AN ABSTRACT OF THE THESIS OF

Michael B. Craven for the degree of Master of Science in Forest Engineering presented on June 10, 2011.

Title: Assessment of Airborne Light Detection and Ranging (LiDAR) for use in Common Forest Engineering Geomatic Applications

Abstract approved:

_____

Michael G. Wing

Airborne Light Detection and Ranging (LiDAR) has become a popular remote sensing technology to create digital terrain models and provide forest inventory information. However, little research has been done to investigate the accuracy of using airborne LiDAR to perform measurement tasks common to Forest Engineering. This thesis contains two manuscripts investigating different measurement scenarios.

The first manuscript examines the use of airborne LiDAR to measure existing forest roads in support of a road assessment under four different canopy conditions. It was found that along existing centerlines the LiDAR data had a vertical RMSE of 0.28 m and a horizontal RMSE of 1.21 m. Road grades were estimated to within 1% slope of the value measured in the field and horizontal

curve radii were estimated with an average absolute error of 3.17 m. The results suggest that airborne LiDAR is an acceptable method to measure forest road grade, but some caution should be used in measuring horizontal curve radii, particularly on sharp curves.

The second manuscript compares profile corridor measurements using airborne LiDAR-derived elevations across different forest canopy types and terrain slopes ranging from 37 to 49%. Both LiDAR-derived DEM and raw LiDAR point elevations were compared to field data. The DEM elevations had an average RMSE error of 0.43 m across all canopy types compared to the field data, while the nearest LiDAR point had an average RMSE of 0.49 m compared to the field data. A skyline payload analysis suggested that profiles based on the DEM outperformed profiles based on nearest point elevations by 5% on average when compared to the field measured profiles. Results suggest that a forest engineer should consider using the DEM value rather than the nearest LiDAR point elevation for terrain elevations at discrete locations, particularly when forest canopy occludes locations of interest.

Assessment of Airborne Light Detection and Ranging (LiDAR) for use in Common Forest Engineering Geomatic Applications

by

Michael B. Craven

A THESIS

submitted to

Oregon State University

in partial fulfillment of
the requirements for the
degree of

Master of Science

Presented June 10, 2011

Commencement June 2012

Master of Science thesis of Michael B. Craven presented on June 10, 2011.

APPROVED:

_____

Major Professor, representing Forest Engineering

_____

Head of the Department of Forest Engineering, Resources and Management

_____

Dean of the Graduate School

I understand that my thesis will become part of the permanent collection of Oregon State University libraries. My signature below authorizes release of my thesis to any reader upon request.

_____

Michael B. Craven, Author

ACKNOWLEDGMENTS

I would like to thank Dr. Michael Wing, Dr. John Sessions, Dr. Michael Olsen, and Dr. Brian Paul for serving on my committee and for all their help with this project. I would also like to thank Dr. James Kiser for providing any field supplies I needed and was also instrumental in my success while at OSU. Perhaps one day yet I will learn to take the time so it takes less.

A special thank you is deserved by the people who helped with the field data collection: Kevin Brown, Jereme Frank, Elijah Allensworth, Katie Hall, and Mark Mathre.

I would also like to thank my family, without them I would not have made it so far. I am especially grateful to Katie who probably now knows more about LiDAR than she ever wanted. Thank you to Emily and Kelley for helping to make sure everything made sense.

CONTRIBUTION OF AUTHORS

Dr. Michael Wing made significant contributions to this project across all aspects of the planning, fieldwork, and data analysis, particularly for Chapter 4. I would like to recognize Dr. John Sessions for his contributions for Chapter 4. Jeff Wimer was also instrumental in the planning of Chapter 4.

TABLE OF CONTENTS

Page

TABLE OF CONTENTS (Continued)

Page

LIST OF FIGURES

LIST OF TABLES

LIST OF APPENDIX FIGURES

LIST OF APPENDIX TABLES

CHAPTER 1: INTRODUCTION

Measurement plays a large role in many of the design decisions required of a forest engineer and many tasks cannot be completed without proper measurement. These measurements span a wide range of subjects from tree measurements for volume estimation and equipment sizing, to measurements of the ground surface for road design and harvest unit layout (Wing and Kellogg 2004). Two common areas of assessment in forest engineering are transportation networks and determination of the ground profile beneath a planned cable harvesting corridor. The intent of this project is to quantify the ability of airborne Light Detection and Ranging (LiDAR) to perform these measurements.

In any type of forest operation the transportation network is a crucial element. Forest engineers typically need to measure and assess the segment from landing to county road or highway within the road network. In the Pacific Northwest (PNW) this segment of the network is typically a road that is either rocked or has a native surface. In the aforementioned context the majority of these roads were built to be used by standard stinger-steered log trucks. Having been built decades ago, there is little engineering record of their design or location. Information pertaining to these roads is primarily derived from aerial photos and topographic maps.

A variety of harvesting projects now require trucks with different operating characteristics from those of a standard stinger-steered log truck. With the utilization of different vehicles and operating equipment, forest or land managers

need to obtain more information about existing roads to determine if they are suitable for the proposed operations. One such operation is biomass harvesting, which is gaining popularity and typically requires the use of chip vans to haul the product through the forest. Chip vans have different operating characteristics than traditional logging trucks (Sessions et al. 2010) and therefore may require modification of existing roads/ existing roads maybe inadequate.

Aside from hauling biomass in chip vans, there are cases were non-standard vehicles need to access the road network. Some land owners are hauling logs longer than fifty feet to allow for more bucking options at the sawmill and potentially lower hauling costs (Sessions et al. 2009). This creates a longer load than the standard maximum log lengths of forty feet and can impact a truck's ability to navigate the road. The delivery of harvesting equipment, particularly large towers, also continues to pose a challenge on the road network just as oversized construction equipment, such as a pile driver needed for some bridge foundations, tests the road networks capabilities.

When a large vehicle (besides a stinger-steered log truck) needs to access the road network the forest engineer is responsible for conducting a road assessment to determine if the vehicle is capable of navigating the network. To make this determination a series of measurements must be taken on the existing roads; these measurements then form the foundation of the road assessment.

A second common measurement task for a forest engineer is the determination of the ground profile beneath a planned cable harvesting corridor.

The corridor information is used to make engineering decisions about harvesting feasibility, equipment selection, tailspar/intermediate support locations, production, and harvesting costs. Historically, these measurements have been made with a hand held compass, string-box, and clinometer (Solmie et al 2003).

This project focuses on determining how well airborne LiDAR can perform the measurements outlined above. In Chapter 2 the basics of LiDAR are discussed and a review of relative literature is presented. Chapter 3 examines the use of airborne LiDAR for measuring existing forest roads across different silvicultural systems. Part one of the chapter is devoted to examining the spatial accuracy of airborne LiDAR along the existing road, and the second portion investigates how well the LiDAR can determine road grade and curve radius simulating a road assessment.

Chapter 4 investigates the ability of airborne LiDAR to measure skyline profile corridors across a variety of canopy types. Comparisons are made using a gridded digital elevation model produced from the LiDAR data, and to the LiDAR points themselves. A brief payload analysis was conducted to show the difference in estimated payload of a skyline logging system using the different elevation inputs.

The ultimate goal of this research is to show that airborne LiDAR has sufficient precision and accuracy to perform some of the measurements common in forest engineering. Specifically the ability of airborne LiDAR to measure the horizontal and vertical alignment of an existing forest road, and measure skyline

profile corridors in support of a payload analysis for a cable harvesting operation. By showing that airborne LiDAR can perform these measurements, it will allow forest engineers to be more efficient in cable harvest design and road assessment.

CHAPTER 2. BACKGROUND AND REVIEW OF RELEVANT LITERATURE

What is LiDAR?

LiDAR is a remote sensing technology (Jenson 2007). That is, LiDAR does not require the user to physically visit an object to measure it. Rather, the measuring is done from a distance. Furthermore, LiDAR is considered to be an active remote sensing system in that LiDAR sends its own energy to a target rather than relying on the energy of the sun (Jenson, 2007).

The first LiDAR systems were developed by NASA in the 1970s. LiDAR for surveying and mapping purposes did not become fully developed until after the advent of the global positioning system (GPS) in the late 1980s. Interest in airborne laser scanning strongly increased beginning in the late 1990s and has continued through today (Baltsavais 1999b, Akay et al. 2009).

There are primarily two types of laser scanners used in LiDAR systems. The first system uses pulses of laser light while the second uses continuously emitted light, known as continuous wave (CW) lasers (Wehr and Lohr 1999). The pulse method is really a time-of-flight measurement system and is typically used in Airborne LiDAR scanners. It has been well established that in a vacuum light travels with a constant speed of c = 299,792,458 m/s. The speed of light does depend on the medium it travels through, but it remains constant for a given medium. As light travels from the source to an object and back to the source, the time it takes is recorded. Knowing the time and speed of light, the distance

between the source and object can be calculated. Again, this method is known as time-of-flight (Beraldin et al. 2010) and distance is calculated with the equation:

$$distance = \frac{c}{n} \times \frac{time}{2}$$

where c is the speed of light, n is the refractive index, and time is the round trip travel time for the laser pulse.

As the laser light travels from the scanner to the object, it will spread out. The footprint or spot size depends on the flying height of the aircraft and laser beam divergence. As an example, at a flying height of 750 meters the laser footprint size would be 0.75 meters in diameter for a typical laser (Baltsavias 1999a). Multiple objects (Figure 2.1) may lie within the laser's footprint. Part of the laser energy will reflect off the first object encountered, while the remaining energy will continue. When energy is reflected back towards the scanner it is known as a return (Beraldin et al. 2010, Jensen 2007).

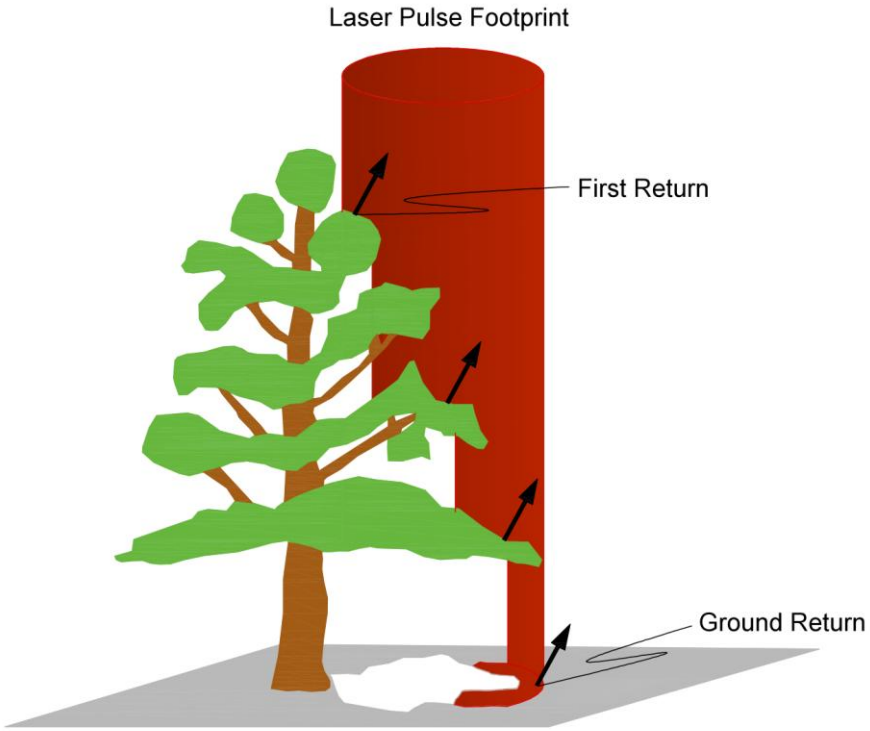

Figure 2.1: Example of multiple returns from a single laser pulse.

The scanner used in this project has the ability to detect up to four returns per laser pulse. Ideally, in a forested situation (Figure 2.1) the first three returns will be off vegetation, while the last return is off the ground. This allows for ground modeling under a forested canopy, as well as the opportunity to measure tree heights if the first return is near the top of the tree. If the only object in the laser's footprint is ground, than there will be only one solid return. If the canopy is too thick then there is a good chance that none of the laser's energy will reach the ground leaving a gap in the ground coverage.

Newer scanners have the ability to measure the entire waveform of the returning energy, and are not limited to detecting a set number of returns. These

scanners are called “full waveform” (Beraldin et al. 2010). Full waveform scanners require more processing and storage space, but offer a greater level of detail.

In addition to multiple returns, LiDAR measures the intensity, the amount of energy that is reflected back from the object being scanned. There are many factors that can affect the intensity including target material properties, range to target, angle of incidence, and atmospheric dispersion (Jenson 2007). Different materials can have different intensity values, and be used for identification of features. This can be seen in figure 2.2, where the rocked road surface has a different intensity value than the surrounding trees and landscape, enabling detection of the road by intensity differences.

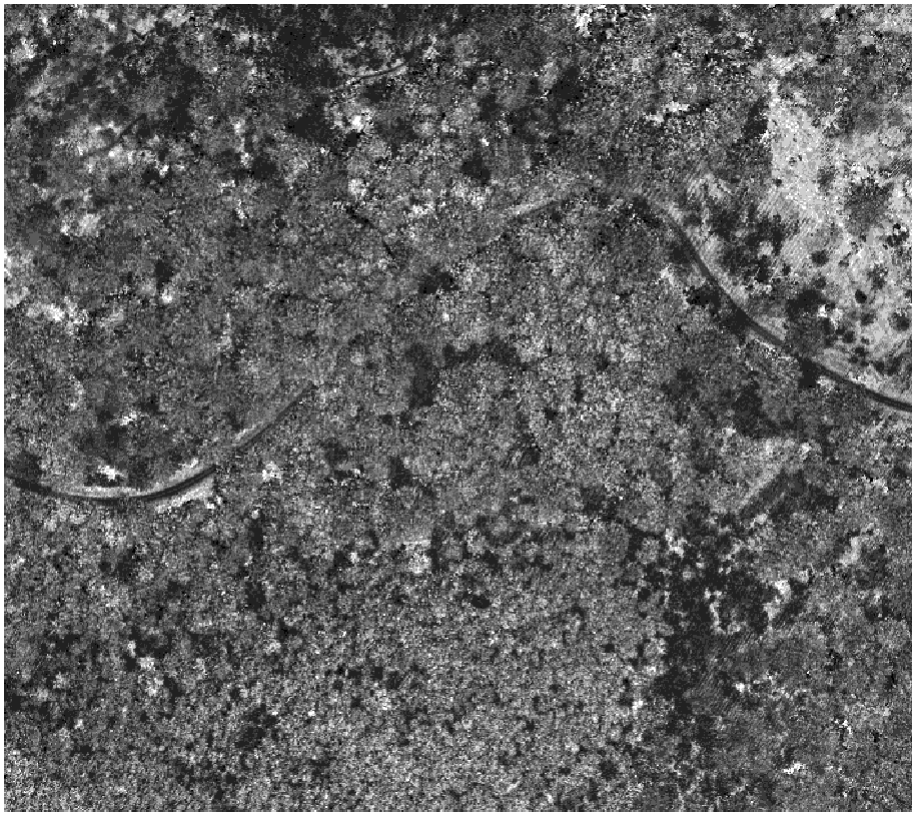

Figure 2.2: Example intensity image of forest road

The data from the scanner is often called a point cloud (Figure 2.3). A point cloud is a 3D series of points, or returns that have their coordinate values determined by the distance and angle from the laser scanner. Therefore, the point cloud coordinates are referenced to the scanner location. In the case of airborne LiDAR, the scanner location is constantly changing with the motion of the aircraft. Two other systems are needed to account for the scanner location and angular orientation, which in turn will allow for the point cloud to be registered into a known coordinate system.

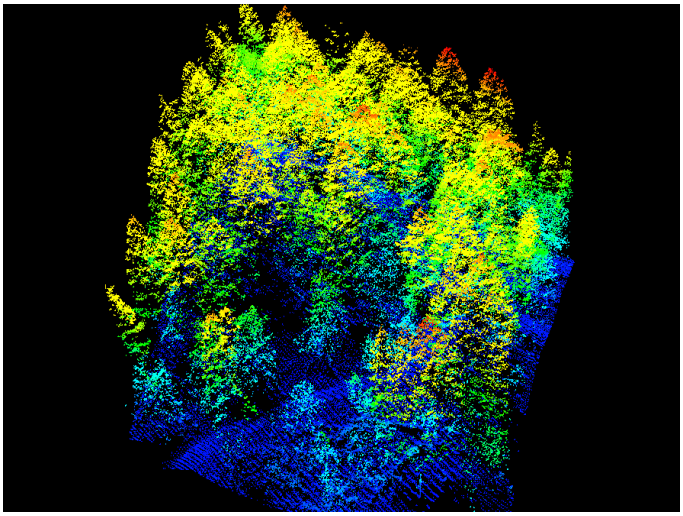

Figure 2.3: Example point cloud with points color coded by elevation

Airborne LiDAR has three main components: the laser scanner, an inertial measurment unit (IMU), and high frequency kinematic GPS (Beraldin et al. 2010). The GPS requires two receivers: one is located on the plane with the laser scanner while the other is located on a stationary known point close to the survey area. During the course of the flight both GPS receivers run simultaneously. After the flight, data from both units are post-processed. The resulting data will yield the

location of the GPS antenna on the aircraft during the flight. With careful calibration the relation of the scanner to GPS antenna can be determined (Jenson 2007).

The aircraft does not fly perfectly level for the entire flight. Rather, the aircraft will have some pitch, yaw, and roll, or rotations about the y, z, and x axes. The IMU device can record the amount of pitch, yaw, and roll, which can be used to correct the scanner data to account for these rotations (Beraldin et al. 2010). By combining the GPS and IMU data the orientation of the each laser pulse can be determined and the resulting returns referenced into a standard coordinate system.

LiDAR Accuracy

There have been many studies conducted to assess the accuracy of LiDAR and LiDAR-based digital terrain models (DTM). As with every study the results are specific to that study and depend on a variety of conditions. Technological improvements have also made LiDAR more accurate today than it was at its conception, and as technology continues to improve, so should the accuracy.

Technical Limitations

One of the limits of LiDAR technology is the ability to measure time accurately, which is one of the key components in a time of flight system. Baltsavais (1999) showed that for an average laser pulse time of 10 ns there is a rise time of 1ns from no to full energy. The rise time corresponds to a range of 15 cm. Measuring time precisely plays a critical role in the accuracy and precision of a LiDAR time of flight system. As technology improves for both shorting rise time

and time measurement, the amount of error in a LiDAR measurement decreases. However, there are certain limits that technology cannot seemingly overcome. As an example, in a heavily forested area the canopy will always reflect a large portion of the laser pulse resulting in a sparse number of returns on the forest floor.

Vertical Accuracy

The terrain in which the LiDAR data are being collected plays a large role in the final accuracy. Forested areas present a challenge in that the canopy cover over the ground surface is highly variable in both spatial distribution and density as species and structure changes. Therefore, it is hard to predict how much of the forest will prevent the LiDAR energy from reaching the ground surface and producing a ground return. Understanding the canopy structure above the ground surface is a key step in assessing the LiDAR's accuracy in the forested environment.

One of the earliest and often referenced studies on LiDAR and the forest is Kraus and Pfeifer (1998). The study was conducted in a wooded area outside of Vienna; no information was provided on the type of forest cover. The combination of the scanner used and the forest cover resulted in a ground return occurring, on average, every 2.5 m. Check points were collected terrestrially to provide a baseline elevation of the ground. Across the study site the total vertical root mean squared error (RMSE) was 0.57 m.

Another early example of vertical accuracy assessment is from the Boreal forest in southern Finland. Hyyppä et al. (2000) conducted an accuracy assessment

as part of their development of a new terrain model creation algorithm. They found that for flat areas in their study, the LiDAR versus true ground elevation had a standard error of 15 cm. Areas with slopes of 40% had a standard error of 40 cm, lending some evidence that slope can affect LiDAR accuracy. Hyyppä et al. (2000) determined elevation accuracies along roads in their study area. The methods involving the roads were not included in paper, nor any details regarding the roads, but their results show an elevation difference of 8.5 cm between ground and LiDAR points along the roads.

Hodgson and Bresnahan (2004) also examined the influence of surface conditions on LiDAR accuracy. Their study site was located in forested area in South Carolina. The RMSE between field measured and LiDAR measured elevations varied from 19, 23, 17 cm for areas of pavement, low grass and evergreen forest respectively. Deciduous forest had the largest RMSE at 26 cm. Using the same data it was noted that elevation error on steeper slopes (47 %) were twice as high as those on flatter slopes (3 %).

Hodgson et al. (2005) assessed another forested area delineated into strata based on land cover. The LiDAR data was collected in North Carolina during what was considered "leaf off" conditions, meaning the deciduous trees did not have leaves at the time the LiDAR was flown. Slopes in the study area were shallow ranging from 0 to 18 %. The land cover categories that were heavily vegetated such as shrubs and Pine had the largest RMSE values at 36.1 and 27.6 cm respectively. Land cover types such as grass and pavement had lower RMSE

values at 14.5 and 22.6 cm respectively. This indicates that tree and shrub ground cover affects the accuracy of LiDAR.

Of particular relevance to this project is the study by, Reutebuch et al (2003) that examined a 500 hectare parcel in Western Washington. The study area was divided into four canopy classes: clearcut, lightly thinned, heavily thinned, and uncut. A gridded DTM model was produced from LiDAR data that had four returns per pulse, averaging 1 ground return per square meter. The grid size on the DTM was 1.52 m x 1.52 m. Over 300 points were surveyed on the ground using total stations for the control. The mean error across all canopy types was 0.22 m, with a standard deviation of 0.24 m. As expected, the clearcut regions had less error than the uncut regions as shown in table 2.1.

Table 2.1: Summary of DTM errors by canopy type from Reutebuch et al. 2003

Canopy Type	Mean DTM Error	Standard Deviation
Clearcut	0.16 m	0.23 m
Lightly Thinned	0.18 m	0.18 m
Heavy Thinned	0.18 m	0.14 m
Uncut	0.31 m	0.29 m

A case study conducted in the Netherlands assessed a LiDAR dataset accuracy specifically for the purposes of road design. Gomes Perira and Janssen (1999) stated that an acceptable vertical RMSE in a LiDAR DTM for the purposes of forest road design would be 25 cm. They used ground-based surveying methods to determine the baseline elevation of the ground surface and then compared those values to the LiDAR DTM. The total vertical RMSE was 29 cm; however, a stratification was completed to separate flat and non flat areas. Flat regions had a

vertical RMSE of 8 cm to 15cm while sloped terrain had a vertical RMSE of 25 cm to 38 cm. Although the total vertical RMSE was above the target of 25 cm, Gomes Pereira and Janssen felt that the results were close enough, and airborne LiDAR would provide a DTM sufficient for road design.

Bowen and Waltermire (2002) conducted a study of LiDAR elevation accuracy in the specific application of measuring river corridor topography. A river corridor may be analogous to a road in that there would be reduced canopy cover over both the river and road. Also the steeper banks along a river might be analogous to the cut banks on forested roads.

Bowen and Waltermire (2002) provided little information on the LiDAR dataset, the number of detectable returns, native pulse density or ground returns per square meter. The control points were collected via GPS and over 200 points were taken. As with many of the other studies, the region was delineated into strata based on land cover and slope: steep slopes 100 % or higher, sand, cobbles, and brush. The RMSE for the whole area was 0.43 m, while the worst performing strata was the steep slopes with an RMSE of 111cm. Bowen and Waltermire (2002) noted their total RMSE is about twice that of other studies and attribute the difference to steep and varied topography surrounding the river corridor. Their results also support those of other studies (Hodgson and Bresnahan 2004, Hodgson et al. 2005) in that LiDAR accuracies decreased as ground slope increased.

By reviewing the studies presented here, there are two main ideas to retain. First as shown best by Reutebuch et al (2003), LiDAR accuracy in measuring the

ground surface is affected by the forest canopy. Secondly, ground slope can also affect the accuracy of LiDAR as shown by many of the studies discussed, but perhaps shown the best by Hodgson and Bresnahan (2004). A summary of the vertical accuracy studies are presented in table 2.2.

Table 2.2: Summary of Vertical LiDAR Accuracies Presented

Study	LiDAR Vertical Accuracy	Land Cover Type
Kraus and Pfeifer (1998)	57 cm, RMSE	Forested Terrain
Hyyppä et al. (2000)	40 cm, Standard error	"Steep" Forested Terrain
Hodgson and Bresnahan (2004)	26 cm, RMSE	Deciduous Forest
Hodgson et al. (2005)	28 cm, RMSE	Pine Forest
Reutebuch et al (2003)	22 cm, Mean error	Across various management regimes in PNW Forest
Bowen and Waltermire (2002)	43 cm, RMSE	River Corridor Area

Horizontal Accuracy

The majority of LiDAR accuracy assessment in the forest environment has been concerned with vertical accuracies. Horizontal accuracies are difficult to obtain because the LiDAR must return off a distinct feature that can be found in the field and measured. Hodgson and Bresnahan (2004) comment that typically flat roofs work well as a reference point for horizontal comparisons between field measurements and LiDAR data. This is due to the fact that roof corners are easily identifiable in the LiDAR data and in the field. Gomes Perira and Janssen (1999) used roof corners in their study area as a point that could be found in the LiDAR data and found in the field. Gomes Perira and Janseen's error in horizontal position was found to be on average 0.21 m. An accepted range of horizontal accuracies for airborne LiDAR are 0.2-1.0 m under good conditions (Beraldin et al. 2010).

In a completely forest environment, with no buildings, studies have been conducted that use tree location to assess horizontal accuracy. Renslow et al. (2000) reported a horizontal RMSE of 0.90 m using tree tops as a horizontal location. Hyyppä et al. (2000) also used tree top locations as a gauge for horizontal accuracy with a reported RMSE of 0.98 m.

The horizontal accuracy of airborne LiDAR is larger than that of vertical accuracy as a result of laser footprint size (Beraldin et al. 2010, Renslow et al. 2000). Due to laser beam divergence and flying height of aircraft used in Airborne LiDAR, the laser beam footprint is considerably large (0.75 m), as shown in the Baltsavais (1999a) example. A rule of thumb is that the horizontal accuracy will be within twice the size of the laser beam foot print (Renslow et al. 2000). Flying at low elevations such as with a helicopter would reduce the laser footprint and improve the horizontal accuracy.

Forestry Applications

Airborne LiDAR has been shown to be a valuable tool in forestry applications (Maas 2010, Jenson 2007). The ability of LiDAR to capture multiple returns typically results in a return from the top of the canopy and the final return from the ground surface. By subtracting the difference between the two returns, the height of the canopy and thus tree height is estimated. Collecting data in 3D LiDAR has some advantage over 2D image based techniques when it comes to calculating forest structure estimates, such as leaf area index (LAI) (Maas 2010). With current LiDAR technology the resulting point cloud is dense enough that

individual trees can be measured (Hyyppä and Inkinen 1999). Airborne LiDAR has even been found to measure successfully single trees and snags in burned areas (Wing et al. 2010). Using all the returns has so far been primarily used in inventory related applications, while ground surface modeling only requires the last return, if indeed the last return is from the ground.

Akay et al. (2009) provides an overview of the research surrounding applications in forestry. Once it was established that LiDAR could measure individual trees and canopy conditions, LiDAR based data sets became the foundation for many different research areas. Examples include Patenaude et al. (2004) who conducted a study that used LiDAR measurements to quantify above ground carbon content. Another example is Hyde et al. (2005) who used LiDAR to analyze forest structure and produce large scale maps for wildlife habitat management.

The primary interest of this project is the characteristics of the terrain, so the ground returns play the key role. There has been a variety of research conducted that has used LiDAR based terrain models under forested canopy. One such example is using the high resolution Digital Elevation Model (DEM) produced from LiDAR as a way to optimize forest road design. Aruga et al (2003) developed an algorithm to optimize the vertical alignment of a road based on earthwork volumes. Having an accurate DEM was crucial to the algorithm's success. In another design example Chung (2003) used a LiDAR based DEM to

optimize road locations and cable harvest layout over a 230 acre region. In these examples LiDAR data was used, but an accuracy assessment was not conducted.

Field Equipment Incorporated in Project

Global Positioning System (GPS)

The LiDAR data used in this project had been geo-referenced with a projection in the Universal Transmercator (UTM). In order to make comparisons the data collected in the field would need to be referenced in the same projection. This leaves two options: 1) use existing control points that have existing coordinate values, or 2) establish new control points in the field. A review of the College of Forestry database for known survey control indicated that Public Land Survey System Corners (PLSS) were the only control points located with in the forest. PLSS corners can have established horizontal coordinates but typically not in UTM coordinates and lack vertical control. Thus, establishing control points was the preferred option.

Control points can be established in a variety of ways (Schofield 2001), but today GPS is commonly used. There are currently three types of GPS receivers available, the most accurate and precise being survey grade receivers. The unit used for this project was a HiperLite+ manufactured by Topcon, figure 2.4. The HiperLite+ is a dual frequency receiver, in that it can receive the L1 and L2 frequencies broadcast by the satellites. The time delay caused by the ionosphere affects the L1 and L2 frequencies differently. By modeling the difference between

the frequencies the receiver can estimate the error caused by the ionosphere (Van Sickle 2008b).

Figure 2.4: Topcon HiperLite+ Survey Grade GPS receiver

In order to obtain more accurate coordinates, GPS solutions need to be post-processed to account for a variety of conditions, one of the most notable being satellite orbit (Van Sickle 2008a). In the United States, one of the common ways to post-process the data is via the National Geodetic Survey's Online Positioning User Service (OPUS). OPUS is available online, and is free for anyone to use. The requirements for OPUS are a raw GPS observation file, antenna height, and antenna model. Depending on the length of the GPS observation, different algorithms are used. As the length of the observation increases, errors due to

ambiguities or multipath can be reduced. In order to use the strongest algorithm in OPUS a two hour observation, or longer, must be taken (NGS 2011).

Once a user's data is submitted and it is over two hours in length, it is analyzed via a program called Pages. Pages computes the GPS receiver's coordinates via three independent baselines from the closest three continually operating reference stations (CORS). These baseline solutions are all double-differenced and carrier-phase. Under ideal conditions the Pages program should be able to resolve the GPS unit's position to within a few centimeters in all three directions (NGS 2011).

Knowing the GPS satellite orbits precisely is key in obtaining quality results. The GPS system can be thought of as trilateration, where the measurement of distances is used to fix positions (as opposed to angles as in triangulation). In order to determine the location of a position on the Earth, the distance from a GPS satellite to the point on the Earth must be known, but so must the position of the satellite (Van Sickle 2008a). In order to know the satellite's position the satellite orbit must be known.

There are two basic types of GPS satellite orbits available: broadcast and precise (ASCE 2000, Van Sickle 2008a). The broadcast ephemeris is the predicted satellite position that is sent to the satellites as part of the control segment of GPS. The broadcast ephemeris is determined via the measurements from tracking stations that monitor each GPS satellite's orbit (ASCE 2000).

The precise ephemeris is determined by tracking the GPS satellites and post-processing the data to produce more accurate satellite positions (ASCE 2000). The International GPS Service (IGS) provides precise GPS orbits to the scientific community and other users. The IGS is comprised of over 200 organizations in eighty different countries. They have more than 300 permanent continuously operating GPS stations that provide the tracking data to the IGS's analysis centers (Kouba 2009). Currently, there are eight analysis centers. Examples include: National Geodetic Survey, located within the National Oceanic and Atmospheric Administration, NASA's Jet Propulsion Laboratory JPL, and Scripps Institute of Oceanography (NGS 2009, Kouba 2009).

For the OPUS observations Pages uses either a rapid orbit or a final precise orbit. The rapid orbits are delayed anywhere from 17-41 hours from the time of the observation. The final precise orbits are updated every GPS week, which translates into a delay of 11 to 17 days (NGS 2009).

For this project the GPS observation times were predetermined to be 8 hours. This is more than triple the minimum needed for Pages, extended time would theoretically mitigate the likelihood of multipath errors in the forested environment. Final precise orbits were used for all the OPUS solutions.

There are no absolute rules in determining if an OPUS solution is highly accurate (NGS 2011). However, there are a number of indicators provided with an OPUS solution that will suggest if the solution is of quality. One such indicator is the estimation of the root mean square (RMS) error for the observed point, and if

this value is less than 3 cm the solution is considered to be acceptable (NGS 2011). Soler et al. (2005) examined OPUS solution quality for five sites throughout the United States using observation times ranging from 1 hour to 4 hours. Their results reflected the comments by the National Geodetic Survey; the longer the observation, the more accurate the OPUS solution will be. Using 2 hour observations the RMS was 0.8 cm, 2.1 cm and 3.4 cm in the northing, easting, and elevation respectively. A 3 hour observation improved the elevation RMS to 2.0 cm.

By following the suggestions of NGS (2011) and Soler et al. (2005) and using longer observation of times of 8 hours, the OPUS solutions for this project should have similar accuracies to those reported in Soler et al. (2005). Each OPUS solution used in this project was checked to make sure it met the recommendations by NGS (2011) for what is considered to be a quality solution. See the appendix for a table detailing the specifics of the OPUS results.

In addition to the GPS used to establish control points, a second method of GPS technology was utilized for the skyline profile analysis segment of the project discussed in chapter 4. Real Time Kinematic (RTK) GPS, and was used in the areas that had no canopy cover and would allow for quality results.

In its classical application, RTK consists of two survey grade GPS receivers. One receiver is setup on a tripod over a known control point; this receiver is known as the base. The second receiver is mounted on a range pole and is known as the rover, because the unit moves between different measurement

positions while the base station remains static throughout the survey. The two receivers communicate with each other via a radio link, and both units are run simultaneously. The base station calculates its position based off the GPS satellite signals, and compares its calculated position with its control point coordinates. Corrections are developed to account for the difference between the calculated and control point coordinates. These corrections are transmitted in real time to the rover unit. The rover unit takes its calculated coordinates and applies the corrections from the base station to produce more accurate coordinates (Van Sickle 2008a).

Total Stations

A total station is a digital instrument comprised of two main parts: 1) Electronic Distance Measurement (EDM) and 2) Angular measurement (Wolf and Ghilani, 2006a). EDM, in this case, works by sending out a pulse of energy to a target and measures the difference in phase of the returned energy. With known wavelength of energy and number of cycles through modulation, the distance to the target can be computed (Wolf and Ghilani, 2006b).

The angular measurement on a total station is conducted via electronics. The system works by passing a beam of collimated light through finely spaced graduations. It is important to note that unlike a magnetic or solar instrument, a total station has no internal mechanism to determine what direction it is pointing. The total station must be pointed in the direction of a known bearing, or azimuth, and that direction must be input into the total station's computer for it to orientate

itself in the horizontal direction. In the vertical direction the initial direction is determined by an automatic compensator. The compensator uses the direction of gravity to vertically align the instrument. Both the horizontal and vertical angle measurements require that the total station be level to operate properly (Wolf and Ghilani, 2006a).

The specific total station used was a Nikon Nivo 5c (figure 2.5). The unit used was a 5” model, meaning the instrument is accurate up to five seconds of arc when measuring angles. The stated distance accuracy is 3mm plus 2 parts per million of distance measured (Nikon, 2010).

Figure 2.5: Nikon Nivo 5c Total Station

LiDAR Dataset:

The LiDAR dataset used in this project was flown with a fixed wing aircraft by Watershed Sciences, Inc. of Corvallis, Oregon. The data was collected in April of 2008 using a Leica ALS 50 scanner. The ALS 50 is capable of recording up to four returns per laser pulse and produced a native point density of 10 points/m^2. On average, 1.12 points/m^2 reached the ground across the forest (Watershed Sciences 2008). This indicates the canopy prevented many of the points from reaching the ground.

The LiDAR data was referenced in the Universal Transverse Mercator (UTM) coordinates using the NAD 83 (CORS 96) horizontal datum and the NAVD88 (Geoid03) vertical datum. Real time kinematic GPS was used to measure points along two roads in clearcuts in the northern part of the forest at the same time the LiDAR was being flown. This allowed for a comparison between the GPS points and the LiDAR points to yield an initial accuracy assessment. A total of 510 points were taken along and road in a cleartcut, and the average difference between the field measured elevation and the LiDAR elevation was 0.007 m, with the maximum being 0.077 m (Watershed Sciences, 2008).

Watershed Sciences delivered the data in two formats: raw data points and a 1-meter DEM. In addition to the positional data, a 0.5 meter intensity image was also provided. Rather than use a statistical technique to determine grid cell values in the DEM, Watershed Sciences determined grid cell elevations by sampling from a triangular irregular network (TIN) surface (Russ Fox, pers. comm., Watershed

Sciences, Feb. 5, 2011). A TIN surface is basically a series of triangular faces that represent the terrain, (Figure 2.6). In this case the vertices of the triangles are LiDAR points. The TIN allows for the DEM elevations to be interpolated between LiDAR points. Without the TIN surface as the basis for the DEM, there would be many grid cells with a no data value or "hole". This is due to the nature of the canopy and how it prevents ground returns from occurring with every laser pulse.

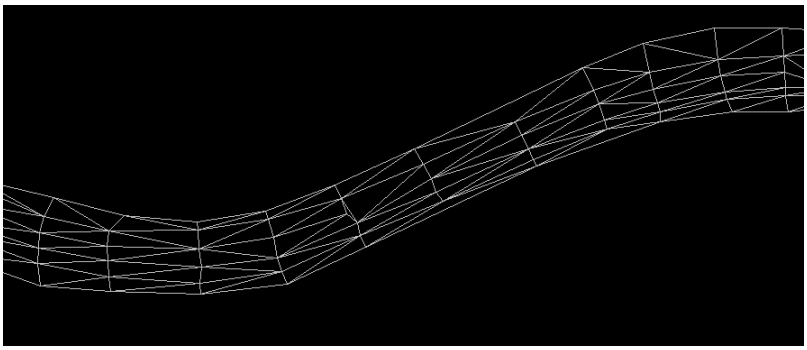

Figure 2.6: Example of a Tin Surface From Field Survey, Road Segment E4

Summary

This chapter provides a background of the equipment and data used in this project, as well as provide a sense for the previous research involving forestry and LiDAR accuracy. This review indicates that many studies have shown LiDAR accuracy varies with the type of forest cover and ground slope. Generally, less cover above the forest floor, correlates with better accuracy and conversely, more cover with worse accuracy. Steep slopes appear to have less accurate LiDAR measurements than do flat areas. The majority of the accuracy studies involving forestry have taken a general approach to LiDAR accuracy and have not examined specific applications. This project evaluates the accuracy of specific application in

two areas. First, the measurement of existing roads were the forest canopy over the road is typically less than the surrounding stand, but not completely open. Second, the replacement of field measurement of skyline profile corridors, which require both precision and accuracy on steep slopes to model payload analysis.

References

Akay, A., H. Oguz, I. Karas, and K. Aruga. 2009. Using LiDAR technology in forestry activities. *Environ. Monit. Assess.* 151(1):117-25.

Aruga, K., J., Sessions, and A. Akay. 2005. Application of an airborne laser scanner to forest road design with accurate earthwork volumes. *Journal of Forest Research* 10(2): 113-123.

American Society of Civil Engineers (ASCE). 2000. Operational Theory of NAVSTAR GPS. P 3-26. in *NAVSTAR Global Position System Surveying*. American Society of Civil Engineers, Boston, MA.

Baltsavias, E. 1999a. Airborne Laser Scanning: Basic Relations and Formulas. *ISPRS Journal of Photogrammetry & Remote Sensing*. 54(1999): 199-214.

Beraldin, J-A., F., Balis, and U. Lohr. 2010. Laser Scanning Technology. P. 1-42 in *Airborne and Terrestrial Laser Scanning,* Vosselman, G., and H-G., Mass (eds.). Whittles Publishing, Dunbeath, Scotland, UK.

Bowen, Z.H., and R.G. Waltermire. 2002. Evaluation of Light Detection and Ranging (LiDAR) for measuring river corridor topography. *Journal of the American Water Resources Association*. 38(1):33-41.

Chung, W. 2003. *Optimization of Cable Logging Layout Using a Heuristic Algorithm for Network Programming.* Ph.D. Thesis, Oregon State University, Corvallis OR. 198 p.

Gomes Pereira, L.M., and L.L.F. Janssen. 1999. Suitability of laser data for DTM generation: a case study in the context of road planning and design. *ISPRS Journal of Photogrammetry & Remote Sensing*. 54(1999):244-253.

Hodgson M., P., Bresnahan. 2004. Accuracy of Airborne Lidar-Derived Elevation: Empirical Assessment and Error Budget. *Photogrammetric Engineering and Remote Sensing* 70(3): 331-339.

Hodgson, M., J., Jensen, G., Raber, J., Tullis, B., Davis, G., Thompson,and K., Schuckman. 2005. An Evaluation of Lidar-derived Elevation and Terrain Slope in Leaf-off Conditions. *Photogrammetric Engineering & Remote Sensing* 71 (7): 817-823.

Hyde, P., R. Dubayah, R., B., Peterson, J., Blair, M., Hofton, and C., Hunsaker. 2005. Mapping forest structure for wildlife habitat analysis using waveform

LiDAR. Validation of montane ecosystems. *Remote Sensing of the Environment* 96(4): 427-437.

Hyyppä, J., and M. Inkinen. 1999. Detecting and estimating attributes for single trees using laser scanner. *The Photogrammetric Journal of Finland* 16(2): 27-42.

Hyyppä, J., U., Pyysalo, H., Hyyppä, and A. Samberg. 2000. Elevation Accuracy of Laser Scanning-Derived Digital Terrain and Target Models in Forest Environment. P. 139-147 in Proceedings of EARsEL-SIG Workshop LIDAR. Dresden Germany.

Jenson, J.R. 2007. LiDAR Remote Sensing. P. 335-355 in *Remote Sensing of the Environment*, Howard, J., D. Kaveney, K. Schiaparelli, E. Thomas (eds.). Pearson Education, Inc, Upper Saddle River, NJ.

Kouba, J. 2009. A Guide to Using International GNSS Service (IGS) Products. Geodetic Survey Division, Natural Resources Canada. Ottawa, On. P. 1-29

Kraus, K., and N. Pfeifer. 1998. Determination of terrain models in wooded areas with airborne laser scanner data. *ISPRS Journal of Photogrammetry & Remote Sensing.* 53 (1998): 193-203.

Maas, H. 2010. Forestry Applications. P. 213-235 *in Airborne and Terrestrial Laser Scanning*, Vosselman, G., and H-G., Mass (eds.). Whittles Publishing, Dunbeath, Scotland, UK.

NOAA National Geodetic Survey (NGS). 2009. Precise GPS Orbits. Available online at http://www.ngs.noaa.gov/orbits/; last accessed Apr. 4, 2011.

NOAA National Geodetic Survey(NGS). 2011. What is OPUS?. Available online at: http://www.ngs.noaa.gov/OPUS/about.jsp#about; last accessed Apr. 4, 2011.

Nikon. 2010. Nikon Nivo M Series Total Stations Specification Sheet. Available online at: http://trl.trimble.com/docushare/dsweb/Get/Document-468108/022505-100B_NivoMseries_SS_0909_LR.pdf; last accessed Apr. 4, 2011.

Patenaude, G., R., Hill, R., Milne, D., Gaveau, B., Briggs, and T., Dawson. (2004). Quantifying forest above ground carbon content using LiDAR remote sensing. *Remote Sensing of the Environment* 96(3): 368-380.

Renslow, M., P. Greenfield, T. Guay. 2000. *Evaluation of multi-return LiDAR for forestry applications*. USDA Forest Service - Engineering, Remote Sensing Applications Center RSAC-2060/4180-RPT1. 17 p.

Reutebuch, S., R. McGaughey, H. Andersen, and W. Carson. 2003. Accuracy of high-resolution lidar terrain model under a conifer forest canopy. *Can. J. Remote Sensing*. 29(5):527-535.

Schofield, W. 2001. Control surveys. P. 252-306 in *Engineering Surveying*. Butterworth Heinemann, Oxford, UK.

Soler, A., P. Michalak, N. Weston, R. Snay, and R. Foote. 2005. Accuracy of OPUS solutions for 1- to 4-h observing sessions. *GPS Solutions.* 10(1): 45-55.

Van Sickle, J. 2008a. GPS Surveying Techniques. P. 177-228 in *GPS for Land Surveyors.* CRC Press, Boca Raton, FL.

Watershed Sciences. 2008. LiDAR remote sensing data collection: McDonald-Dunn Research Forest. Corvallis, Oregon, Watershed Sciences Inc.: 20 p.

Wing, M., A., Eklund, and J., Sessions. 2010. Applying LiDAR technology for tree measurements in burned landscapes. *International Journal of Wildland Fire* 19(1): 104-114.

Wolf, P.R., C.D., Ghilani. 2006a. Total Station Instruments; Angle Measurements. P. 187-226 in *Elementary Surveying an Introductin to Geomatics,* Svendsen E., D., Bernhard, V., O'Brien, D., George, R., Kernan (eds.). Pearson Prentice Hall, Upper Saddle River, NJ.

Wolf, P.R., C.D., Ghilani. 2006b. Electronic Distance Measurement. P. 145-164 in *Elementary Surveying an Introductin to Geomatics,* Svendsen E., D., Bernhard, V., O'Brien, D., George, R., Kernan (eds.). Pearson Prentice Hall, Upper Saddle River, NJ.

CHAPTER 3: APPLYING AIRBORNE LiDAR FOR FORESTED ROAD GEOMATICS

Michael Craven and Michael Wing

Department of Forest Engineering, Resources and Management

Oregon State University

Corvallis, OR 97331

Introduction

Traditionally, forest roads have been designed for a stinger-steered log truck with log lengths close to forty feet. Stinger-steered log trucks have three primary advantages over traditional tractor/trailer combinations. First, the stinger portion of the truck allows for articulation of the trailer, which in turn allows for sharper curves to be negotiated. The minimum safe radius for a stinger-steered log truck is 15 m or 50 ft (B.C Ministry of Forests 2002, Kramer 2001).

The second advantage of a stinger-steered log truck is its ability to climb steeper grades while unloaded. This is realized by the capacity to “piggy back” the rear portion of the trailer onto the truck. The result is an increase in weight over the drive wheels, which in turn produces a greater normal force at the wheel contact area. The larger the normal force, the more traction the wheels can develop, and the more traction the truck has, the steeper the grade it can climb (Sessions 2007, Sessions et al. 2009). The third advantage also comes from the stinger-steered truck's unloaded state. With the trailer placed on the truck, the wheel base is shorter and allows for smaller truck turnarounds out in the forest (Sessions et al. 2010).

If a landowner wants to haul forest products that do not fit on the standard stinger-steered log truck, the road that is going to be hauled on needs to be assessed. As an example, Sessions et al. (2010) showed that chip vans hauling biomass have different requirements in terms of gradeability and horizontal geometry compared to a stinger-steered log truck.

There are a variety of methods available to measure and assess forest roads. Each road segment could be visited and surveyed manually. Depending on the accuracy and precision, the time and cost of manual surveying may not make it feasible for large road networks.

A more practical method to measure forest roads on a large scale would be with a remote sensing technique. Traditionally, the principal remote sensing technique for forestry has been aerial photography, with origins beginning in the 1930's (Paine and Kiser 2003). Camera technology and analytical methods have advanced greatly since the early days of photogrammetry. Depending on the level of effort and equipment, very precise measurements can be made on the ground to the centimeter level (Wolf and Dewitt 2000). This level of detail is not often practiced in the forested environment, but rather on engineering projects were such precision is justified.

Typically in forestry applications, direct measurements are taken from photos. The accuracy and precision of directly measuring from photos is greatly influenced by topographic displacement and the motions of the aircraft/camera (Kiser 1991). While aerial photos are an excellent tool for making measurements and interpreting features on the ground, they do have a drawback in the forested environment: the user cannot determine what is underneath the forest canopy. However, there are other remote sensing technologies that can detect the ground surface beneath trees. One such technology is Light Detection and Ranging (LiDAR).

There were two main objectives of this study. The first was to assess the horizontal and vertical accuracy of LiDAR along existing forest roads. The second objective was to investigate the ability to measure road grade and horizontal curve radius from LiDAR in support of a road assessment.

Methods

Study site and sample design

We conducted our research within McDonald Research Forest which is managed by the Oregon State University College of Forestry (44° 37” N, 123° 18” W). McDonald Forest is located within a 11.25 km radius of Corvallis. The forest is comprised of a mixture of silvicultural regimes, but is predominately covered with Douglas-fir (pseudotsuga menziesii).

McDonald Forest is an ideal research site due to its close proximity to Oregon State University campus and its variety of forest management practices. Forest staff have compiled an extensive geographic database including individual stand data, roads, streams, digital elevation models (DEMs), and ownership boundaries. McDonald Forest was also convenient because most of the people involved with the project were familiar with the forest in general.

Using the GIS road data, there is approximately 81.88 km (50.88 mi) of road located within McDonald Forest. Due to the time constraints and available personnel, five percent of the road lengths were selected for sampling. This resulted in 4.09 km (2.54 mi) of road being sampled.

Due to the fact that the forest is not comprised of a homogenous stand, the road system within McDonald Forest were stratified based on surrounding stand types. Stand types were stratified using descriptions in the GIS stands layer: clearcut, evenage, unevenage, and mature. We selected these stratifications as we believed that different canopy conditions would affect the number of LiDAR returns that were from the road surface (Reutebuch et al. 2003, Hodgson and Bresnahan 2004, Hodgson et al. 2005).

After initial stratification, a check was done to determine if the strata assigned to each road appeared correct. A primary concern was with stands that were labeled as "clearcut" in the GIS layer, but had been last harvested in the 1980's and had not had database updates that evidenced subsequent forest growth. A combination of aerial photography from 2009, tree height data from the GIS layers, and harvest year were used to determine if a stand should be stratified as clearcut or evenage. As a general rule, a stand that had an average tree height of 7.6 m (25 ft) or taller was moved into the evenage category. The combination of four strata and the 4.09 km of road to be sampled resulted in 1.03 km (0.64 mi) in each strata being surveyed.

Ideally, there would be, at a minimum, thirty road segments measured. This is because at a sample size of thirty for a given confidence level, the t distribution changes by a small amount as the sample size is increased. However, given the time required to establish measurement control and rigorously survey road

segments, four road segments within each strata were selected for analysis. This resulted in a total of sixteen road segments.

With the number of samples determined, the next task was to randomly select sixteen segments from the forest road network. This required associating each road with one of the four strata. To accomplish this, a combination of GIS operations including a spatial join and an identity overly process was used. The spatial join assigned the strata with the largest length along the road to each road segment in network. The identity feature then delineated the road network into segments that correspond to the four strata values.

There were issues with the topology of the McDonald GIS datasets. Within a single layer the topology appeared to be correct. When comparing two layers to each other, the topology often did not align. The typical case is when in the field a road was the boundary between two different stands. In GIS the road layer did not match the stand layer, resulting in the road criss-crossing the strata boundary. When the identity was run the result was multiple road segments of relatively short length. To overcome this problem, the identity process in ArcGIS has the ability to use a spatial tolerance. Multiple tolerance values were experimented with (1-10 m), and a tolerance of 3 meters appeared to give the best results.

After the roads data were delineated by strata, the next step was to select the sixteen road segments for measurement. Every road segment was numbered consecutively with segments less than 256 m being discarded. The remaining

roads were segregated into categories based on how many potential samples would fit in their length (Table 3.1).

Table 3.1: Number of Samples Based on Segment Length

Road Segment Length (m)	Number of Samples Assigned
256	1
512	2
768	3
1024	4
1280	5
1536	6
1792	7

Each of these potential samples located within a road segment was assigned a sample number. Four random numbers for each strata were generated and indicated which sample would be chosen for measurement. None of the selected segments were exactly divisible by 256 m so a method had to be developed to determine where along the segment the 256 m measurement segment would start.

To determine the starting end of each segment a random number of either one or zero was generated. Zero corresponded to the start of segment as defined by the roads GIS layer, while one corresponded to the end. The remaining distance of road in the segment that was in excess of 256 m was calculated. A random number was then generated within the range of this remainder to quantify how far from the

end of the total segment the 256 m segment would start. Once the 256 m segments were identified, their locations were annotated into the GIS files (Figure 3.1).

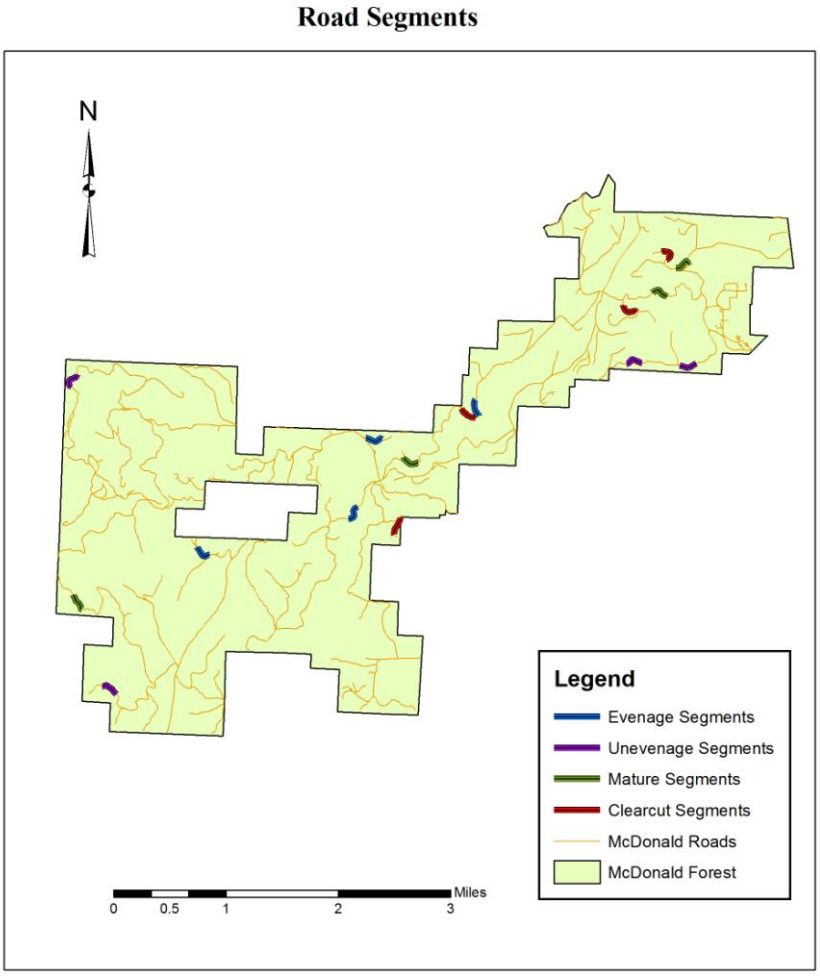

Figure 3.1: Road Segment Locations

Ground based surveying

The objective of the field portion of the project was to establish the baseline road surface to use as a reference in comparison to the LiDAR data. A digital total station was employed to capture the alignment and grade. However, a

total station alone only provides relative measurements on an assumed coordinate system. A survey grade GPS receiver was used to establish control points that the total station measurements could be tied to and provide a ground coordinate system. Thus, the field methods can be thought of in two parts: GPS and total station.

For each road segment two control points were required. One control point was used to fix the X, Y, and Z coordinates of the field survey. The second point was used to establish a bearing between the two control points. By setting up on the first control point and sighting the second control point, the direction the total station was facing would be known. The points were set using a Topcon Hiperlite+ and processed via OPUS solutions as described in Chapter 2.

With control points established via GPS, the remaining survey work was completed with a total station. All distance measurements were made using single prisms. In an effort to keep errors to a minimum, tripod setups were used for all backsights and foresights that were traverse points. A traditional rod was used as a prism mount for all other points. To avoid blunders, once each backsight direction was set, the backsight point was re-measured. This second measurement was inversed in the field against the original coordinates of the backsight point to ensure against measurement blunders.

Each road segment was measured using an assumed coordinate system in the field. The GPS receiver measurements provided coordinates in the UTM projection, but measuring in an assumed system allowed for more flexibility. By

using assumed coordinates, it was not necessary to wait for the final OPUS solution to be computed, and there was also a reduced risk of incorrectly entering the control points in the total station's data collector. The total station data was translated and rotated to match the GPS derived control coordinates within an office setting.

Starting with the beginning point of the road, cross sections were taken with a maximum spacing of 7.62 m. Depending on alignment and other features, such as water bars, cross section intervals were made shorter, as needed. A shorter spacing was used on horizontal curves in an attempt to provide a better definition of the curve.

At each cross section, there were three key points to collect: center line and the two points that marked the edge of the road. Edge of the road is a rather subjective term, and in this case it was defined as the edge of the rocked portion of the road, not necessarily the geometric edge of road. Additional points past the edge of road were taken as necessary to define the cross section including the ditch flow line, geometric edge of road, top of cut, and fill slope. Ideally, the toe of fill would have also been captured, but it was not practical to measure on most road segments due to a high density of trees and poor intervisibility. Each point measured was coded with a descriptor key so that it could be.

Data analysis

The data from the total station work were exported as comma delimited files and imported into AutoCAD Civil 3D 2011. Civil 3D was chosen because of

its ability to easily import survey data and handle terrain modeling. A key feature of 2011 version of Civil 3D is its ability to build point clouds from the standard file format of airborne LiDAR that are stored in the .las format.

With the field surveyed points loaded into Civil 3D, the next step was translation and rotation of the road segment to the control points. The control points were associated with the OPUS derived UTM Zone 10 coordinates, while the road segment was surveyed using an arbitrary local coordinate system. The control point with the best OPUS solution was used to fix the translation, and the inversed bearing between the two control points was used to fix the azimuth.

Once the road segment points were transformed in the UTM Zone 10 coordinates, polylines were drafted connecting the linear features of the road. These linear features included the centerline, edge of road surface, ditch flowline, and grade breaks (Figure 3.2).

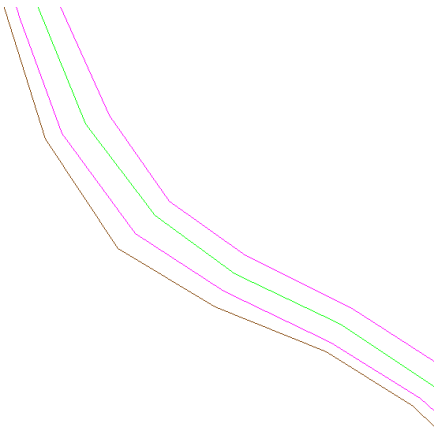

Figure 3.2: Example of centerline, edge of road, and ditch

Horizontal Alignment:

The best estimate location of the centerline of the road was established via total station survey. Moreover, determining the location of the centerline via the LiDAR data was challenging. Unlike the field survey, where points could be taken directly on the centerline, the LiDAR points occurred across the entire landscape. Two methods were explored as potential solutions to determine the road centerline using LiDAR data.

The first method was a manual method digitizing in which an operator traces a digital line over the LiDAR data where they think the road centerline is located. To determine the location of the road two approaches were taken. The first approach used the intensity image as the background data the operator digitizes upon. The second approach uses the raw point cloud data as the digitizing source.

The second method developed a MATLAB script to automatically detect a road centerline and extract it using an initial "guess" at centerline location, such as those created by the digitizing method. The centerline produced from the intensity image digitizing was used as the initial guess centerline. The method utilized an algorithm that filtered points out of a LiDAR dataset based on slope until the only points left are those on the road. The algorithm assumed that the initial centerline guess was located between the edges of the field measured road.

The user is also required to input a possible width, or a distance to either side of the initial centerline a road edge might be located. A possible width of 4

meters to either side of the initial centerline was found to provide good results after experimenting with several tolerances. The other input required from the user is a slope threshold. If the slope to a point from the initial centerline is greater than the specified threshold, the point is filtered out of the dataset. Once only the road points remain, the centerline is reconstructed as a line down the center of the filtered road points.

The workflow for the MATLAB code is as follows:

- Load LiDAR (.mat) file
- Load initial CL points and determine extents of data
- Filter LiDAR points to extents of initial CL data
- Determine CL alignment
    - Inverse between CL points
    - Create points at 90^{o} to CL points at the possible road zone, call these points “end points”
- Locate points near the initial CL points
    - Find LiDAR points that are between the endpoints and the initial CL points
    - Check found points for elevation
        - Compute acceptable elevation range from initial CL to LiDAR point based on slope threshold and distance between points.

        - If elevation of LiDAR point is inside acceptable elevation range accept point
        - Otherwise reject LiDAR point
- Reconstruct the centerline from the LiDAR points determined to be on the road
    - Find LiDAR road point closest to its corresponding end point, this should be the edge of the road
    - Inverse between corresponding road edge LiDAR points
    - Centerline is located a midpoint of the inverse
- Compare initial CL to reconstructed CL
    - Calculate difference in x, y, and total distance between points
- Plot results and save figure
- Save results as .csv file

Road Assessment:

In addition to determining the centerline location, estimating horizontal curve radii is a primary objective of road assessment. Carlson et al. (2005) suggested a variety of methods for estimating curve radii for existing roads. Sessions et al. (2010) also suggest one of the same methods for estimating curve radius known as the three point method:

$$R = \frac{C^2 + 4H^2}{8H}$$

where

R = radius

C = length of chord across curve

H= perpendicular distance from midpoint of chord to curve.

In order to determine LiDAR's ability to estimate curve radii, curve radii needed to be estimated for both the field measured centerline and a LiDAR derived centerline. The intensity based digitized centerline was used for the LiDAR based centerline because it appeared to have the best results in approximating the field centerline. Using Civil 3D the curves on both types of centerlines were measured to obtain the values for C and H resulting in the computation of R.

Vertical:

The vertical assessment was conducted in three phases. The first phase examined elevations along the centerline of the road. The purpose of the vertical analysis was to model the vertical profile of the road, which would be used to determine road grades, and could be used for vertical curve assessments. Initially, corresponding LiDAR elevations were found for field measured centerline points. Two sets of LiDAR elevations were utilized, one set from the DEM grid cells the field points fell in, and the second from the nearest LiDAR ground return in horizontal distance.

The second phase was conducted to simulate estimating road grade from LiDAR for the purposes of road assessment. In phase 1, the LiDAR elevation was determined based on the x and y coordinates of the field measured centerline. In the case of a road assessment from LiDAR there would be no field visit so the x and y coordinates of the actual centerline would be unknown. Therefore, in phase

two the x and y coordinates of the centerline were taken from the centerline digitized from the intensity images. Road grade was determined between every point along the field centerline, which had an average spacing of 7.6 m. Using GIS, the LiDAR elevations were sampled along the intensity based centerline using the same horizontal distance between points as the corresponding field measured centerline.

The third phase examined the effectiveness of aerial LiDAR to model the road surface including the ditch and cutbank. In order to do this, a terrain model was created from the field surveyed data and compared to a terrain model made from the LiDAR points. The type of terrain model chosen was a TIN surface, created through a process known as Delaunay triangulation. Delaunay triangulation connects points with triangles in such a fashion that the triangle is kept as close to equilateral as possible. Delaunay triangulation is the method built into the Civil 3D software and is a common TIN creation method and results in what is known as a constrained Delaunay triangulation (Vosselman and Klein 2010).

Building the terrain surface from the field measured points required the use of the polylines that represented the road edges, ditch flowline, and any grade breaks recorded in the field. In the model creation process, the polylines are converted to what are known as breaklines. Breaklines indicate a break in the terrain, such as the flow line of a ditch. In the TIN model this means that no triangles can cross over a breakline. The triangle edges must align with the

breaklines. The definition of appropriate breaklines greatly improves the accuracy of a surface model (Briese 2010).

With the TIN surface completed for the field measured points, a tin surface needed to be created from the LiDAR. Civil 3D has the ability to open and use the standard airborne LiDAR data format .las. Watershed Sciences, Inc. collected and delivered the LiDAR data with only ground returns, so filtering of the other returns was not necessary. The imported LiDAR points were clipped to a region that was 5 m greater than the surveyed area to ensure complete coverage. This clipped region of LiDAR points was then used to generate the LiDAR based TIN model.

A drawback to Civil 3D is its inability to easily subtract two surfaces from one another. In order to compare the two TINs created, the values of one TIN needed to be subtracted from the other to determine elevation differences. However, gridded elevation models can easily be manipulated in with GIS software. The TIN models were sampled in Civil 3D to produce gridded surface models with a cell size of 5 cm in the form of a GEOTIFF. The raster calculator, found in the spatial analyst extension in ArcGIS, easily subtracted the LiDAR based model from the field base model to produce the elevation difference between the surfaces (Figure 3.3).

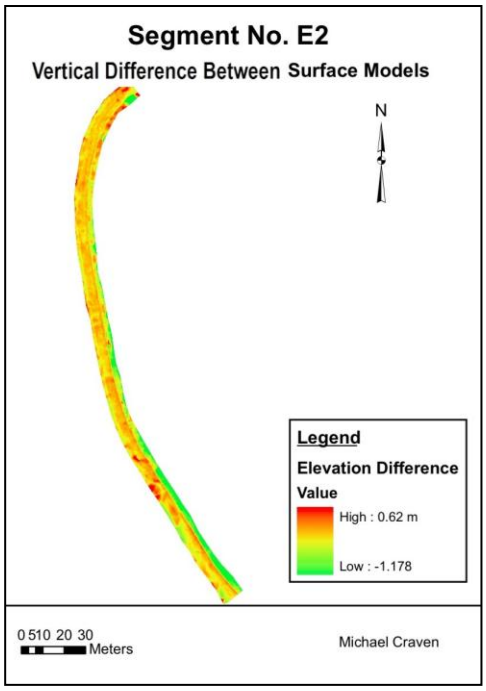

Figure 3.3: Elevation Difference Between Field Model and LiDAR model, Road Segment E2.

Results

Digitized Centerlines

The distance between corresponding points along the field centerline and digitized centerlines were computed to determine RMSE, average, and standard deviation (SD) for each strata and using intensity based centerlines (Table 3.2). The clearcut strata showed the best performance with an average horizontal error of 0.38 m, which was significantly less than the next closest strata mature (0.97 m). The strata with highest average horizontal error was evenage at 1.19 m. The RMSE results reflected the same pattern with clearcut having the best RMSE at 0.44 m with the next closest being mature (1.15 m). The clearcut also had the lowest variance (SD 0.22 m) while both evenage and unevenage had high measures of variance (SD 0.97 m, SD 0.99 m).

Table 3.2: Intensity Based Digitized Centerline Horizontal Position Results (m)

Strata	Average Horizontal Distance	Standard Dev. Horizontal Distance	RMSE Horizontal Distance
Clearcut	0.38	0.22	0.44
Evenage	1.19	0.97	1.54
Mature	0.97	0.62	1.15
Unevenage	1.00	0.99	1.40
Total	0.89	0.83	1.21

The cloud based centerline had a similar pattern of results as did the intensity based centerline (Table 3.3). The clearcut strata performed the best with a RMSE of 1.64 m, while the evenage had the largest at 3.26 m. Results clearly indicate that the intensity based centerline outperformed the cloud based centerline

in every stratum. The average horizontal RMSE across the four strata for the cloud based centerline was almost double (1.92 times greater) that of the intensity based centerline.

Table 3.3: Cloud Based Digitized Centerline Horizontal Position Results (m)

Strata	Average Horizontal Distance	Standard Dev. Horizontal Distance	RMSE Horizontal Distance
Clearcut	1.45	0.77	1.64
Evenage	2.12	2.48	3.26
Mature	1.20	0.83	1.46
Unevenage	2.13	1.30	2.50
Total	1.72	1.57	2.33

In addition to descriptive statistics for both digitized centerlines, analysis of variance statistical techniques (ANOVA) were used to test for significant differences between strata in terms of horizontal accuracy. For both the intensity and cloud based centerlines a natural log transformation was applied to better meet the distribution normality assumption of ANOVA. For the intensity based centerline there was significant evidence ($p<0.001$) of differences among the strata. The ANOVA results for the cloud based centerline also had significant evidence ($p<0.001$) of differences among the strata and the Tukey-Kramer procedure was used to compare each strata to the other strata. For both digitizing methods each strata was found to be different ($p<0.001$).

Extracted Centerline

The extracted centerline was created by filtering LiDAR points until only points that were thought to be on the road were left. The user had to specify an

initial centerline location, which in this case was the intensity digitized centerline. A search window of 4 m on either size of the initial centerline and a slope threshold of 12.5% was found to give the best results (Table 3.4).

Table 3.4: Extracted Centerline Results (m)

Strata	Average Error	Standard Deviation of Error	Average Minimum Error	Average Maximum Error	RMSE
Clearcut	0.73	0.32	0.06	1.76	0.80
Evenage	1.24	0.65	0.10	3.04	1.40
Mature	1.04	0.51	0.08	2.72	1.17
Unevenage	1.30	0.35	0.32	2.34	1.35
Total	1.08	0.46	0.14	2.47	1.34

The total RMSE for the extracted centerline (1.34 m) was lower than the point cloud digitizing (2.33 m) but larger than the intensity based digitizing (1.21 m). As was the case with intensity based digitizing the clearcut strata had the lowest RMSE at 0.80 m, with the next lowest RMSE being the mature strata (1.17 m). The variation in the extracted centerlines was much lower (0.46 m SD) than those of the intensity based (0.83 m SD) and cloud based (1.15 m SD) digitizing centerlines.

ANOVA was used to test if there was a significant difference between strata and the average error between the extracted centerline and the field measured centerline. To better meet the ANOVA assumption for normality, average errors were transformed using a natural log. There was no compelling evidence for statistically significant differences between strata ($p=0.62$).

Horizontal Curves

A total of 23 curves were measured, at least one curve from each road segment, using the field measured centerline and the intensity-based digitized centerline to produce two estimates of curve radius. The difference in radius was computed by taking the field estimated radius and subtracting the intensity based radius. If the difference was positive the intensity based curve would underestimate the field curve and if negative than visa versa.

The results of the curve radius estimations are highly variable. The greatest difference in curve radius was 6.52 m on an evenage road segment, and the smallest difference was 0.71 m also from an evenage road segment. Ten of the 23 comparisons yielded a negative result indicating near uniform distribution of under and over estimated curves using the intensity based centerline. This can also be shown by the total average difference in radius which is -0.24 m (Table 3.5), close to zero and far less than the smallest difference of 0.71 m. If the absolute difference is used to generate an average the difference in curve radius is much greater at 3.17 m. The large amount of variability can also be seen in the magnitude of the standard deviation (2.13 m).

Table 3.5: Average Difference in Estimated Curve Radius (m)

Strata	Average Difference in Radius	Average Absolute Difference In Radius	Standard Deviation of Absolute Difference in Radius
Clearcut	-2.92	4.31	2.49
Evenage	2.60	3.39	2.56
Mature	0.10	3.24	1.99
Unevenage	-1.16	1.92	1.11
Total	-0.24	3.17	2.13

The curve data were tested for statistically significant differences in radius estimates based on strata. The data were tested through an ANOVA and there was no strong statistical evidence to suggest that strata explained any of the variance in the curve estimates ($p=0.32$).

Vertical Accuracy Along the Field Identified Centerline

The initial examination of the vertical accuracy of the LiDAR data involved comparing field measured elevations along the true centerline of the road with elevations for the same horizontal position derived from the LiDAR created DEM and the nearest LiDAR point. The elevation difference between corresponding points was determined by taking the field elevation and subtracting the LiDAR elevation. The absolute difference in elevation was also calculated because the simple average would allow for compensating errors.

Across all the strata and segments the average difference in elevation was positive (0.16 m) indicating that the LiDAR elevation underestimated the elevation along the road centerlines (Table 3.6). On road segments CC1, E3, M2, and M4, the average elevation difference was negative, but the trend still suggests the LiDAR elevations were lower.

Table 3.6: Field Measured Elevation vs LiDAR DEM Elevation (m)

Strata	Average of Elevation Difference	Average of Absolute Elevation Difference	Standard Deviation of Absolute Elevation Difference	RMSE
Clearcut	0.15	0.18	0.19	0.26
Evenage	0.03	0.07	0.06	0.09
Mature	0.28	0.31	0.27	0.43
Unevenage	0.17	0.17	0.14	0.23
Total	0.16	0.19	0.21	0.28

The strata with the best performance was evenage with an RMSE of 0.09 m, while the worst performing was mature with an RMSE of 0.43 m. The variation in the elevation difference followed the same pattern, with evenage having the least variation (0.06 m SD) and mature having the most variation (0.27 m SD).

The absolute average elevation difference was used to test if there was a significant difference between the strata in regards to elevation differences. Using ANOVA, a significant difference was found ($p<0.001$), and the Tukey- Kramer procedure was used to compare each strata to each other. Each strata was found to be different from each other ($p<0.001$) except for clearcut and unevenage strata ($p=0.99$).

Nearest LiDAR point comparisons were also summarized (Table 3.7). The average distance from LiDAR point to field measured point was 0.32 m. The clearcut strata had the shortest distance (0.28 m), while the other three strata were very similar (0.31 m-0.34 m). As with the DEM elevation comparison, using the nearest LiDAR point elevation yielded the same trend in that the LiDAR elevations were lower than the field elevations on average. The road segments

CC1, E3, E4, M2, and M4 had on average LiDAR elevations that were higher than the field elevations. With the exception of E4, these road segments had the same results with the DEM based elevations.

Table 3.7: Field Measured Elevation vs. LiDAR Nearest Point Elevation (m)

Strata	Average of Elevation Difference	Average of Absolute Elevation Difference	Standard Deviation of Absolute Elevation Difference	RMSE	Average Distance to Nearest LiDAR Point
Clearcut	0.15	0.17	0.22	0.27	0.28
Evenage	0.00	0.07	0.06	0.09	0.34
Mature	0.26	0.30	0.25	0.39	0.34
Unevenage	0.16	0.16	0.15	0.22	0.31
Total	0.14	0.17	0.20	0.27	0.32

As shown with the DEM based elevations, the evenage strata had the lowest RMSE at 0.09 m and mature had the highest RMSE at 0.39 m. Unevenage had a lower RMSE (0.2 2m) than clearcut (0.27 m), however, clearcut had more variation (0.22 m SD) than did unevenage (0.15 m SD). Evenage had a much smaller amount of variance (0.06 m) than the other strata.

The absolute average elevation difference was used to test if there was a significant difference between the strata in regards to elevation differences. Using ANOVA a significant difference was found ($p<0.001$), and the Tukey- Kramer procedure was used to compare each strata to each other. Each strata was found to be different from each other ($p<0.001$) except for the clearcut and unevenage strata ($p=0.96$).

Road Grade from Field Centerline and Intensity Digitized Centerline

Slope was determined between points measured in the field along road centerlines, and served as a measure of the best estimate of road. Using the best performing LiDAR derived centerline location (digitized from intensity images) slope was calculated using LiDAR DEM elevations corresponding to the same horizontal interval in the field measured data. The average horizontal distance used to calculate slope was 7.52 m (Table 3.8). The clearcut strata had the best performance with the lowest average difference between slope measured in the field and LiDAR based slope estimates (0.42 %). The evenage strata had the worst performance with an average difference in slope being 0.76 %. Across all the strata the average difference in slope estimates was 0.57 %.

Table 3.8: Field Centerline Slope vs Intensity Digitized Centerline Slope

Strata	Average Absolute Difference In Slope	Single Maximum Difference in Slope
Clearcut	0.42 %	0.83 %
Evenage	0.76 %	9.20 %
Mature	0.51 %	3.95 %
Unevenage	0.48 %	0.42 %
Total	0.57 %	3.60 % (Ave)

The maximum difference between the field measured slope and LiDAR DEM based slope for a single slope estimate yielded interesting results. Clearcut and unevenage strata had a low maximum difference at 0.83 % and 0.42 %, respectively. The evenage strata had a maximum difference in slope of 9.20 %. This large difference in slope estimates came from road segment E3. This segment

had very poor maintenance, and had a small slope failure running across and down the road segment. The field measured slope was 25.87 % through the failure while the LiDAR DEM based slope was 16.67 %, indicating the LiDAR DEM did not have enough resolution with the forest canopy blocking ground returns to adequately define the slope failure.

ANOVA was used to test if there was any significant difference between strata in regards to the slope estimation. The results indicated no statistical difference between strata ($p=0.46$).

TIN Modeling of Road Surface

Using the LiDAR data to model the road area had mixed results. From a visual inspection, the road wearing surface appeared to be at a similar elevation in both the field based TIN model and the LiDAR based TIN. Certainly at the same order of magnitude as the accuracy estimations from the point analysis. The cut bank, ditch, and fill slope areas tended to have relatively large amounts of error in both the positive and negative direction. This means that the LiDAR TIN model was both lower and higher in elevation than the field based model in the cut bank, ditch, and fill slope regions (Table 3.9).

Table 3.9: TIN Modeling Results by Strata (m)

Strata	Average of Min. Elev. Difference	Average of Max. Elev. Difference	Average of Mean Elev. Difference	Average of Absolute Mean Elev. Difference
Clearcut	-0.92	0.75	0.13	0.14
Evenage	-1.26	0.64	-0.04	0.05
Mature	-0.91	1.28	0.28	0.37
Unevenage	-0.61	0.96	0.08	0.08
Total	-0.93	0.90	0.11	0.16

On average, a segment had a section of the model 0.93 m below the field model and 0.94 m above. The worst cases occurred on road segments that had large cut banks (3 m +), with values of 1.5 m below the field surface and 2.44 m above the field surface.

Discussion

Horizontal

The results of the digitized centerlines were not surprising. With both the intensity and cloud based centerlines the clearcut group had the best performance, which makes sense because the clearcut should have the least interference from the canopy. The opposite case was that of the evenage strata where canopy density over the road was typically the greatest. This made it more difficult on the operator to determine the road location in both the intensity image and point cloud. The difference between strata was found to be statistically significant (p-value <0.001).

The intensity based centerline outperformed the cloud based centerline by almost double. Digitizing is highly dependent on the operator, and different operators may have different results. As was shown with this data, the 0.5 m intensity image provided a better picture of where the road was located than the point cloud. The point cloud when made up of just ground returns has many gaps in it where canopy has blocked the laser pulse and does not have the continuous coverage found in the intensity image.

The horizontal accuracy of the intensity centerline (RMSE 1.21 m) is close to the horizontal RMSE reported by Renslow et al. (2000) and Hyyppä et al. (2000) of 0.90 m and 0.98 m, respectively. An issue with road centerlines is that they are subjective, and not as easily definable as say the corner of a roof in the LiDAR data. Because of this, the horizontal accuracy estimate reported here is an estimate of the horizontal error in the LiDAR and the error in the digitizing.

The extracted centerlines had an RMSE (1.34 m) that was close to that of the best performing intensity digitized centerline (1.21 m). The method for extracting the centerlines was not very complicated or difficult to code, and yet provided good results with less variation (0.46 m SD) compared to the intensity digitized centerline (0.83 m SD). A more sophisticated method could be developed that uses slope. However, there are many other ways in which to approach the problem of having a computer extract a centerline. One such method maybe to use image processing and have the computer detect and classify the road location based on a hillshade of the DEM, or from the intensity data. An example of a detection algorithm is presented by Arbelaez et al. (2011).

Computer extracted centerlines would be prove to be useful for land managers who have large road networks. A more sophisticated method could reduce the number of inputs required by the user. Over a large road network, the extracted centerlines would be more efficient to obtain than the effort required to manually digitize the road centerline.

The results of curve radius measurements from the LiDAR derived centerline were highly variable. The average absolute difference was 3.17 m between the two radius estimates. Carlson et al. (2005) found that for highways in Texas, the chord method of estimating curve radii was found to have errors up to 5% of the true value. For this study the average difference was 7%.

The definition of the curve plays a large role in the ability to measure the chord and perpendicular distance in the three point method. Since the LiDAR based measures came from digitized points the operator needs to pay careful attention with digitizing curves, and make sure to tighten the spacing between digitized points to ensure a good definition of the curve. The same goes for the field measurements. As was done in this study, the points collected along the true centerline were taken at shorter intervals when traversing a corner to provide a better definition.

A potential issue with existing forest roads, especially spur roads, is that the road may never have been designed with curves having a specific radius. Trying to model a curve that has no design with a simple circular curve (as was done in this study) will naturally have errors associated with it. With no construction plans or as-built drawings, it is unclear if the curves in this study were designed with a specific radius or not.

Vertical

Using the field location for the centerline, centerline elevation errors were slightly lower if using the nearest LiDAR point (0.27 m) than if using the LiDAR

based DEM (0.28 m) for elevation values. With such a small difference using either elevation source would probably have little effect on determining road grade. This may not be true depending on the resolution of the DEM and the size of the road. In this study the DEM was at a 1m resolution, and the road widths ranged from 4-7m. If the DEM resolution is such that a grid cell overlaps the road surface and includes portions of the side slopes of the road, the grid cell value would probably not represent the elevation of the road surface very well.

Both RMSE values for the nearest LiDAR point (0.27 m) and DEM (0.28 m) elevations were of similar magnitude to Hodgson and Bresnahan (2004) (0.26 m) and Hodgson et al. (2005) (0.28 m). Elevation differences between strata were found to be significant ($p<0.001$) for both the nearest LiDAR point and DEM elevations, except for unevenage compared to clearcut.

It was surprising that for both elevation sources, DEM and nearest point, the evenage strata had the lowest RMSE at 0.09 m for both elevation sources.. One of the reasons for this may be factors that were not considered in the design of the study. With the exception of segment E3, the evenage road segments were located on well maintained mainline roads. This was the result of a random sample, and not the intention of the study. These segments were well brushed and had right of ways clear of trees and other obstructions. They also had well graded and rocked surfaces. Many of the road segments in the other strata were not as well maintained and had grass and other small vegetation growing in the center of the road surface. With the exception of segment E2, the evenage strata did not have

road segments with large cut banks such as those in the mature strata or on segment CC2.

The results from the road grade analysis showed that using a LiDAR derived centerline and elevation values to calculate slope resulted in an average difference of 0.57 % to the field measured road slope for horizontal distances of 7.52 m. A standard tool for measuring existing road slope, as opposed to a total station, is a clinometer (Sessions et al. 2010). A clinometer can only be read to the nearest percent (Suunto 2008) and commonly it is believed that a clinometer is only accurate to within 2 %. The LiDAR derived road slopes are within the accuracy of a clinometer, lending credence to using airborne LiDAR to perform road grade assessments.

Finally, the TIN model analysis of the road surface and surrounding area indicated that airborne LiDAR did not capture the locations of steep side slopes or ditches very well. This can be seen with a visual inspection of the results for each road segment (Figure 3.3). This can also be shown with the average minimum error (-0.93 m) and average maximum error (0.90 m). These large differences are due to a number of factors including: steep cut banks, vegetation growing on side slopes, and the inability to add breaklines to LiDAR data.

The majority of the TIN model was road surface, which LiDAR appeared to model well and the effect can be seen in the average elevation difference across the model. The average absolute elevation difference from the TIN modeling was

0.16 m, which is very comparable to the analysis of the centerline elevations based on the nearest LiDAR point (0.17 m) and LiDAR based DEM (0.19 m).

Conclusion

The increasing interest of hauling products that do not fit on standard stinger-steered log trucks has lead to a demand for conducting road assessments to determine if other vehicles such as chip vans can access the road network. Being able to measure the road network to sufficient precision and accuracy using a remote sensing technique such as LiDAR would be an efficient alternative to measuring the road network in the field.

We examined the accuracy of airborne LiDAR for the purposes of measuring existing forest roads across four stand structures. A variety of methods were used to determine a road's centerline in the LiDAR data, and it was found that manually digitizing the centerline based on intensity images provided the lowest RMSE of 1.21 m. A simple computer algorithm was developed and used to extract the road centerline based on slopes and had an RMSE of 1.34 m. A more sophisticated algorithm would most likely obtain an RMSE equal or better to the digitizing method, and would be a much more efficient method for analyzing large road networks. Estimating horizontal curve radius was also examined and the average absolute difference in field versus LiDAR measurements was 3.17 m. On larger curves a difference of 3 m may not present an issue, but on a curve that maybe limiting to a vehicle 3 m could prove to be critical. Airborne LiDAR would

be a good method to evaluate all the curves on a road network, and highlight curves that are near limiting and need a field inspection.

Vertical accuracies were also assessed along the true centerline of the roads using a LiDAR derived DEM, and the nearest LiDAR point elevations. The RMSE for the DEM was 0.28 m and 0.32 m using the nearest LiDAR point elevations. For the purposes of road assessment typically road grade is the critical vertical measure. In order to emulate a situation where the actual centerline of the road is unknown the intensity digitized centerline was used to calculate road grade. When compared to field measured road grade the difference was 0.6 %. This is within the precision of a clinometer, the standard tool used to measure road grades in a forestry setting. The TIN modeling showed that the airborne LiDAR does not adequately delineate ditches or cut banks with maximum average errors of up to 0.93 m in these areas.

Overall, airborne LiDAR would be an appropriate tool to use for road assessment. Airborne LiDAR's performance on estimating road grade was slightly better than typical field methods used in road assessments and should be sufficient to calculate road grades for assessment. Some caution should be used in measuring horizontal curves with airborne LiDAR. Curves that are limiting or near limiting according to the LiDAR data should be further investigated in the field.

References

Arbelaez, P., M. Maire, C. Fowlkes, and J. Malik. 2011. Contour Detection and Hierarchical Image Segmentation. *IEEE TPAMI* 33(5): 898-916.

B.C. Ministry of Forests. 2002. Road Layout and Design. P. 3-36 in *Forest Road Engineering Guidebook*, For. Prac. Br., B.C. Min. For., Victoria, B.C. Forest Practices Code of British Columbia Guidebook.

Briese, C.. 2010 Extraction of Digital Terrain Models. P. 135-167 in *Airborne and Terrestrial Laser Scanning*, Vosselman, G., and H-G., Mass (eds.). Whittles Publishing, Dunbeath, Scotland, UK.

Carlson, P., M. Burris, K. Black, and E. Rose. 2005. Comparison of Radius-Estimating Techniques for Horizontal Curves. *Transportation Research Record: Journal of the Transportation Research Board*. 1918: 76-83.

Hodgson M., P., Bresnahan. 2004. Accuracy of Airborne Lidar-Derived Elevation: Empirical Assessment and Error Budget. *Photogrammetric Engineering and Remote Sensing* 70(3): 331-339.

Hodgson, M., J., Jensen, G., Raber, J., Tullis, B., Davis, G., Thompson,and K., Schuckman. 2005. An Evaluation of Lidar-derived Elevation and Terrain Slope in Leaf-off Conditions. *Photogrammetric Engineering & Remote Sensing* 71 (7): 817-823.

Hyyppä, J., U., Pyysalo, H., Hyyppä, and A. Samberg. 2000. Elevation Accuracy of Laser Scanning-Derived Digital Terrain and Target Models in Forest Environment. P. 139-147 in Proceedings of EARsEL-SIG Workshop LIDAR. Dresden Germany.

Kiser, J. 1991. *Photogrammetric Uses of a New-generation Analytical Stereoplotter in Forestry*. M.Sc. thesis, Oregon State University, Corvallis, OR. 156 p.

Kramer, B. 2001. *Forest Road Contracting, Construction, and Maintenance for Small Forest Woodland Owners*. Research Contribution 35, Forest Research Laboratory, Oregon State University, Corvallis, OR. 79 p.

Paine, D. and J., Kiser. 2003. Environmental Monitoring. P. 378-393 in *Aerial Photography and Image Interpretation*. John Wiley and Sons, Hoboken, NJ.

Renslow, M., P. Greenfield, T. Guay. 2000. *Evaluation of multi-return LiDAR for forestry applications*. USDA Forest Service - Engineering, Remote Sensing Applications Center RSAC-2060/4180-RPT1. 17 p.

Reutebuch, S., R. McGaughey, H. Andersen, and W. Carson. 2003. Accuracy of high-resolution lidar terrain model under a conifer forest canopy. *Can. J. Remote Sensing*. 29(5):527-535.

Sessions, J., J. Wimer, F., Costales, and M., Wing. 2010. Engineering Considerations in Road Assessment for Biomass Operations in Steep Terrain. *West. J. Appl. For*. 25(3): 144-153.

Sessions, J., J. Wimer, and K., Boston. 2009. Increasing Value and Reducing Costs through Hauling Longer Logs: Opportunities and Issues. *West. J. Appl. For.* 23(3): 157-162.

Sessions, J. 2007. Trucks. P. 161-188 in *Logging Mechanics Class Notes*. Department of Forest Engineering, Oregon State University, Corvallis, OR.

Suunto. 2008. Optical Height Meter. P. 4 in *Sunnto PM-5 USER'S GUIDE.* Suunto Oy, Valimotie, Finland.

Vosselman, G., and R. Klein. 2010 Visualisation and Structuring of Point Clouds. P. 45-81 in *Airborne and Terrestrial Laser Scanning*, Vosselman, G., and H-G., Mass (eds.). Whittles Publishing, Dunbeath, Scotland, UK.

Wolf, P.R., B.A., Dewitt. 2000. Introduction to Analytical Photogrammetry. P. 233-259 in *Elements of Photogrammetry*, Munson, E (eds.). McGraw-Hill, Boston, MA.

CHAPTER 4: LiDAR- DERIVED DEM AND RAW HEIGHT COMPARISONS ALONG PROFILE CORRIDOR GRADIENTS WITHIN A FOREST

Michael Craven, Michael Wing, John Sessions, and Jeff Wimer

Department of Forest Engineering, Resources and Management

Oregon State University

Corvallis, OR 97331

Introduction

Profile corridors are linear transects or pathways along which terrain gradients and elevations are measured. Profile corridor measurements involve collecting elevation measurements at discrete points along a linear transect. Relating to forest engineering, profile corridor measurements are typically collected to support cable logging operations but might also be collected to support various design projects including road and trail construction, fish passage creation, and stream channel restoration.

Profile elevation measurements can be collected using several different techniques and a variety of field and remotely based measurement tools are available for profile corridor measurements. Profile corridor measurement techniques vary in cost, efficiency, and accuracy. Elevation data can be collected directly either through the use of differential leveling equipment or through a global positioning system (GPS) receiver. Elevation can also be measured indirectly using analog vertical angle measurement equipment, such as an abney or clinometer, and tape measures to record distances between points. Trigonometry is then applied to calculate elevations. Typically for cable logging profiles measurements are made using a string-box or tape measure for distance and a clinometer for slope (Solmie et al. 2003).

We collected profile corridor measurements using rigorous field based techniques across a forested landscape that had also been measured using airborne LiDAR scanning. We compared field based and LiDAR derived profile corridor

measurements across a range of different forest canopy types and terrain. Our primary objectives were to examine whether varying canopy cover and ground slope influenced LiDAR derived profile corridor measurements. We examined both LiDAR-derived digital elevation model (DEM) and point elevation models in our comparisons. A secondary objective included conducting a cable logging payload analysis using field measured profile elevations and comparing the results to the same analysis using LiDAR derived profile elevations.

Methods

LiDAR Data Set:

The LiDAR dataset used in this study was flown by Watershed Sciences, Inc. of Corvallis, OR. The data was collected in April of 2008, which was still in the "leaf-off" period for that year. The laser scanner used was a Lecia ALS 50, which is capable of recording four returns per laser pulse, and produces a native density of eight plus points per square meter. Actual results were 10 points/m^2, and 1.12 ground return points/m^2 (Watershed Sciences 2008). Raw point returns were provided as well as a one meter digital elevation model (DEM) produced by Watershed Sciences.

Site Determination:

We included six sites in McDonald-Dunn Research Forest (western Oregon, USA) for our study. Each site needed to contain enough area for four profile corridors. Other initial criteria for site selection included that both forested sites and a measurement control site free of overhead canopy during the LiDAR

flight be included. Criteria for forested site selection included that a range of stand characteristics representing trees per ha, basal area, and conifer/hardwood forest be represented across the sites, and that sites should not include any standing timber that had been harvested in a 20 year period previous to the LiDAR flight. We also strove, however, to find areas that had been thinned or harvested since the LiDAR flight, with minimal ground disturbance, in order to improve field data collection operations (Table 4.1).

Table 4.1: Study Site Stand Characteristics

Profile sites	Mean slope %	Trees / ha	BA / ha	Avg. DBH (m)	Dominant tree species/cover	Description
Meadow	27	-	-	-	Grasses 0.3 m tall	Uniform slope
Clearcut	43	-	-	-	Some logging debris	Uniform slope
Low density forest	49	294	339	0.28	Douglas-fir (*Pseudotsuga menziesii*)	Undulating slope
Medium density forest	37	331	381	0.31	Douglas-fir (*Pseudotsuga menziesii*)	Uniform slope
High density forest	35	509	450	0.29	Douglas-fir (*Pseudotsuga menziesii*)	Undulating slope
Mixed forest	46	257 (hardwood) 356 (conifer)			Bigleaf Maple (*Acer macrophyllum*)	Uniform slope

In terms of a measurement control site, we initially included an area that had been clearcut before the LiDAR flight but became concerned upon visiting the site that on-the-ground harvesting residue present during the LiDAR flight might

bias ground elevations from the LiDAR. We retained the clearcut site but also included an open meadow site as measurement control.

At all forest sites, including the clearcut site, another criterion was that ground slopes exceed 35% on average. This slope threshold is often associated with forested areas that require cable logging versus a ground based system. We relaxed this slope requirement for the meadow site as no other open areas were available in the research forest that met all other criteria.

Field Procedures:

We measured elevation at points located along four profile lines at each study site. Points were taken along each profile at changes in the ground slope. If there was no appreciable change in ground slope, we attempted to maintain a maximum spacing between points of approximately 7.5 m. Average point spacing across all profiles was below 7.5 m, but due to field conditions some profiles had average spacing greater than 7.5 m.

Depending on whether the selected site had canopy or no canopy at the time of the field surveying dictated the field approach. The meadow, of course, had no canopy and the mixed forest and low density stands were clearcut harvested so they had no canopy as well. These three sites were surveyed with Real Time Kinematic (RTK) GPS as discussed in Chapter 2. A control point was set at each site and a static four hour or longer observation was conducted. The resulting data was then processed into a control point using the National Geodetic Survey's

Online Positioning User Service (OPUS). Using the control point as the base station for the RTK setup, four profiles were measured in each of the three sites.

Extra points were taken along each profile to provide some measure of the precision of the RTK measured points. Approximately every fifth point was staked and measured with the initial pass along the profile. After some time had passed, at least 15 minutes, which allowed the satellite constellation to move, the staked points were revisited and measured a second time. The difference in horizontal distance and elevation values were calculated for each pair of points (Table 4.2).

Table 4.2: Summary of RTK GPS re-measured points (m)

Stand	Mean Difference (Horizontal)	Mean Difference (Vertical)	Max Difference (Horizontal)	Max Difference (Vertical)
Mixed Forest	0.019	0.026	0.033	0.090
Low Density	0.038	0.033	0.158	0.083
Clearcut	0.055	0.049	0.124	0.233
Meadow	0.021	0.015	0.071	0.040

The medium and high density stands were thinned since the LiDAR was flown, and both had too much canopy coverage to make RTK GPS practical. Instead these sites were measured with total stations. Control still had to be located at each site, so the nearest canopy opening that would provide a GPS solution was located. Two control points are required when using a total station, one point is used to control the X,Y,Z coordinates, while the second point controls the orientation of the total station. The control point used to control the X,Y,Z coordinate values was measured with a four hour plus static GPS observation processed with OPUS. The second control point was set using three minute RTK

observation using the OPUS processed control point as the base station location. The second control point was used to establish the angular orientation of the total stations. For both sites two total station setups were required to traverse from the control location to the designated profile site.

To reduce potential errors in the total station work each backsight was taken using a tripod/tribrach setup. By using the tripod potential errors from a un-plumb rod could be avoided. As a check, once each backsight was completed and the total station coordinate system established, the backsight point was re-measured. The original backsight point and the re-measured point were inversed in the field to ensure that a blunder had not been made. Once measurement of the profiles began the measurement of the profile points were kept to a straight line as much as possible by locking the azimuth on the total stations, and using preset stakeout points to control the azimuth on the RTK GPS.

The LiDAR data used in this study (discussed in Chapter 2) was flown by Watershed Sciences, Inc, of Corvallis, Oregon was provided in Universal Transverse Mercator (UTM) coordinates using the NAD 83 (CORS96) datum. The OPUS solutions on the control points were also available in the same UTM coordinates and datum, so all field points were collected in the same projection and datum as the LiDAR.

Data Analysis:

The LiDAR data provided two different elevation sources: a 1-meter gridded DEM and raw ground point elevations. A separate comparison was made for each elevation source. First, for each profile point elevation that was surveyed in the field, we subtracted the LiDAR DEM value that was associated with the same location. Second, we also subtracted the nearest LiDAR point elevation from each profile point elevation. These calculations were performed with a geographic information system (GIS). We also investigated whether ground slopes influenced differences between field measured and LiDAR-derived elevations. The ground slope associated with each profile point was calculated by taking the average of the percent slope as indicated by field measurements to the next uphill and next downhill points. In the case of the initial profile point, we only used the next downhill point slope; for the final corridor point, only the next uphill point slope was used.

We relied upon root mean square errors and average errors between the field surveyed and LiDAR elevations for descriptive statistical comparisons. For statistical analysis, we used the absolute value of elevation differences in order to avoid compensating errors from using average differences. Statistical analyses included analysis of variance (ANOVA) and Tukey multiple range tests. We used a base 10 logarithmic transformation of the absolute errors so that data distributions approximated normality and supported parametric statistics.

We also conducted a third comparison that considered a cable logging payload analysis based on field measured profile elevations and differences that resulted by using LiDAR-derived elevations for the same profiles. The primary reason for creating profile corridors is to determine the limiting payload for a cable logging operation. Our comparison considered the differences among payloads associated with the three data sources. The steepest profile was selected from each of the six sites for payload analysis. Three versions of the each profile were analyzed and included field measured elevations, LiDAR DEM elevations, and nearest LiDAR point elevations. The analysis software used was Skyline XL which enables payload analysis within an Excel spreadsheet interface. Skyline XL is produced by the US Forest Service and is freely available (USFS 2010). To provide a more rigorous approach the limiting payloads were computed using the phase II analysis option in Skyline XL, which also accounts for line stretch in the payload analysis (Figure 4.1).

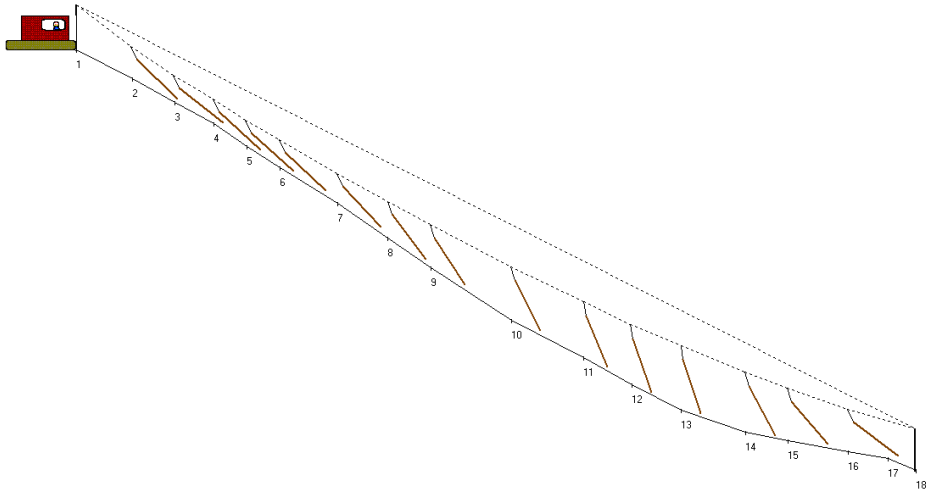

Figure 4.1: Skyline Analysis Graphic for Clearcut Profile No. 1

Each profile was analyzed using the same parameters so that relative comparisons could be made. Key parameters included the cable system, yarder and carriage combination, rigging heights, and log sizes and clearances (Table 4.3). While most profiles allowed a 9.14 m (30 ft) tailspar, the medium and high density forest profiles both required a tailspar height of 15.24 m (50 ft) to support a payload. One might consider a multi-span setup instead of a taller tailspar under actual conditions, but our common parameter set enables comparisons between the three data sources. The choice of a Koller 501 yarder was purposeful because a smaller yarder (10.06 m) accentuates the differences in payload capacity compared to a taller yarder.

Table 4.3: Payload Analysis Variables

Parameter	Value
Cable system	Standing
Yarder	Koller 501
Tower height	10.1 m
Carriage	Acme 10
Carriage weight	454 kg
Tailspar height (standard)	9.1 m
Tailspar height (medium/high density sites)	15.2 m
Log length	12.9 m
Log diameter	0.31 m
Front end log clearance	1.2 m

Results

We measured the elevations of 505 profile points covering 3,524 m of profile corridors at the six study sites. The smallest number of profile points was

collected at the medium forest density site (39) while the largest number was collected at the high density forest site (158). Overall, there was an average of 7.33 m that separated profile point locations within the corridors. The lowest average point separation occurred in the medium density forest site (6.15 m) while the highest was in the hardwood site (9.04 m).

Field Measured Profile and DEM Elevations

We subtracted LiDAR DEM values from the profile point elevations to determine RMSE, average, and standard deviation (SD) of elevation differences (Table 4.4). The meadow site had the lowest overall average elevation RMSE (0.38 m) and the clearcut site had the highest (0.50 m). The four forested sites had average RMSE values that ranged from 0.41 to 0.46 m. The overall average elevation differences for DEM values were negative for all study sites with a combined average of -0.09 m (SD 0.22). This indicates that LiDAR DEMs tend to overestimate actual heights. We found that there were statistically significant differences between the profile point and DEM elevation differences among the six study sites ($p = 0.03$). The medium forest density site had the lowest average elevation error (-0.02 m, 0.21 SD) and the clearcut site had the highest (-0.22 m, 0.19 SD).

Table 4.4: Field Profile and DEM Elevation Results

Site	Average Elev. Difference	Average Absolute Elev. Difference	RMSE Absolute Elev. Difference
Meadow Total	-0.09	0.14	0.38
Clearcut Total	-0.22	0.25	0.50
Low Density Total	-0.11	0.21	0.46
Medium Density Total	-0.02	0.17	0.41
High Density Total	-0.04	0.18	0.43
Mixed forest	-0.14	0.20	0.45
Grand Total	-0.09	0.19	0.43

A Tukey multiple range test determined that these were the only two study sites that were statistically different from one another. Two other study sites, however, had individual corridors with positive elevation differences. This included corridors 3 (0.03 m) and 4 (0.02 m) on the medium density forest site and corridor 3 on the high density forest site (0.03 m).

We also tested whether field measured ground slopes were related to profile point and DEM elevation differences, and found no statistically significant association ($p = 0.21$).

Field Measured Profile and Nearest LiDAR Point Elevations

We compared the elevation of each profile point to the nearest LiDAR point by subtracting LiDAR point elevations. Overall, the nearest LiDAR point was located an average of 0.62 m from the nearest profile point (Table 4.5). Average distances were smallest for the meadow (0.32 m) and clearcut (0.33 m) sites. Average separation distance was relatively consistent for the forested sites and ranged from 0.68 m for the mixed forest site to 0.75 m for the medium and

high density forested sites. We used regression to test the influence of profile point and nearest LiDAR point separation difference and found no statistically significant differences ($p = 0.98$).

Table 4.5: Field Profile and Nearest LiDAR Point Elevations

Site	Average Difference In Elev.	Average Absolute Elev. Difference	RMSE Absolute Z Difference
Meadow Total	-0.11	0.12	0.35
Clearcut Total	-0.23	0.24	0.49
Low Density Total	0.01	0.32	0.57
Medium Density Total	-0.13	0.28	0.53
High Density Total	-0.01	0.23	0.48
Mixed forest	0.07	0.28	0.53
Grand Total	-0.07	0.24	0.49

Average elevation RMSE for nearest LiDAR point was 0.49 m across all study sites. Nearest LiDAR elevation comparisons were lowest for the meadow site (0.35 m) and highest for the low density forest site (0.57 m). The other three forest categories had RMSE that ranged between 0.48 m (high density forest) and 0.53 m (medium density forest and mixed forest). The clearcut site had a RMSE of 0.49 m.

Average elevation differences for the nearest LiDAR point were -0.07 m across all six study sites but included considerable variation (0.33 SD) and two sites with average differences that were not negative (low density forest (0.01 m) and mixed forest (0.07 m)). Among the 24 individual corridors, there were six corridors at three sites that had positive average elevation differences. The overall trend, however, suggests that LiDAR elevations overestimate actual heights.

We found statistically significant differences in the average elevation differences between profile point and LiDAR point elevations ($p < 0.01$). Tukey multiple range tests determined that the meadow site was different from the clearcut, medium density, and mixed forest sites. The lowest average elevation difference was determined at the low forest density (0.01 m) and high forest density (-0.01 m) sites. The maximum elevation average elevation difference was measured at the clearcut site (-0.23 m).

Field measured ground slopes were determined to be related to average elevation differences between profile point and LiDAR point elevations ($p < 0.01$) but the correlation was nonexistent ($r^2 = 0.01$).

Profile Analysis

For each profile the critical terrain point or the point that caused the limiting payload occurred at the same distance from the yarder regardless of the elevation values used. This result is expected because the elevation difference at any given point between the three profiles is not more than a couple of meters, resulting in the same general geometry for each profile.

Using the field measured profiles as a baseline the percent difference in limiting payload was calculated for the DEM elevation and nearest point elevation based profiles. On average the DEM based profiles under estimated the limiting payload by 6%, with a range of 39% below to 18% over estimation. The nearest point based profiles performed worse with an average over estimation of 11% and a range of 20% below to 39% above.

Discussion

We found that average RMSE elevation errors were slightly lower for profile point to LiDAR DEM values (0.43 m) as contrasted to profile point to nearest LiDAR elevation point (0.49 m) comparisons across our six study sites. The elevation differences between these two methods of extracting elevations from LiDAR are relatively small and likely have little influence on applications such as terrain and hydrologic modeling. The elevation differences become more pronounced however when the four forested sites are considered and the meadow and clearcut sites are not. Average RMSE values for the four forested sites were 0.43 m for the LiDAR DEM and 0.53 m for the nearest LiDAR point.

One possible explanation for the lower LiDAR DEM errors when contrasted to nearest LiDAR point elevation errors could be the distance that separated field-collected profile points from the nearest LiDAR elevation. The average separation distance was 0.62 m but some differences in individual corridors reached nearly a meter. LiDAR DEMs represent an interpolated surface that is based on an averaged elevation created from a neighborhood of raw LiDAR points. The interpolated surface may represent a better fit then the nearest point due to the terrain elevation averaging, particularly as the distance to the nearest point increases.

Our overall RMSE results for LiDAR DEM values (0.43 m) as compared to nearest LiDAR elevation point (0.49 m) are lower than those reported by one previous study that focused on DEM elevation comparisons (Su and Bork 2006).

However, our errors were higher than those reported by several earlier studies that utilized LiDAR-derived DEM elevations (Gomes-Pereira and Janssen 1999, Hodgson and Bresnahan 2004, Hodgson et al. 2005). There are doubtlessly site factors that influence the differences. For instance, our average slope gradients (38%) exceeded those reported by several of the studies (Hodgson and Bresnahan 2004, Hodgson et al. 2005, Su and Bork 2006). We note that while Hodgson and Bresnahan 2004 considered 47% slopes, results were based on scaling the results from lower slope values. It is also unlikely that forested sites were very similar in structure between any two studies. In addition, seasonality and LiDAR technology (hardware and software) also influence study results.

RMSE values have been typically used by previous LiDAR elevation studies but at times average errors have been the focal statistic. Our overall average errors for LiDAR DEM values (-0.09 m) and nearest LiDAR elevation points (-0.07 m) were lower than the overall average (0.22 m) reported by a previous study (Reutebuch et al. 2003). The site slopes in our study, however, were greater than those reported by Reutebuch et al. 2003. Given the advances in scanner technology that have occurred since this earlier study, we would anticipate reduced errors. In addition, the density of LiDAR pulses was enhanced in our study (10 points per m^2) in comparison to the earlier study (4 points per m^2).

Some previous studies determined an association between steeper slopes and increased errors in LiDAR elevations (Kraus and Pfeifer 1998, Gomes-Pereira and Janssen 1999, Hodgson and Bresnahan 2004, Su and Bork 2006) while other

studies have either not found a correlation (Reutebuch et al. 2003) or determined an inconsistent relationship depending on study site. Hodgson et al. (2005) found that only the low grass land cover category exhibited increasing slope errors as terrain slope increased.

We found no statistically significant association of field measured ground slopes to profile point and DEM elevation differences ($p = 0.21$). We did, however, discover that field measured ground slopes were significantly related to average elevation differences between profile point and LiDAR point elevations ($p < 0.01$) but the correlation was relatively weak ($r^2 = 0.01$). Given these results, it appears that greater slopes may have at times a small influence on LiDAR accuracies but the influence is likely negligible within the study sites in our study. This finding may be a result of the way in which we determined ground slopes at our field sites. Ground slopes were determined based on the average slope between each profile point and its upslope and downslope neighboring profile points.

Payload analysis is at times an inexact process, as a large number of variables can affect results. We held most of the variables in our analysis constant with the exception of the tailspar height. Our payload analysis considered where the limiting payload occurred relative to the yarder and results were consistent among all study sites. The DEM-based profile appeared to outperform the nearest point profile by 5% on average and appears to be the preferred LiDAR elevation source for payload analysis.

Conclusion

Our results suggest that forest analysts should consider using the nearest LiDAR DEM value rather than the nearest LiDAR point elevation for terrain heights at discrete locations, particularly when forest canopy occludes locations of interest. We base this recommendation on the slightly improved performance of the LiDAR DEM over the nearest LiDAR point profile elevation comparisons, and note that further performance increases when only forested sites were concerned. We also observed an improved performance of the LiDAR DEM in our payload analysis.

In addition, with DEMs being readily accessed in GIS packages it is typically easier for an analyst to access and manipulate a LiDAR DEM-derived profile rather than trying to draw values from the nearest point elevations. This circumstance lends more incentive to use LiDAR DEMs as a source of elevation data for profile analysis.

References

Gomes Pereira, L.M., and L.L.F. Janssen. 1999. Suitability of laser data for DTM generation: a case study in the context of road planning and design. *ISPRS Journal of Photogrammetry & Remote Sensing*. 54(1999):244-253.

Hodgson M., P., Bresnahan. 2004. Accuracy of Airborne Lidar-Derived Elevation: Empirical Assessment and Error Budget. *Photogrammetric Engineering & Remote Sensing and Remote Sensing* 70(3): 331-339.

Hodgson, M., J., Jensen, G., Raber, J., Tullis, B., Davis, G., Thompson,and K., Schuckman. 2005. An Evaluation of Lidar-derived Elevation and Terrain Slope in Leaf-off Conditions. *Photogrammetric Engineering & Remote Sensing* 71 (7): 817-823.

Kraus, K., and N. Pfeifer. 1998. Determination of terrain models in wooded areas with airborne laser scanner data. *ISPRS Journal of Photogrammetry & Remote Sensing.* 53 (1998): 193-203.

Reutebuch, S., R. McGaughey, H. Andersen, and W. Carson. 2003. Accuracy of high-resolution lidar terrain model under a conifer forest canopy. *Can. J. Remote Sensing*. 29(5):527-535.

Solmie, D., L. Kellogg, J. Kiser, and M. Wing. 2003. Comparing Strategies for Skyline Corridor Layout. In *Proc. Of Council on Forest Engineering (COFE) "Forest Operations Amoung Competing Forest Users"*, Bar Harbor, ME.

Su, J. and E. Bork. 2006. Influence of vegetation, slope and Lidar sampling angle on DEM accuracy. *Photogrammetric Engineering and Remote Sensing*. 72(11): 1265-1274.

USFS. 2010. Index of Programs. Available online at: http://www.fs.fed.us/r6/nr/fp/FPWebPage/FP70104A/Programs.htm; last accessed Mar. 28, 2011.

CHAPTER 5. CONCLUSION

This thesis has presented two different manuscripts investigating the usage of airborne LiDAR to perform common measurement tasks faced by forest engineers and forest land managers. The goal was to show that airborne LiDAR could be used to perform these measurements, reducing time spent on the ground and therefore, the cost of these measurement activities.

Chapter 2 provided background information regarding basic theory and properties of LiDAR. A literature review was also presented that covered previous vertical and horizontal accuracy assessments of airborne LiDAR in forested environments and LiDAR applications in forestry. Background information on the field equipment used in both manuscripts was also provided.

Results from Chapter 3 indicate that airborne LiDAR can successfully measure road grade to within 1% slope of the best grade estimate regardless of four canopy types in the study. It is important to note that slopes were calculated over a relatively short horizontal distance of 7.5 m (24.6 ft) on average. When estimating horizontal curve radius the average LiDAR based radius was 3.17 m (10.4 ft) different from the field measured radius. On the smaller radius curves, for example, radius of 16 m (52 ft) a difference of 3.17 m could easily be the difference between a chip van navigating a corner or not. If a curve radius is small and near limiting for the vehicle in question a field visit is warranted.

Chapter 4 produced results that indicated the DEM elevations performed better than the nearest LiDAR point elevations. The difference can be seen in the

total RMSE for DEM (0.43 m) compared to that of the nearest LiDAR point elevations (0.49 m). The payload analysis showed that DEM profiles were on average 12% different from field profiles, while nearest LiDAR points profiles were on average 24% different. The field measured profiles in Chapter 4 were measured using survey grade instruments. In practice profile corridors are typically measured with instruments that have much lower precision and accuracy. Therefore, it is difficult to say with confidence if LiDAR DEM derived profiles can replace those measured by traditional field methods, but it appears the LiDAR data provides sufficient profile corridors for cable analysis.

Opportunities for further research

As mentioned in Chapter 3 there is an excellent opportunity to develop a computer algorithm that automatically extracts the road centerline from the LiDAR data. This would be particularly helpful for large road networks, where digitizing may not be feasible, or would prove to be cost prohibitive. The accuracy and precision of digitizing is also highly dependent on the skill of the operator. As suggested in Chapter 3, a possible method would be create a hillshade of the LiDAR based DEM and use image processing techniques to identify roads in the hillshade.

Another opportunity that was not explored in this thesis is the use of non-ground returns in assisting with road assessments. One of the safety concerns with horizontal curves is safe sight distance. Generally in a forested environment the inside of a horizontal curve is forested and prohibits a driver from seeing very far

down the curve. By utilizing the non-ground returns the height and position of the vegetation on the inside of a curve would be known and a model could be built that would estimate how far a driver could see and consequently what the safe speed limit would be.

Another possible opportunity comes from mobile scanning. Mobile scanning is analogous to airborne LiDAR except that the scanner is mounted to a ground based vehicle instead of the laser scanner being mounted to an aircraft. There has been a large interest in mobile scanning for urban corridors such as highways, dense city streets, and rail lines (Kutterer 2010). The current cost of the mobile systems does not make it practical for forestry use. However, as technology progresses and the prices lower, mobile scanning may be a viable option for forest roads. The scanner used in mobile scanning would be able to gather many more points per square meter than the airborne system. As a result, mobile scanning should be able to model the cutbanks and ditches to a much higher accuracy than the airborne data used in this thesis.

BIBLIOGRAPY

Akay, A., H. Oguz, I. Karas, and K. Aruga. 2009. Using LiDAR technology in forestry activities. *Environ. Monit. Assess.* 151(1):117-25.

Arbelaez, P., M. Maire, C. Fowlkes, and J. Malik. 2011. Contour Detection and Hierarchical Image Segmentation. *IEEE TPAMI* 33(5): 898-916.

Aruga, K., J., Sessions, and A. Akay. 2005. Application of an airborne laser scanner to forest road design with accurate earthwork volumes. *Journal of Forest Research* 10(2): 113-123.

American Society of Civil Engineers (ASCE). 2000. Operational Theory of NAVSTAR GPS. P 3-26. in *NAVSTAR Global Position System Surveying*. American Society of Civil Engineers, Boston, MA.

B.C. Ministry of Forests. 2002. Road Layout and Design. P. 3-36 in *Forest Road Engineering Guidebook*, For. Prac. Br., B.C. Min. For., Victoria, B.C. Forest Practices Code of British Columbia Guidebook.

Baltsavias, E. 1999a. Airborne Laser Scanning: Basic Relations and Formulas. *ISPRS Journal of Photogrammetry & Remote Sensing*. 54(1999): 199-214.

Baltsavias, E. 1999b. A Comparison Between Photogrammetry and Laser Scanning. *ISPRS Journal of Photogrammetry & Remote Sensing*. 54(1999): 83-94.

Beraldin, J-A., F., Balis, and U. Lohr. 2010. Laser Scanning Technology. P. 1-42 in *Airborne and Terrestrial Laser Scanning*, Vosselman, G., and H-G., Mass (eds.). Whittles Publishing, Dunbeath, Scotland, UK.

Briese, C.. 2010 Extraction of Digital Terrain Models. P. 135-167 in *Airborne and Terrestrial Laser Scanning*, Vosselman, G., and H-G., Mass (eds.). Whittles Publishing, Dunbeath, Scotland, UK.

Bowen, Z.H., and R.G. Waltermire. 2002. Evaluation of Light Detection and Ranging (LiDAR) for measuring river corridor topography. *Journal of the American Water Resources Association*. 38(1):33-41.

Carlson, P., M. Burris, K. Black, and E. Rose. 2005. Comparison of Radius-Estimating Techniques for Horizontal Curves. *Transportation Research Record: Journal of the Transportation Research Board*. 1918: 76-83.

Chung, W. 2003. *Optimization of Cable Logging Layout Using a Heuristic Algorithm for Network Programming.* Ph.D. Thesis, Oregon State University, Corvallis OR. 198 p.

Edson, C. 2011. *Light Detection and Ranging(LiDAR): what we can and cannot see in the forest for the trees*. PhD Dist., Oregon State University, Corvallis, OR. 262 p.

Gomes Pereira, L.M., and L.L.F. Janssen. 1999. Suitability of laser data for DTM generation: a case study in the context of road planning and design. *ISPRS Journal of Photogrammetry & Remote Sensing*. 54(1999):244-253.

Hodgson M., P., Bresnahan. 2004. Accuracy of Airborne Lidar-Derived Elevation: Empirical Assessment and Error Budget. *Photogrammetric Engineering and Remote Sensing* 70(3): 331-339.

Hodgson, M., J., Jensen, G., Raber, J., Tullis, B., Davis, G., Thompson,and K., Schuckman. 2005. An Evaluation of Lidar-derived Elevation and Terrain Slope in Leaf-off Conditions. *Photogrammetric Engineering and Remote Sensing* 71 (7): 817-823.

Hyde, P., R. Dubayah, R., B., Peterson, J., Blair, M., Hofton, and C., Hunsaker. 2005. Mapping forest structure for wildlife habitat analysis using waveform LiDAR. Validation of montane ecosystems. *Remote Sensing of the Environment* 96(4): 427-437.

Hyyppä, J., and M. Inkinen. 1999. Detecting and estimating attributes for single trees using laser scanner. *The Photogrammetric Journal of Finland* 16(2): 27-42.

Hyyppä, J., U., Pyysalo, H., Hyyppä, and A. Samberg. 2000. Elevation Accuracy of Laser Scanning-Derived Digital Terrain and Target Models in Forest Environment. P. 139-147 in Proceedings of EARsEL-SIG Workshop LIDAR. Dresden Germany.

Jenson, J.R. 2007. LiDAR Remote Sensing. P. 335-355 in *Remote Sensing of the Environment*, Howard, J., D. Kaveney, K. Schiaparelli, E. Thomas (eds.). Pearson Education, Inc, Upper Saddle River, NJ.

Kiser, J. 1991. *Photogrammetric Uses of a New-generation Analytical Stereoplotter in Forestry*. M.Sc. thesis, Oregon State University, Corvallis, OR. 156 p.

Kouba, J. 2009. A Guide to Using International GNSS Service (IGS) Products. Geodetic Survey Division, Natural Resources Canada. Ottawa, On. P. 1-29

Kramer, B. 2001. *Forest Road Contracting, Construction, and Maintenance for Small Forest Woodland Owners*. Research Contribution 35, Forest Research Laboratory, Oregon State University, Corvallis, OR. 79 p.

Kraus, K., and N. Pfeifer. 1998. Determination of terrain models in wooded areas with airborne laser scanner data. *ISPRS Journal of Photogrammetry & Remote Sensing.* 53 (1998): 193-203.

Kutterer, H. 2010. Mobile Mapping. P. 293-309 in *Airborne and Terrestrial Laser Scanning*, Vosselman, G., and H-G., Mass (eds.). Whittles Publishing, Dunbeath, Scotland, UK.

Maas, H. 2010. Forestry Applications. P. 213-235 *in Airborne and Terrestrial Laser Scanning*, Vosselman, G., and H-G., Mass (eds.). Whittles Publishing, Dunbeath, Scotland, UK.

NOAA National Geodetic Survey (NGS). 2009. Precise GPS Orbits. Available online at http://www.ngs.noaa.gov/orbits/; last accessed Apr. 4, 2011.

NOAA National Geodetic Survey(NGS). 2011. What is OPUS?. Available online at: http://www.ngs.noaa.gov/OPUS/about.jsp#about; last accessed Apr. 4, 2011.

Nikon. 2010. Nikon Nivo M Series Total Stations Specification Sheet. Available online at: http://trl.trimble.com/docushare/dsweb/Get/Document-468108/022505-100B_NivoMseries_SS_0909_LR.pdf; last accessed Apr. 4, 2011.

Paine, D. and J., Kiser. 2003. Environmental Monitoring. P. 378-393 in *Aerial Photography and Image Interpretation*. John Wiley and Sons, Hoboken, NJ.

Patenaude, G., R., Hill, R., Milne, D., Gaveau, B., Briggs, and T., Dawson. (2004). Quantifying forest above ground carbon content using LiDAR remote sensing. *Remote Sensing of the Environment* 96(3): 368-380.

Renslow, M., P. Greenfield, T. Guay. 2000. *Evaluation of multi-return LiDAR for forestry applications*. USDA Forest Service - Engineering, Remote Sensing Applications Center RSAC-2060/4180-RPT1. 17 p.

Reutebuch, S., R. McGaughey, H. Andersen, and W. Carson. 2003. Accuracy of high-resolution lidar terrain model under a conifer forest canopy. *Can. J. Remote Sensing*. 29(5):527-535.

Schofield, W. 2001. Control surveys. P. 252-306 in *Engineering Surveying*. Butterworth Heinemann, Oxford, UK.

Soler, A., P. Michalak, N. Weston, R. Snay, and R. Foote. 2005. Accuracy of OPUS solutions for 1- to 4-h observing sessions. *GPS Solutions.* 10(1): 45-55.

Sessions, J., J. Wimer, F., Costales, and M., Wing. 2010. Engineering Considerations in Road Assessment for Biomass Operations in Steep Terrain. *West. J. Appl. For.* 25(3): 144-153.

Sessions, J., J. Wimer, and K., Boston. 2009. Increasing Value and Reducing Costs through Hauling Longer Logs: Opportunities and Issues. *West. J. Appl. For.* 23(3): 157-162.

Sessions, J. 2007. Trucks. P. 161-188 in *Logging Mechanics Class Notes*. Department of Forest Engineering, Oregon State University, Corvallis, OR.

Solmie, D., L. Kellogg, J. Kiser, and M. Wing. 2003. Comparing Strategies for Skyline Corridor Layout. In *Proc. Of Council on Forest Engineering (COFE) "Forest Operations Amoung Competing Forest Users"*, Bar Harbor, ME.

Su, J. and E. Bork. 2006. Influence of vegetation, slope and Lidar sampling angle on DEM accuracy. *Photogrammetric Engineering and Remote Sensing*. 72(11): 1265-1274.

Suunto. 2008. Optical Height Meter. P. 4 in *Sunnto PM-5 USER'S GUIDE.* Suunto Oy, Valimotie, Finland.

Van Sickle, J. 2008a. GPS Surveying Techniques. P. 177-228 in *GPS for Land Surveyors.* CRC Press, Boca Raton, FL.

Van Sickle, J. 2008b. Biases and Solutions. P. 35-60 in *GPS for Land Surveyors.* CRC Press, Boca Raton, FL.

Vosselman, G., and R. Klein. 2010 Visualisation and Structuring of Point Clouds. P. 45-81 in *Airborne and Terrestrial Laser Scanning,* Vosselman, G., and H-G., Mass (eds.). Whittles Publishing, Dunbeath, Scotland, UK.

USFS. 2010. Index of Programs. Available online at: http://www.fs.fed.us/r6/nr/fp/FPWebPage/FP70104A/Programs.htm; last accessed Mar. 28, 2011.

Watershed Sciences. 2008. LiDAR remote sensing data collection: McDonald-Dunn Research Forest. Corvallis, Oregon, Watershed Sciences Inc.: 20 p.

Wing, M., A., Eklund, and J., Sessions. 2010. Applying LiDAR technology for tree measurements in burned landscapes. *International Journal of Wildland Fire* 19(1): 104-114.

Wing, M., and L. Kellogg. 2004. Locating and Mobile Mapping Techniques for Forestry Applications. *Geographic Information Sciences* 10(2): 175-182.

Wolf, P.R., B.A., Dewitt. 2000. Introduction to Analytical Photogrammetry. P. 233-259 in *Elements of Photogrammetry*, Munson, E (eds.). McGraw-Hill, Boston, MA.

Wolf, P.R., C.D., Ghilani. 2006a. Total Station Instruments; Angle Measurements. P. 187-226 in *Elementary Surveying an Introductin to Geomatics,* Svendsen E., D., Bernhard, V., O'Brien, D., George, R., Kernan (eds.). Pearson Prentice Hall, Upper Saddle River, NJ.

Wolf, P.R., C.D., Ghilani. 2006b. Electronic Distance Measurement. P. 145-164 in *Elementary Surveying an Introductin to Geomatics,* Svendsen E., D., Bernhard, V., O'Brien, D., George, R., Kernan (eds.). Pearson Prentice Hall, Upper Saddle River, NJ.

APPENDIX

Table A1: Summary of OPUS Solutions

Segment	Date	Orbit Type	RMS	Obs. Used	Amb. Fixed	Peak to Peak Error X	Y	Z
CC11	19-Jul-10	Final	0.02m	90%	88%	0.05m	0.00m	0.01m
CC12	19-Jul-10	Final	0.02m	84%	85%	0.03m	0.01m	0.01m
M21	20-Jul-10	Final	0.02m	66%	84%	0.09m	0.07m	0.07m
M22	20-Jul-10	Final	0.02m	64%	86%	0.14m	0.10m	0.20m
E41	15-Jul-10	Final	0.02m	89%	86%	0.04m	0.02m	0.03m
E42	15-Jul-10	Final	0.02m	87%	87%	0.02m	0.04m	0.01m
CC2&E21	12-Aug-10	Final	0.01m	89%	98%	0.02m	0.02m	0.01m
CC2&E22	12-Aug-10	Final	0.01m	77%	92%	0.02m	0.03m	0.03m
CC3&M31	13-Aug-10	Final	0.02m	86%	90%	0.06m	0.05m	0.04m
CC3&M31	13-Aug-10	Final	0.02m	67%	74%	0.13m	0.11m	0.14m
U41	16-Aug-10	Final	0.02m	62%	86%	0.07m	0.13m	0.06m
U42	16-Aug-10	Final	0.02m	65%	70%	0.12m	0.11m	0.11m
CC4&M41	23-Aug-10	Final	0.01m	98%	96%	0.03m	0.02m	0.02m
CC4&M42	23-Aug-10	Final	0.01m	98%	100%	0.03m	0.02m	0.02m
U11	26-Aug-10	Final	0.02m	88%	92%	0.03m	0.03m	0.01m
U12	26-Aug-10	Final	0.02m	88%	93%	0.04m	0.04m	0.03m
M11	31-Aug-10	Final	0.02m	66%	73%	0.33m	0.59m	0.35m
M12	31-Aug-10	Final	0.02m	59%	87%	0.03m	0.10m	0.20m
E31	30-Aug-10	Final	0.02m	79%	89%	0.08m	0.05m	0.04m
E32	30-Aug-10	Final	0.02m	75%	86%	0.09m	0.03m	0.17m
E11	4-Oct-10	Final	0.02m	65%	77%	0.11m	0.06m	0.09m
E12	4-Oct-10	Final	0.02m	67%	85%	0.03m	0.06m	0.12m
U3	11-Jul-09	Final	N/A	N/A	N/A	N/A	N/A	N/A
U3	11-Jul-09	Final	N/A	N/A	N/A	N/A	N/A	N/A

U3 was set and coordinates provided by Edson (2011).

Table A2: Individual Segment Results- Intensity Digitized Centerline

Segment	Horizontal Error				
	Average	Minimum	Maximum	Standard Deviation	RMSE
Clearcut Total	**0.38 m**	**0.00 m**	**1.26 m**	**0.22 m**	**0.44 m**
CC1	0.35 m	0.01 m	1.26 m	0.26 m	0.44 m
CC2	0.30 m	0.00 m	0.96 m	0.25 m	0.39 m
CC3	0.34 m	0.00 m	0.66 m	0.12 m	0.37 m
CC4	0.51 m	0.06 m	0.83 m	0.16 m	0.53 m
Evenage Total	**1.19 m**	**0.00 m**	**4.01 m**	**0.97 m**	**1.54 m**
E1	1.39 m	0.20 m	2.64 m	0.89 m	1.65 m
E2	1.01 m	0.00 m	2.23 m	0.58 m	1.17 m
E3	1.98 m	0.01 m	4.01 m	0.99 m	2.21 m
E4	0.23 m	0.06 m	0.70 m	0.12 m	0.26 m
Mature Total	**0.97 m**	**0.00 m**	**3.21 m**	**0.62 m**	**1.15 m**
M1	1.11 m	0.00 m	1.98 m	0.38 m	1.17 m
M2	0.91 m	0.15 m	2.42 m	0.42 m	1.00 m
M3	1.29 m	0.00 m	3.21 m	0.89 m	1.56 m
M4	0.55 m	0.01 m	1.43 m	0.38 m	0.67 m
Unevenage Total	**1.00 m**	**0.00 m**	**3.39 m**	**0.99 m**	**1.40 m**
U1	0.41 m	0.00 m	1.14 m	0.19 m	0.45 m
U2	2.66 m	2.06 m	3.39 m	0.32 m	2.68 m
U3	0.46 m	0.00 m	0.87 m	0.15 m	0.49 m
U4	0.46 m	0.00 m	1.37 m	0.28 m	0.54 m
Grand Total	**0.89 m**	**0.00 m**	**4.01 m**	**0.83 m**	**1.21 m**

Table A3: Individual Segment Results- Point Cloud Digitized Centerline

Segment	Horizontal Error				
	Average	Minimum	Maximum	Standard Deviation	RMSE
Clearcut Total	**1.45 m**	**0.07 m**	**3.38 m**	**0.77 m**	**1.64 m**
CC1	0.90 m	0.26 m	2.34 m	0.34 m	0.96 m
CC2	1.73 m	0.07 m	3.00 m	0.50 m	1.80 m
CC3	2.28 m	0.19 m	3.38 m	0.77 m	2.41 m
CC4	0.94 m	0.11 m	1.60 m	0.35 m	1.01 m
Evenage Total	**2.12 m**	**0.00 m**	**8.12 m**	**2.48 m**	**3.26 m**
E1	5.89 m	1.63 m	8.12 m	2.04 m	6.23 m
E2	0.66 m	0.00 m	1.64 m	0.40 m	0.77 m
E3	1.42 m	0.01 m	3.96 m	1.21 m	1.87 m
E4	0.59 m	0.00 m	1.31 m	0.27 m	0.65 m
Mature Total	**1.20 m**	**0.00 m**	**3.89 m**	**0.83 m**	**1.46 m**
M1	0.77 m	0.00 m	2.86 m	0.68 m	1.03 m
M2	1.40 m	0.58 m	2.86 m	0.52 m	1.49 m
M3	1.96 m	0.25 m	3.89 m	0.88 m	2.14 m
M4	0.69 m	0.12 m	2.21 m	0.40 m	0.80 m
Unevenage Total	**2.13 m**	**0.45 m**	**5.80 m**	**1.30 m**	**2.50 m**
U1	1.94 m	0.62 m	3.05 m	0.64 m	2.04 m
U2	3.86 m	1.79 m	5.80 m	1.19 m	4.04 m
U3	1.54 m	0.79 m	2.83 m	0.48 m	1.61 m
U4	1.12 m	0.45 m	2.52 m	0.52 m	1.23 m
Grand Total	**1.72 m**	**0.00 m**	**8.12 m**	**1.57 m**	**2.33 m**

Table A4: Individual Segment Results- Slope Filtered Extracted Centerline

Segment	Horizontal Error				
	Average	Standard Deviation	Minimum	Maximum	RMSE
Clearcut Total	**0.73 m**	**0.32 m**	**0.06 m**	**1.76 m**	**0.80 m**
CC1	1.06 m	0.33 m	0.12 m	1.94 m	1.11 m
CC2	0.38 m	0.24 m	0.00 m	1.27 m	0.45 m
CC3	0.89 m	0.49 m	0.05 m	2.42 m	1.02 m
CC4	0.57 m	0.24 m	0.04 m	1.42 m	0.62 m
Evenage Total	**1.24 m**	**0.65 m**	**0.10 m**	**3.04 m**	**1.40 m**
E1	1.50 m	0.85 m	0.14 m	3.37 m	1.72 m
E2	0.99 m	0.54 m	0.08 m	2.70 m	1.13 m
E3	2.08 m	1.00 m	0.14 m	5.07 m	2.30 m
E4	0.41 m	0.21 m	0.03 m	1.02 m	0.46 m
Mature Total	**1.04 m**	**0.51 m**	**0.08 m**	**2.72 m**	**1.17 m**
M1	1.15 m	0.39 m	0.16 m	2.55 m	1.21 m
M2	0.95 m	0.42 m	0.08 m	2.49 m	1.04 m
M3	1.33 m	0.78 m	0.07 m	3.58 m	1.54 m
M4	0.75 m	0.45 m	0.02 m	2.25 m	0.87 m
Unevenage Total	**1.30 m**	**0.35 m**	**0.32 m**	**2.34 m**	**1.35 m**
U1	1.30 m	0.39 m	0.19 m	2.27 m	1.36 m
U2	2.68 m	0.45 m	1.02 m	4.08 m	2.71 m
U3	0.60 m	0.26 m	0.04 m	1.44 m	0.65 m
U4	0.61 m	0.32 m	0.02 m	1.57 m	0.69 m
Grand Total	**1.08 m**	**0.46 m**	**0.14 m**	**2.47 m**	**1.34 m**

Table A5: Individual Segment Results- Curve Radius Estimates

Segment	Average of Radius Difference	Average of Absolute Radius Difference
Clearcut Total	**-2.92 m**	**4.31 m**
CC1	1.76 m	1.76 m
CC2	-5.64 m	5.64 m
CC3	-6.22 m	6.22 m
CC4	1.73 m	1.73 m
Evenage Total	**2.60 m**	**3.39 m**
E1	2.14 m	4.54 m
E2	6.52 m	6.52 m
E3	2.04 m	2.04 m
E4	0.71 m	0.71 m
Mature Total	**0.10 m**	**3.24 m**
M1	3.53 m	3.53 m
M2	-6.16 m	6.16 m
M3	2.26 m	2.26 m
M4	-1.28 m	2.00 m
Unevenage Total	**-1.16 m**	**1.92 m**
U1	-0.73 m	2.12 m
U2	-0.85 m	0.85 m
U3	-0.53 m	1.42 m
U4	-3.61 m	3.61 m
Grand Total	**-0.24 m**	**3.17 m**

Table A6: Individual Segment Results- Centerline Elevations Field vs LiDAR DEM

Segment	Average of Elevation Difference	Average of Absolute Elevation Difference	Standard Deviation of Absolute Elevation Difference	RMSE
Clearcut Total	**0.15 m**	**0.18 m**	**0.19 m**	**0.26 m**
CC1	-0.07 m	0.07 m	0.08 m	0.11 m
CC2	0.11 m	0.11 m	0.05 m	0.12 m
CC3	0.50 m	0.50 m	0.06 m	0.50 m
CC4	0.05 m	0.06 m	0.03 m	0.06 m
Evenage Total	**0.03 m**	**0.07 m**	**0.06 m**	**0.09 m**
E1	0.02 m	0.03 m	0.02 m	0.04 m
E2	0.13 m	0.13 m	0.05 m	0.13 m
E3	-0.03 m	0.07 m	0.08 m	0.11 m
E4	0.00 m	0.03 m	0.03 m	0.04 m
Mature Total	**0.28 m**	**0.31 m**	**0.27 m**	**0.43 m**
M1	0.52 m	0.52 m	0.06 m	0.52 m
M2	-0.02 m	0.04 m	0.04 m	0.06 m
M3	0.63 m	0.63 m	0.06 m	0.63 m
M4	-0.02 m	0.05 m	0.04 m	0.06 m
Unevenage Total	**0.17 m**	**0.17 m**	**0.14 m**	**0.23 m**
U1	0.03 m	0.04 m	0.02 m	0.04 m
U2	0.32 m	0.32 m	0.15 m	0.35 m
U3	0.25 m	0.25 m	0.04 m	0.26 m
U4	0.07 m	0.07 m	0.03 m	0.08 m
Grand Total	**0.16 m**	**0.19 m**	**0.21 m**	**0.28 m**

Table A7: Individual Segment Results- Centerline Elevations Field vs LiDAR Nearest Point

Segment	Average of Elevation Difference	Average of Absolute Elevation Difference	Standard Deviation of Absolute Elevation Difference	RMSE	Average Distance to Nearest LiDAR Point
Clearcut Total	**0.15 m**	**0.17 m**	**0.22 m**	**0.27 m**	**0.28 m**
CC1	-0.03 m	0.06 m	0.08 m	0.09 m	0.30 m
CC2	0.06 m	0.07 m	0.05 m	0.09 m	0.28 m
CC3	0.54 m	0.54 m	0.04 m	0.54 m	0.29 m
CC4	0.03 m	0.03 m	0.02 m	0.04 m	0.26 m
Evenage Total	**0.00 m**	**0.07 m**	**0.06 m**	**0.09 m**	**0.34 m**
E1	0.02 m	0.03 m	0.03 m	0.04 m	0.27 m
E2	0.10 m	0.10 m	0.06 m	0.11 m	0.39 m
E3	-0.06 m	0.10 m	0.07 m	0.12 m	0.38 m
E4	-0.02 m	0.03 m	0.03 m	0.04 m	0.29 m
Mature Total	**0.26 m**	**0.30 m**	**0.25 m**	**0.39 m**	**0.34 m**
M1	0.43 m	0.43 m	0.09 m	0.44 m	0.31 m
M2	-0.04 m	0.05 m	0.04 m	0.06 m	0.28 m
M3	0.61 m	0.61 m	0.08 m	0.61 m	0.35 m
M4	-0.02 m	0.04 m	0.04 m	0.05 m	0.40 m
Unevenage Total	**0.16 m**	**0.16 m**	**0.15 m**	**0.22 m**	**0.31 m**
U1	0.03 m	0.03 m	0.02 m	0.04 m	0.22 m
U2	0.31 m	0.32 m	0.18 m	0.37 m	0.45 m
U3	0.23 m	0.23 m	0.02 m	0.23 m	0.26 m
U4	0.04 m	0.05 m	0.03 m	0.05 m	0.30 m
Grand Total	**0.14 m**	**0.17 m**	**0.20 m**	**0.27 m**	**0.32 m**

Table A8: Individual Segment Results- Road Grade Estimations Field Grade Compared to Intensity Based Centerline with DEM Elevations

Strata	Average Absolute Difference In Slope	Maximum Difference in Slope
Clearcut Total	**0.42%**	**0.56%**
CC1	0.91%	0.36%
CC2	0.09%	0.70%
CC3	0.23%	0.83%
CC4	0.46%	0.36%
Evenage Total	**0.76%**	**3.30%**
E1	0.06%	0.69%
E2	0.08%	1.62%
E3	1.86%	9.20%
E4	1.05%	1.70%
Mature Total	**0.63%**	**1.38%**
M1	0.54%	0.09%
M2	0.53%	3.95%
M3	0.00%	1.09%
M4	1.44%	0.38%
Unevenage Total	**0.48%**	**0.21%**
U1	0.06%	0.03%
U2	0.36%	0.24%
U3	0.50%	0.42%
U4	1.00%	0.17%
Grand Total	**0.57%**	**1.41%**

Table A9: Individual Segment Results- Road Modeling with TIN Surface

Segment	Average of Min. Elev. Difference	Average of Max. Elev. Difference	Average of Mean Elev. Difference	Average of Absolute Mean Elev. Difference
Clearcut Total	**-0.92 m**	**0.75 m**	**0.13 m**	**0.14 m**
CC1	-0.90 m	0.79 m	-0.02 m	0.02 m
CC2	-1.57 m	0.95 m	0.08 m	0.08 m
CC3	-0.77 m	1.05 m	0.45 m	0.45 m
CC4	-0.42 m	0.19 m	0.01 m	0.01 m
Evenage Total	**-1.26 m**	**0.64 m**	**-0.04 m**	**0.05 m**
E1	-1.52 m	0.91 m	0.01 m	0.01 m
E2	-1.18 m	0.62 m	0.01 m	0.01 m
E3	-1.01 m	0.45 m	-0.13 m	0.13 m
E4	-1.34 m	0.58 m	-0.04 m	0.04 m
Mature Total	**-0.91 m**	**1.28 m**	**0.28 m**	**0.37 m**
M1	-0.51 m	2.44 m	0.69 m	0.69 m
M2	-1.26 m	0.56 m	-0.14 m	0.14 m
M3	-0.84 m	1.41 m	0.61 m	0.61 m
M4	-1.04 m	0.69 m	-0.04 m	0.04 m
Unevenage Total	**-0.61 m**	**0.96 m**	**0.08 m**	**0.08 m**
U1	-0.76 m	0.71 m	0.01 m	0.01 m
U2	-0.78 m	1.08 m	0.10 m	0.10 m
U3	-0.31 m	0.64 m	0.20 m	0.20 m
U4	-0.60 m	1.40 m	-0.01 m	0.01 m
Grand Total	**-0.93 m**	**0.90 m**	**0.11 m**	**0.16 m**

Road Extraction Matlab Code:

```
% Michael Craven

% Program to filter points based on slope, with the purpose of defining a
% road segment.  Then taking filtered points and reconstructing a
% centerline from said points.  Has the ability to be run in multiple runs
% through the code to try different search windows and slope thresholds.

% Program requires lidar points already be stored as .mat files, and that
% coordinates for the original centerline and initial centerline be stored
% in the .csv format.  Written in Matlab R2008b.

% last mod 15 MAY 2011

% clear screen/variables & format

format long g
clear all;
clc;

% ------------------------------------
% Parameters to Control Batch Process & Files to Load
%-------------------------------------

% cell array of cl files to open
toopen={'CC1_intensity1.csv';'CC2_intensity1.csv';'CC3_intensity1.csv';'CC4_intensity1.
csv';'E1_intensity1.csv';'E2_intensity1.csv';'E3_intensity1.csv';'E4_intensity1.csv';'O1_inte
nsity1.csv';'O2_intensity1.csv';'O3_intensity1.csv';'O4_intensity1.csv';'U1_intensity1.csv';'
U2_intensity1.csv';'U3_intensity1.csv';'U4_intensity1.csv'};

% save base is a cell array of the names of the lidar files for each
% segment
savebase={'CC1_LiDAR.mat';'CC2_LiDAR.mat';'CC3_LiDAR.mat';'CC4_LiDAR.mat';'E
1_LiDAR.mat';'E2_LiDAR.mat';'E3_LiDAR.mat';'E4_LiDAR.mat';'O1_LiDAR.mat';'O2_
LiDAR.mat';'O3_LiDAR.mat';'O4_LiDAR.mat';'U1_LiDAR.mat';'U2_LiDAR.mat';'U3_L
iDAR.mat';'U4_LiDAR.mat'};

%segment names
names={'CC1';'CC2';'CC3';'CC4';'E1';'E2';'E3';'E4';'O1';'O2';'O3';'O4';'U1';'U2';'U3';'U4'};

% figure names
figure={'CC1.tiff';'CC2.tiff';'CC3.tiff';'CC4.tiff';'E1.tiff';'E2.tiff';'E3.tiff';'E4.tiff';'O1.tiff';'O
2.tiff';'O3.tiff';'O4.tiff';'U1.tiff';'U2.tiff';'U3.tiff';'U4.tiff'};
```

```
% cell array of field cl files to open
truecl={'CC1_topo1.csv';'CC2_topo1.csv';'CC3_topo1.csv';'CC4_topo1.csv';'E1_topo1.csv
';'E2_topo1.csv';'E3_topo1.csv';'E4_topo1.csv';'O1_topo1.csv';'O2_topo1.csv';'O3_topo1.c
sv';'O4_topo1.csv';'U1_topo1.csv';'U2_topo1.csv';'U3_topo1.csv';'U4_topo1.csv'};


%save too is a cell array of the names of the csvs to create
saveto={'CC1_output.csv';'CC2_output.csv';'CC3_output.csv';'CC4_output.csv';'E1_outpu
t.csv';'E2_output.csv';'E3_output.csv';'E4_output.csv';'O1_output.csv';'O2_output.csv';'O3
_output.csv';'O4_output.csv';'U1_output.csv';'U2_output.csv';'U3_output.csv';'U4_output.c
sv'};

numseg=16; % number of segments

totalsumsqer=0;  % sum of all the sqrd error for over all RMSE calc
totalcount=0; % count of all points used in total RMSE calc

% Account for field setups starting in the middle of segment
%-------------------------------------------------------
% which col x or y does data need to be sorted on to account for how it was
% measured in the field
colsort=[2;1;1;2; %cc group
        2;2;1;1; % e group
        2;1;1;1; % o group
        2;1;1;1]; % u group
 %-------------------------------------------------------

% ------------------------------------
% Parameters to Control Road Area
%------------------------------------


% * * * * * * * * * * * * * * * * * * * * * * * * *
% variables user must specify
% * * * * * * * * * * * * * * * * * * * * * * * * *

perc = [.05;.075;.1;.125;.15];
widths =[4;6;8;10];

% define results cell array to store diff in cls

results={};

% read in the road width we are looking at and percent for z diff calc

run=1; % index for number of runs so we can save results
```

```
% START RUNS ------------------------------------------------------------

% loop over possible widths values
for k=1:1%length(widths)

   %loop over possible elevation thresholds
   for n =1:1%length(perc);

      possiblewidth=4;%widths(k); % possible road half width in ft/meters
      percent=.125;%perc(n); % percent slope that is allowable for z determination

      % Start looping over segments
      for m=1:numseg

         %Load Files from Directory
         %---------------------------

         % load lidar file
         load(savebase{m,1});

         fprintf('Loading Segment %s\n',names{m,1});

         %load initial cl file
         clpts = dlmread(toopen{m,1},'\t'); % read file with comma delimiter


         inputcl= clpts; % change variable name


         % find the initial points that are closest to the field points
         % load field points

         fieldcl= dlmread(truecl{m,1},'\t');

         % loop through field cl to find the corresponding intial cl
         % points


         initalcl=[];%zeros(length(inputcl)-1,4); % allocate size
         topo1cl=[];

         counter=1;

         % find which is longer (not exact length due to digitizing)
         togo=0;

         if length(fieldcl)>=length(inputcl)
```

```
   togo=length(inputcl);

elseif length(inputcl)>length(fieldcl)

   togo=length(fieldcl);

end

% assign input cl coords to the variables used later on
% room for improvement in this coding

for i =1:togo % togo is the length of the shorter CL, field or intensity digitized

   if i==1
      % get 1st point
      initalcl(1,1)=inputcl(1,2);% x % cl in acad format PNEZD
      initalcl(1,2)=inputcl(1,3);% y
      %initalcl(1,3)=inputcl(1,4);%z
      initalcl(1,4)=inputcl(1,1); % assign a pt number

      % get corresponding field cl point
      topo1cl(1,1)=fieldcl(1,2);
      topo1cl(1,2)=fieldcl(1,3);% y
      topo1cl(1,3)=fieldcl(1,4);%z
      topo1cl(1,4)=fieldcl(1,1); % assign a pt number
   end

   if mod(i,10) ==0  % grab every 100th point

      initalcl(counter,1)=inputcl(i,2);% x % cl in acad format PNEZD
      initalcl(counter,2)=inputcl(i,3);% y
      initalcl(counter,3)=inputcl(i,4);%z
      initalcl(counter,4)=inputcl(i,1); % assign a pt number
      topo1cl(counter,1)=fieldcl(i,2);
      topo1cl(counter,2)=fieldcl(i,3);% y
      %topo1cl(counter,3)=fieldcl(i,4);%z
      topo1cl(counter,4)=fieldcl(i,1); % assign a pt number

      counter=counter+1;

   end

   if i==length(inputcl) % grab last point
      initalcl(counter,1)=inputcl(i,2);% x % cl in acad format PNEZD
      initalcl(counter,2)=inputcl(i,3);% y
      initalcl(counter,3)=inputcl(i,4);%z
      initalcl(counter,4)=inputcl(i,1); % assign a pt number
```

```
      topo1cl(counter,1)=fieldcl(i,2);% x % cl in acad format PNEZD
      topo1cl(counter,2)=fieldcl(i,3);% y
      %topo1cl(counter,3)=fieldcl(i,4);%z
      topo1cl(counter,4)=fieldcl(i,1); % assign a pt number
   end
end

temp = sortrows(initalcl,colsort(m)); % sort road by x values to make sure it is
cont. rather than as it was collected

initalcl =temp;

% plot intial data

%plot(initalcl(:,1),initalcl(:,2));


% determine max and min of input cl with buffer

buffer =20;% buffer to include more a bit more than just road area

xmax=max(initalcl(:,1))+buffer;
ymax=max(initalcl(:,2))+buffer;
xmin=min(initalcl(:,1))-buffer;
ymin=min(initalcl(:,2))-buffer;

out=length(lidarpts);

% loop through and keep on the lidar points that are in the region

fprintf('Number of Lidar Pts Starting: %i \n\n',out);

keepnum=1;

for i=1:length(lidarpts)

   if lidarpts(i,1)<=xmax && lidarpts(i,1) >= xmin && lidarpts(i,2) <=ymax &&
   lidarpts(i,2)>=ymin

      keep(keepnum,1)=lidarpts(i,1);
      keep(keepnum,2)=lidarpts(i,2);
      keep(keepnum,3)=lidarpts(i,3);
      keep(keepnum,4)=lidarpts(i,4);
      keepnum=keepnum+1;

   end
end % i loop
```

```
fprintf('Number of Lidar Pts After Bounding: %i \n\n',keepnum-1);

% assign lidar pts as keep

clear lidarpts

lidarpts=zeros(length(keep),5);

for i =1:length(keep)
      lidarpts(i,1)=keep(i,1);%x
      lidarpts(i,2)=keep(i,2);%y
      lidarpts(i,3)=keep(i,3);%z
      lidarpts(i,4)=keep(i,4);%p
end



%************************************************
% Need to calculate alignment between CL points
%************************************************

% need to determine # of CL points

numcl = length(initalcl);

% need to determine # of CL points

numlidar = length(lidarpts);

% calc alignment

% creat array that holds distance,direction,p,perpa,perpb
alignment = zeros(numcl,5);

% structure to hold half way pts
half =struct('x',0,'y',0);

for i=1:numcl

   % set beg. to point to zero distance and az
   if i == 1
     alignment(i,1)=0;
     alignment(i,2)=0;
     alignment(i,3)=1;
     alignment(i,4)=0;
     alignment(i,5)=0;
   else
      % inverse
```

```
        dx = initalcl(i,1)-initalcl(i-1,1);

        dy = initalcl(i,2)-initalcl(i-1,2);

        dist=(dx^2+dy^2)^.5; % calc distance

        az = atan2(dx,dy);%atan2(dy,dx); % calc azmuith

        perpa = az-pi/2;% calc perpendicular azmuith

        perpb = az+pi/2;% calc perpendicular azmuith

        % calculate halfway point

        half(i).x = initalcl(i-1,1)+dx/2;

        half(i).y = initalcl(i-1,2) +dy/2;


        % store values in alignment array

        alignment(i,1)=dist;
        alignment(i,2)=az;
        alignment(i,3)=i;
        alignment(i,4)=perpa;
        alignment(i,5)=perpb;

    end  % end if

end% for loop
% go back and fill in perps for point 1 base on point 1-2

alignment(1,4)=alignment(2,4);
alignment(1,5)=alignment(2,5);
display('Alignment Complete');

% calculate endpoints of each perp at possible width

% initilize end points

endptsa=zeros(numcl,4); % x,y,z,clpt
endptsb=zeros(numcl,4); % x,y,z,clpt

% calculate end points
for i=1:numcl
    % a side
    dx=sin(alignment(i,4))*possiblewidth; % diff in x
```

```
    dy=cos(alignment(i,4))*possiblewidth; % diff in y

    dz = possiblewidth*crownslope; % diff in z

    endptsa(i,1) = initalcl(i,1)+dx; % add diff in cl coord
    endptsa(i,2) = initalcl(i,2)+dy;
    endptsa(i,3) = initalcl(i,3)-dz;% subtract for crowned road in z
    endptsa(i,4)=initalcl(i,4); % corresponding inital pt number

    %b side
    dx=sin(alignment(i,5))*possiblewidth;

    dy=cos(alignment(i,5))*possiblewidth;

    endptsb(i,1) = initalcl(i,1)+dx;
    endptsb(i,2) = initalcl(i,2)+dy;
    endptsb(i,3) = initalcl(i,3)-dz;% subtract for crowned road in z
    endptsb(i,4)=initalcl(i,4); % corresponding inital pt number


end % for loop

% check data
plot(initalcl(:,1),initalcl(:,2),endptsa(:,1),endptsa(:,2),endptsb(:,1),endptsb(:,2));


% * * * * * * * * * * * * * * * * * * * * * * * * * * * * *
% FIND POINTS NEAR CL POINTS
% * * * * * * * * * * * * * * * * * * * * * * * * * * * * *


% loop though intial cl pts and find the lidar pts that are near by and
% within the z value diff

roadpts=[];
nroadpts=1;
for i=1:length(initalcl)

    % loop through lidar pts to see which ones are with in the distance

    for j=1:length(lidarpts)

        distance = ((initalcl(i,1)-lidarpts(j,1))^2+(initalcl(i,2)-lidarpts(j,2))^2)^.5;

        if distance <= possiblewidth

            % check difference in z
```

```
        zdiff = initalcl(i,3)-lidarpts(j,3);

        alwz = possiblewidth*percent; % allowable difference in z

        if zdiff <= alwz

           %save point
           roadpts(nroadpts,1) = lidarpts(j,1);
           roadpts(nroadpts,2) = lidarpts(j,2);
           roadpts(nroadpts,3) = lidarpts(j,3);
           nroadpts=nroadpts+1;
        end % if  elev

     end % if distance

  end % j loop


end % i loop

% write out road pts

% Option to write out roadpts for debug purposes etc.
%dlmwrite(filename,roadpts,'delimiter',',','precision',9)


fprintf('Number of Points on Road %f\n',nroadpts)

%  * * * * * * * * * * * * * * * * * * * * * * * * * * * * *
% reconstruct the centerline
%  * * * * * * * * * * * * * * * * * * * * * * * * * * * * *

% find the points closest to the endptsa and endptsb, these should be the
% the outer edge points

outera=zeros(length(endptsa),4);
outerb=zeros(length(endptsa),4);

for i =1:length(endptsa)

  bestdist=100000; % set to large number

  % loop through road pts

  for j=1:length(roadpts)

     %calc distance between road pts and outer pts
     distance = ((endptsa(i,1)-roadpts(j,1))^2+(endptsa(i,2)-roadpts(j,2))^2)^.5;
```

```
        if distance < bestdist

            bestdist = distance; % save the best distance yet seen

            outera(i,1)=roadpts(j,1); % save pt data
            outera(i,2)=roadpts(j,2);
            outera(i,3)=roadpts(j,3);
            outera(i,4) = distance; % save the distance

        end % best dis

    end % j loop

end % i loop

% repeat for the b side
for i =1:length(endptsb)

    bestdist=100000; % set to large number

    % loop through road pts

    for j=1:length(roadpts)

        distance = ((endptsb(i,1)-roadpts(j,1))^2+(endptsb(i,2)-roadpts(j,2))^2)^.5;

        if distance < bestdist

            bestdist = distance;

            outerb(i,1)=roadpts(j,1); % save pt data
            outerb(i,2)=roadpts(j,2);
            outerb(i,3)=roadpts(j,3);
            outerb(i,4) = distance; % save the distance

        end % best dis?

    end % j loop

end % i loop

% - - - - - - - - - - - - - - - - - - - - - - - - - - - - - - -
% now determine the midpoint between corresponding outer points
% - - - - - - - - - - - - - - - - - - - - - - - - - - - - - - -

cl=zeros(length(outera),4);
```

```
for i=1:length(outera)

   % determine distance between corresponding points
   dx = outera(i,1) - outerb(i,1);
   dy = outera(i,2) - outerb(i,2);


   dist = (dx^2 + dy^2)^.5;

   if outera(i,1) == outerb(i,1)
      %used for debug.
      %dist = -9999; % this is an alert in the event there is
      %only 1 point on the road in this section
   end

   az = atan2(dx,dy);%atan2(dy,dx); % calc azmuith

   toclx = sin(az)*dist/2; % x distance to cl

   tocly = cos(az)*dist/2; % y distance to cl

   cl(i,1) = outera(i,1) - toclx;
   cl(i,2) = outera(i,2) - tocly;
   cl(i,3) = dist;
   cl(i,4) = az;

end % i loop


% compare the Cl to the intial cl
% * * * * * * * * * * * * * * * * * * * * * * * * * * * * *

cldiff=zeros(length(cl),3);

for i =1:length(cl)

   cldiff(i,1) = initalcl(i,1)-cl(i,1);

   cldiff(i,2) = initalcl(i,2)-cl(i,2);

   cldiff(i,3) = (cldiff(i,1)^2 + cldiff(i,2)^2)^.5;

end % iloop

% save stats for how the difference between initial cl and the
% extracted centerline

meanxdiff = mean(cldiff(:,1));
```

```
meanydiff = mean(cldiff(:,2));
meandiff = mean(cldiff(:,3));
maxdiff= max(cldiff(:,3));
mindiff= min(cldiff(:,3));
stdv=std(cldiff(:,3));


fprintf('mean x diff %f\n', meanxdiff)
fprintf('mean y diff %f\n', meanydiff)
fprintf('mean diff %f\n', meandiff)

%**********************************
% Load and compare to the original FIELD CL
%**********************************


topo12int=zeros(length(cl),4);

for i =1:length(topo1cl)

    topo12int(i,1) = topo1cl(i,1)-cl(i,1); % delta x

    topo12int(i,2) = topo1cl(i,2)-cl(i,2); % delta y

    topo12int(i,3) = (topo12int(i,1)^2 + topo12int(i,2)^2)^.5; % distance

    topo12int(i,4) = topo12int(i,3)^2; % this is the squared error for RMSE

end % iloop

% determine the error between the extracted cl and the field
% measured cl
meanxerror = mean(topo12int(:,1));
meanyerror = mean(topo12int(:,2));
meanerror = mean(topo12int(:,3));
maxerror= max(topo12int(:,3));
minerror= min(topo12int(:,3));
stdv_err=std(topo12int(:,3));
RMSE = (sum(topo12int(:,4))/length(topo12int))^.5;

 totalsumsqer=totalsumsqer+sum(topo12int(:,4));  % sum of all the sqrd error for
over all RMSE calc
totalcount=totalcount+length(topo12int); % count of all points used in total RMSE
calc

 %write out the segment results for debug
 csvwrite(saveto{m},topo12int);
```

```
        % save plot!

       plot(topo1cl(:,1),topo1cl(:,2),endptsa(:,1),endptsa(:,2),endptsb(:,1),endptsb(:,2),cl(:,
       1),cl(:,2))

        saveas(gcf,figure{m},'jpg');

        % Save the cldiff to a cell array so we can examine with

        result{run,1}=names{m}; % segment name
        result{run,2}=meanxdiff; % mean error in x for seg
        result{run,3}=meanydiff; % mean error in y for seg
        result{run,4}=meandiff; % mean total error for seg
        result{run,5}=maxdiff; %
        result{run,6}=mindiff; %
        result{run,7}=stdv; %
        result{run,8}=percent; % save percent for z calc
        result{run,9}=possiblewidth; % save the road width seach zone
        result{run,10}=meanxerror; % mean error in x for seg
        result{run,11}=meanyerror; % mean error in y for seg
        result{run,12}=meanerror; % mean total error for seg
        result{run,13}=maxerror; %
        result{run,14}=minerror; %
        result{run,15}=stdv_err; %
        result{run,16}=RMSE; %


        run=run+1;

        fprintf('Finished Segment %s !\n\n* * * * * *\n\n',names{m,1});

      end % M, numseg loop
   end % n loop, changes percent for z calc

end % K loop, change in possible road width


% ---------------------------------------------------------------
% write result array out
% ---------------------------------------------------------------
% because result is a cell array, low level functions have to be used to
% write out the array as opposed to dlmwrite etc.

% write file as csv
fid=fopen('slopefilter_7_0_b.csv','wt');

% print header
```

```
fprintf(fid,'Segment,meanxdiff,meanydiff,meandiff,maxdiff,mindiff,stdv,percent,width,me
anxerror,meanyerror,meanerror,maxerror,minerror,stdev_error,RMSE\n');

for i=1:length(result)
   % print data
   fprintf(fid,'%s,',result{i,1});

        fprintf(fid,'%f,%f,%f,%f,%f,%f,%f,%f,%f,%f,%f,%f,%f,%f,%f,%f\n',result{i,2},result
        {i,3},result{i,4},result{i,5},result{i,6},result{i,7},result{i,8},result{i,9},result{i,10}
        ,result{i,11},result{i,12},result{i,13},result{i,14},result{i,15},result{i,16});

end

fclose(fid); % close the output file

%uncomment if doing a single run and desire total RMSE
%Total_RMSE=(totalsumsqer/totalcount)^.5 % print out the total RMSE, is only correct
for a single run....



% END
```

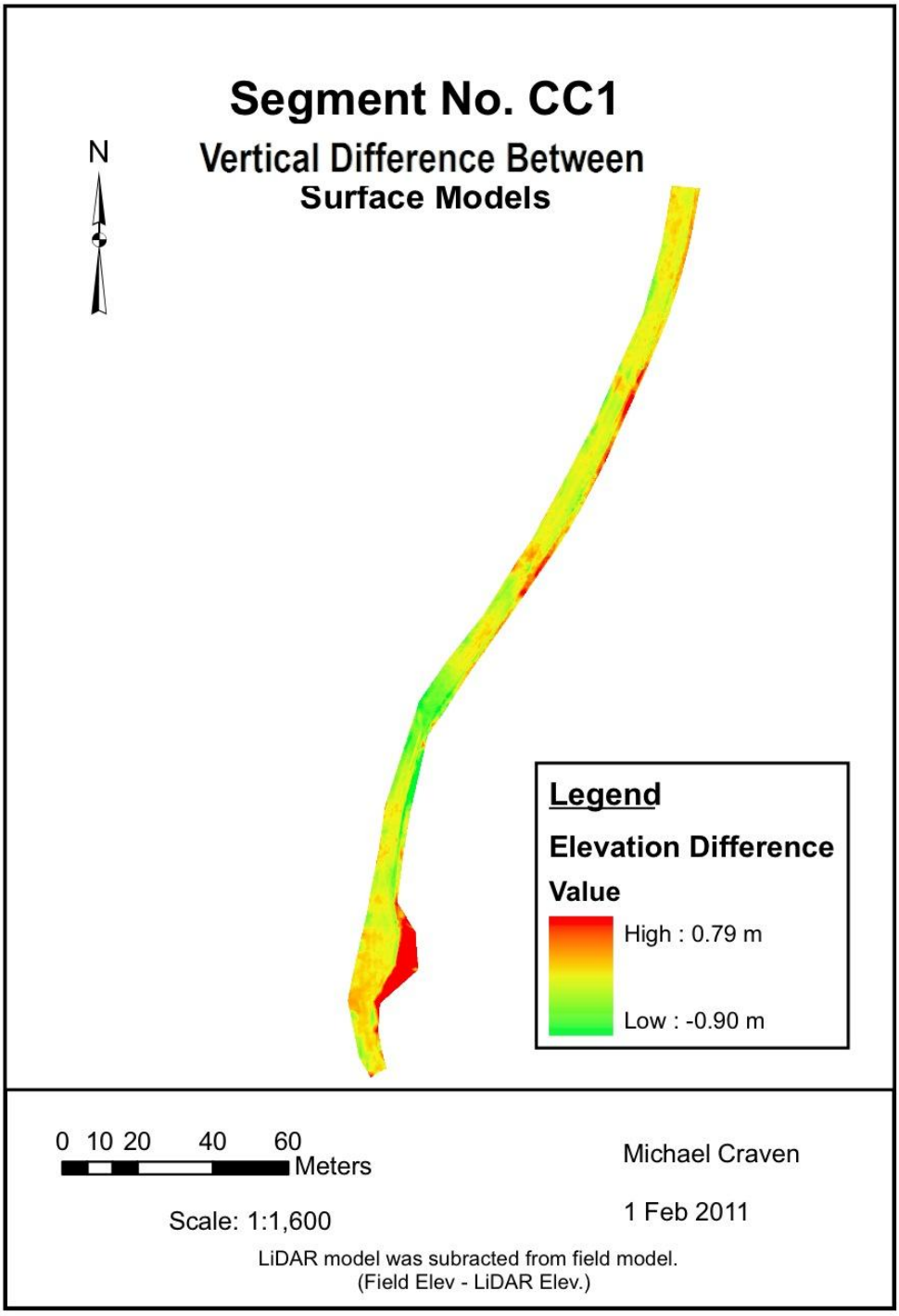

Figure A1: Elevation Difference Between TIN Models- Segment CC1

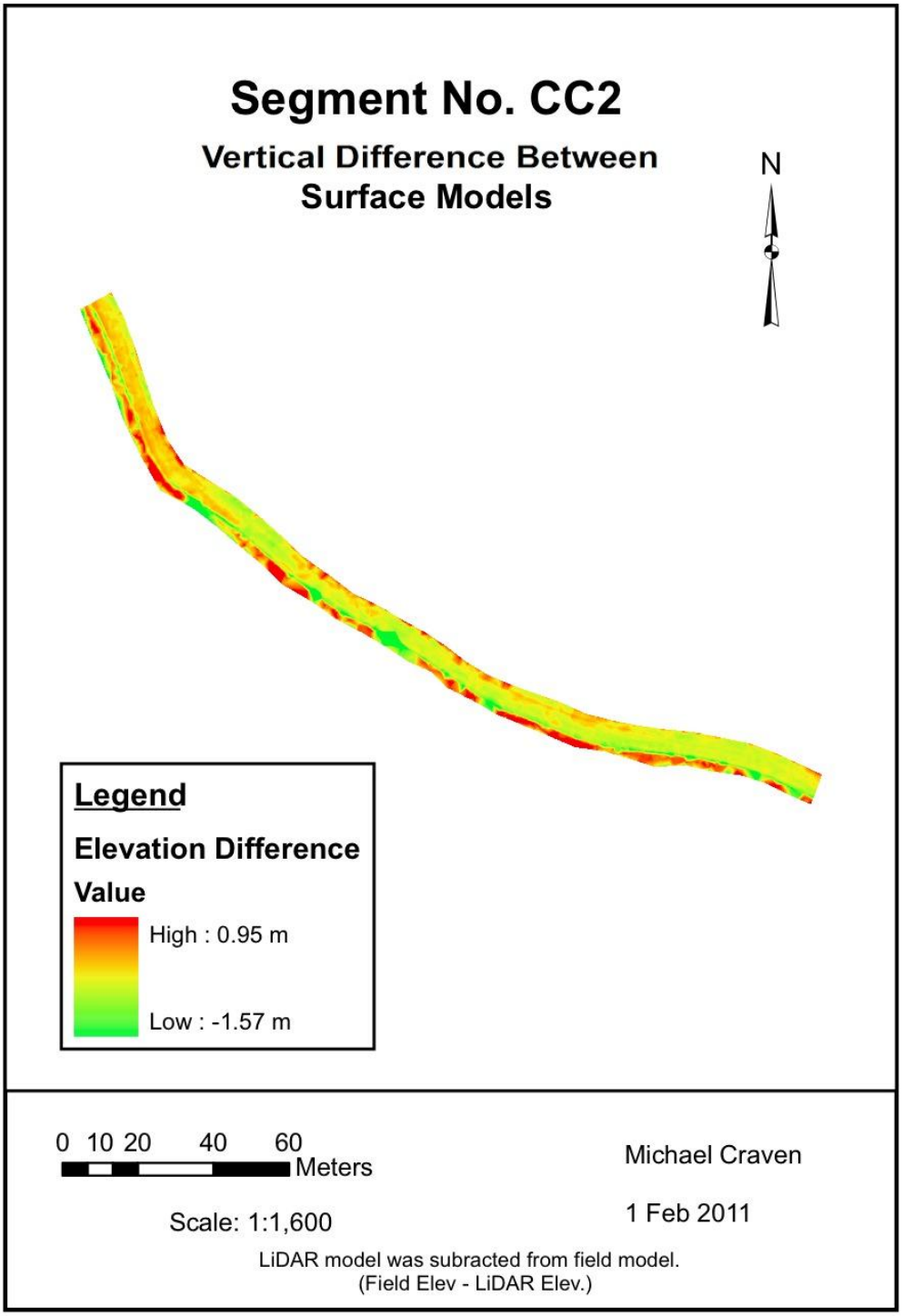

Figure A2: Elevation Difference Between TIN Models- Segment CC2

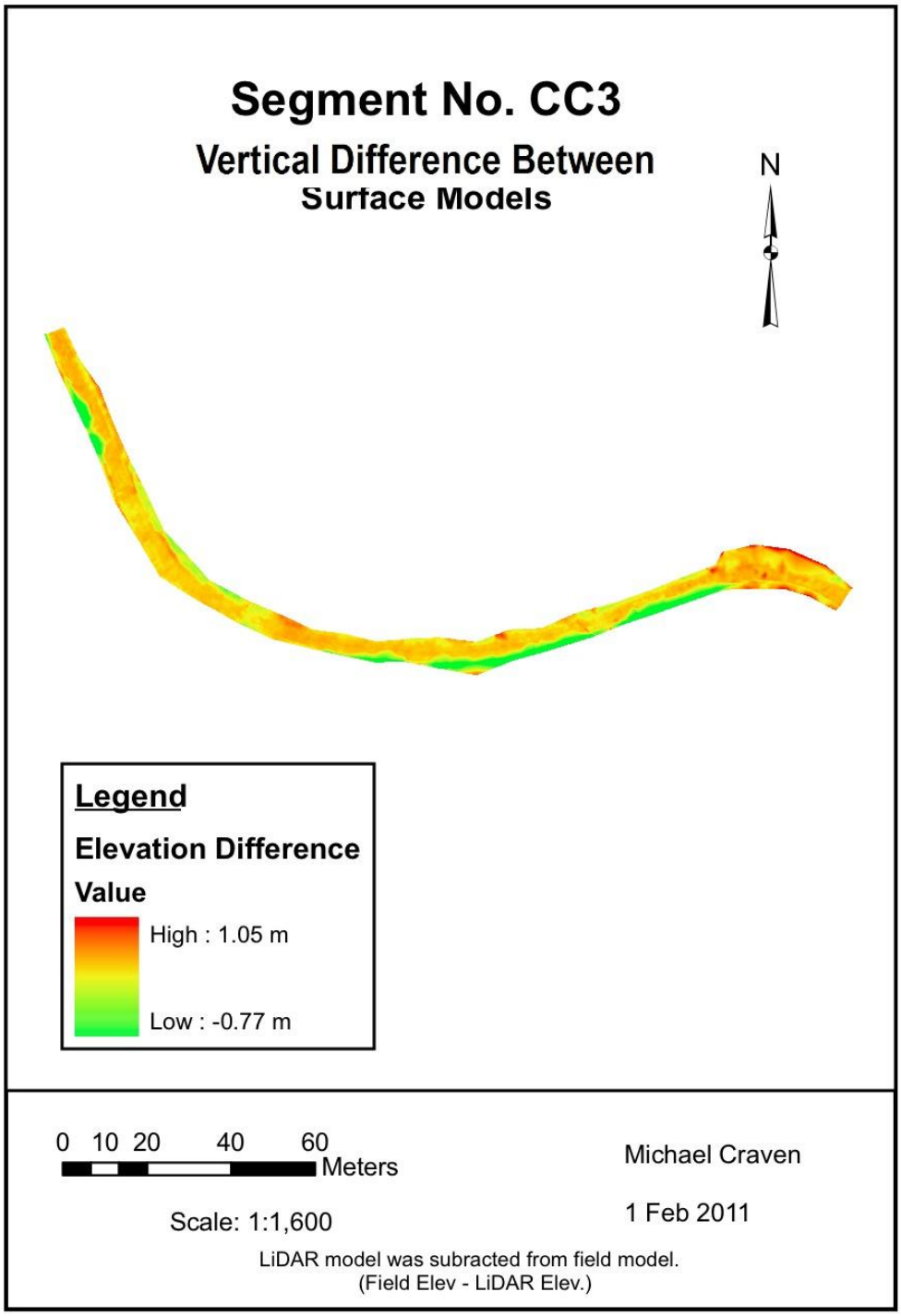

Figure A3: Elevation Difference Between TIN Models- Segment CC3

Figure A4: Elevation Difference Between TIN Models- Segment CC4

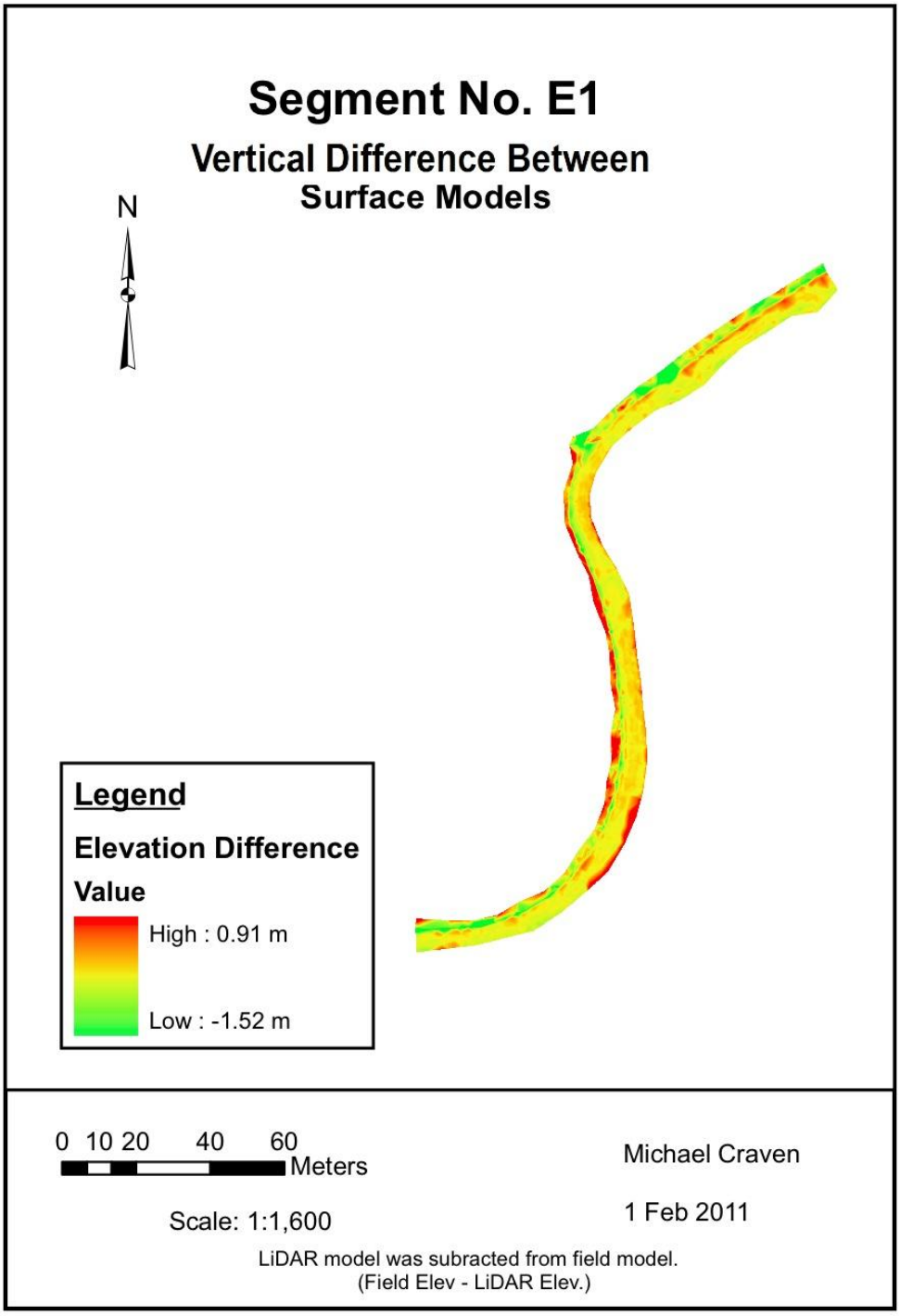

Figure A5: Elevation Difference Between TIN Models- Segment E1

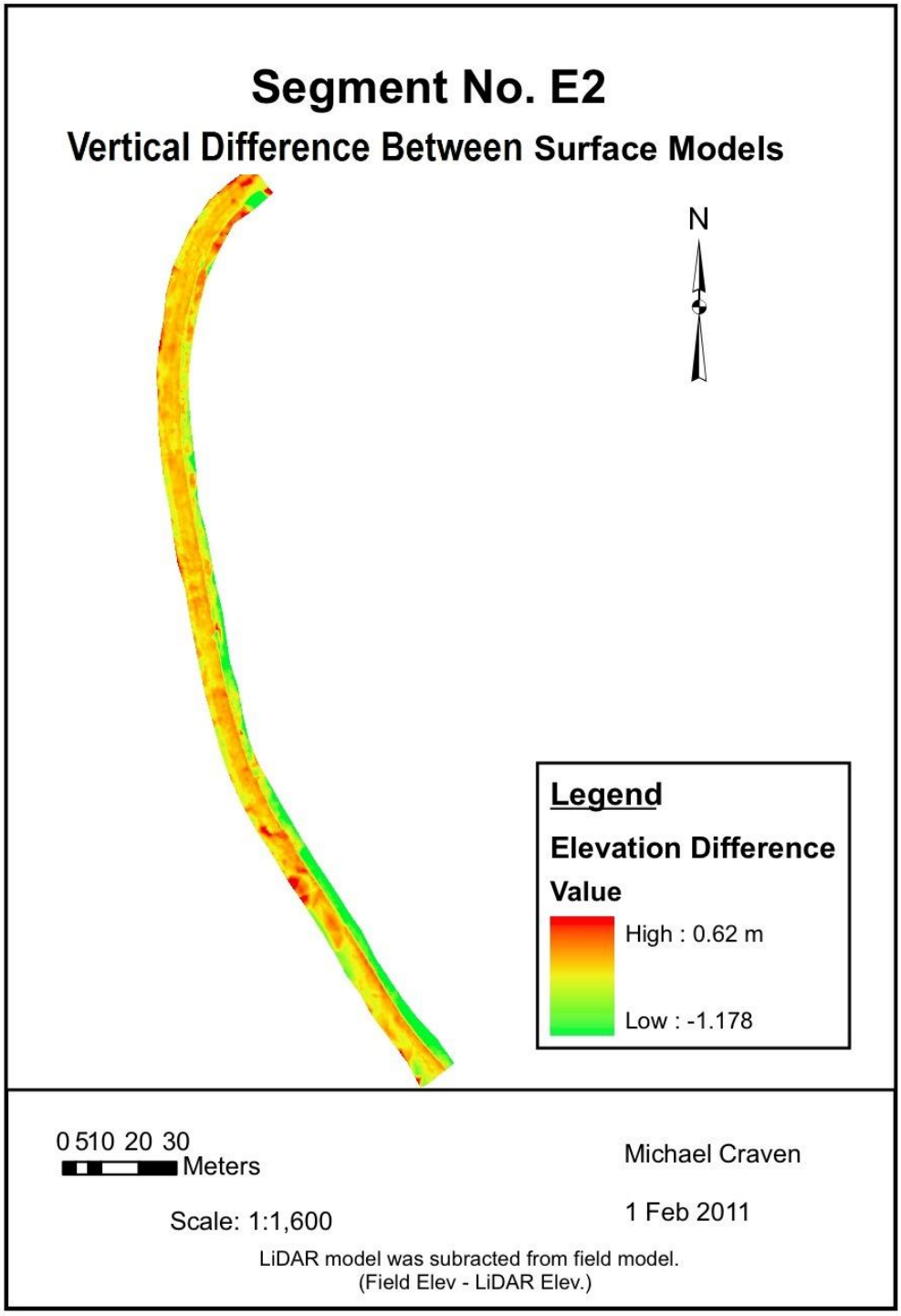

Figure A6: Elevation Difference Between TIN Models- Segment E2

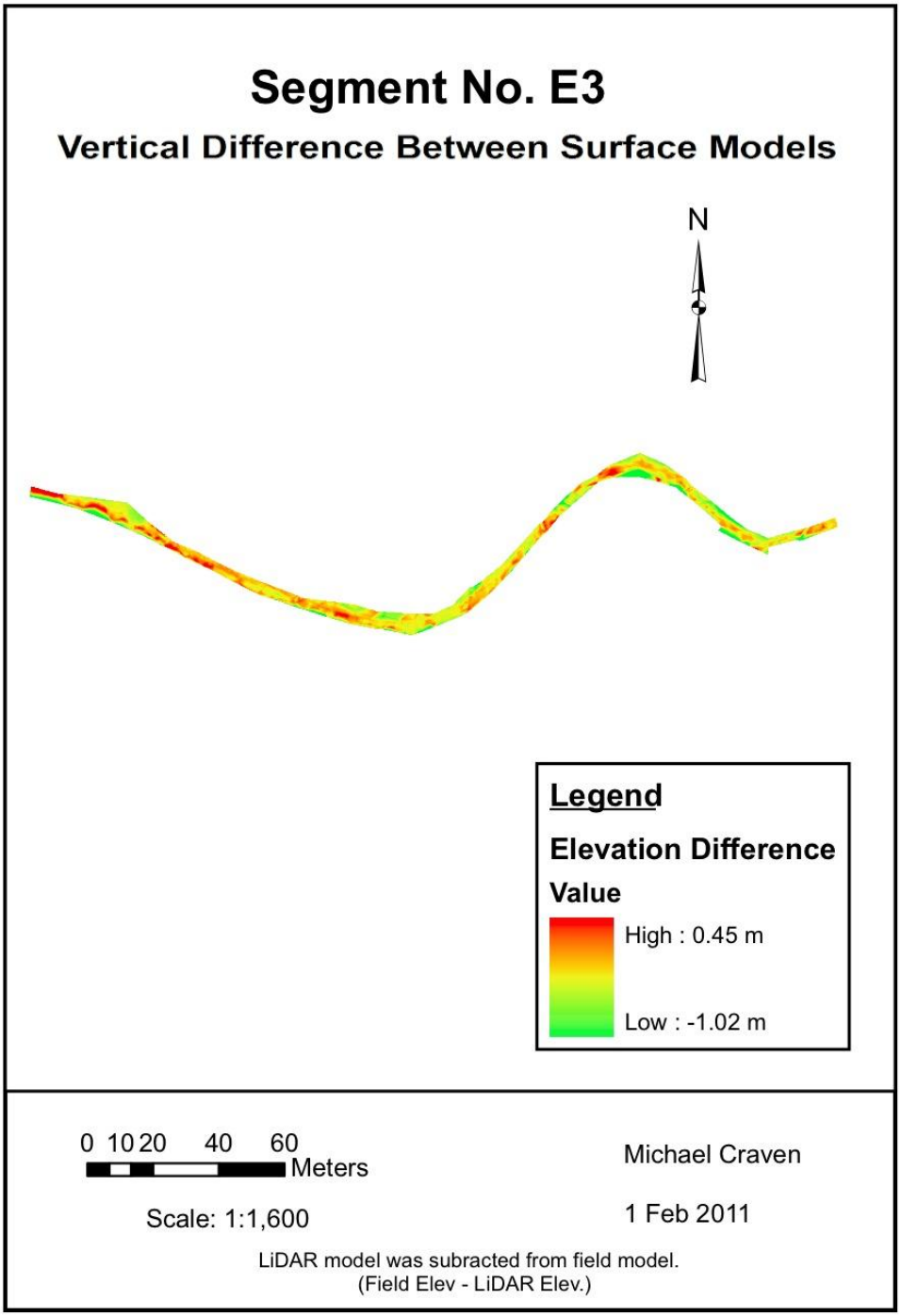

Figure A7: Elevation Difference Between TIN Models- Segment E3

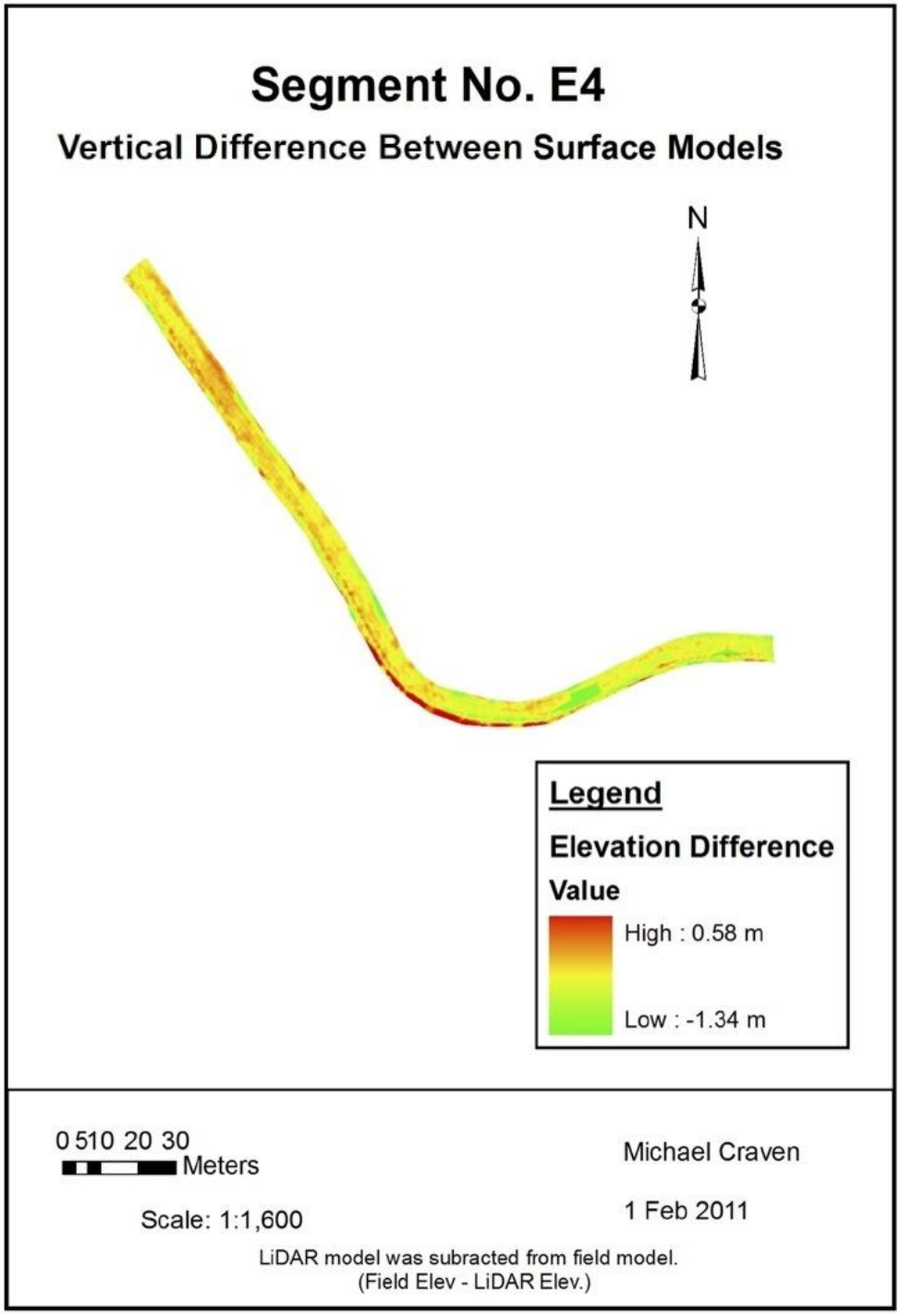

Figure A8: Elevation Difference Between TIN Models- Segment E4

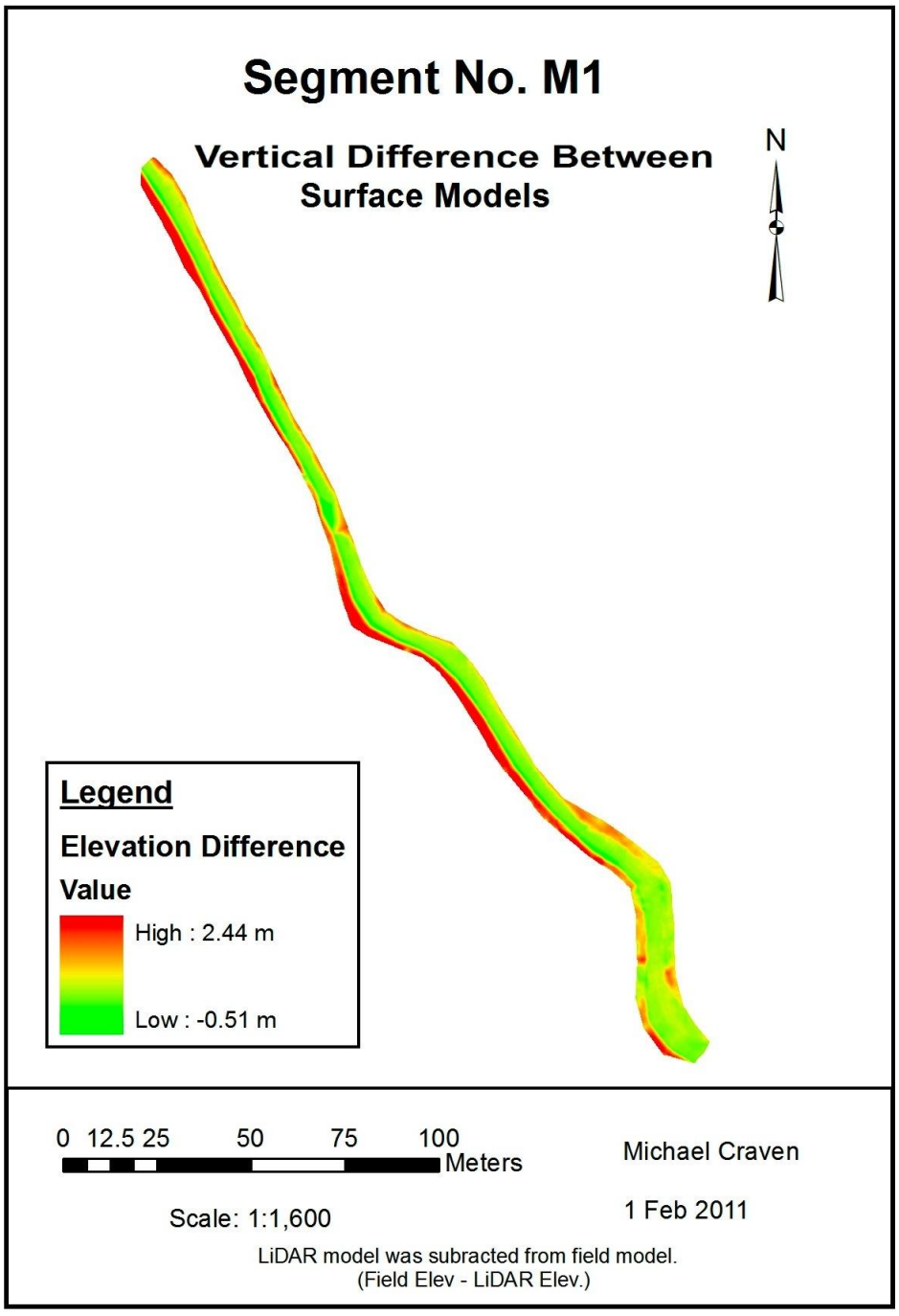

Figure A9: Elevation Difference Between TIN Models- Segment M1

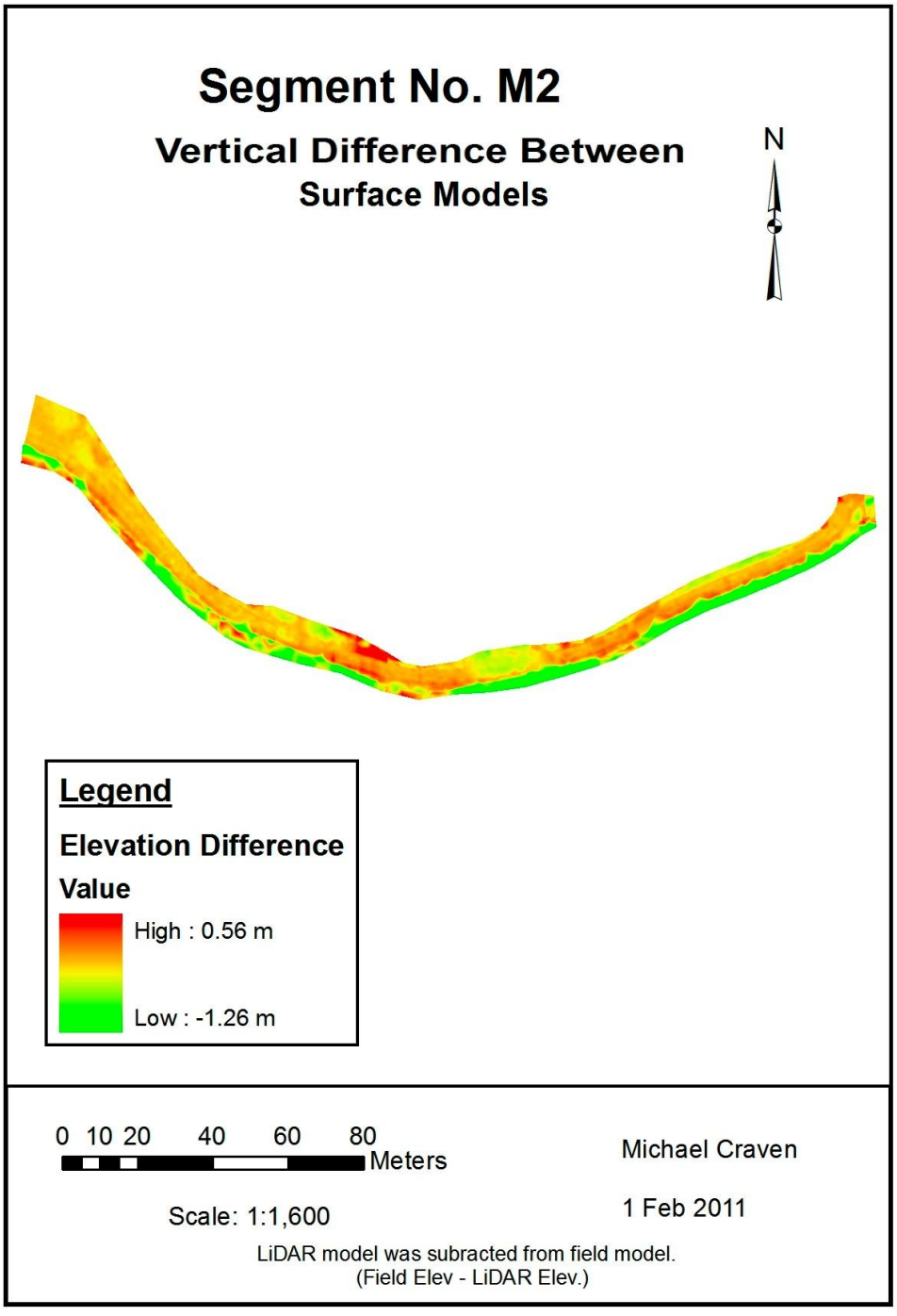

Figure A10: Elevation Difference Between TIN Models- Segment M2

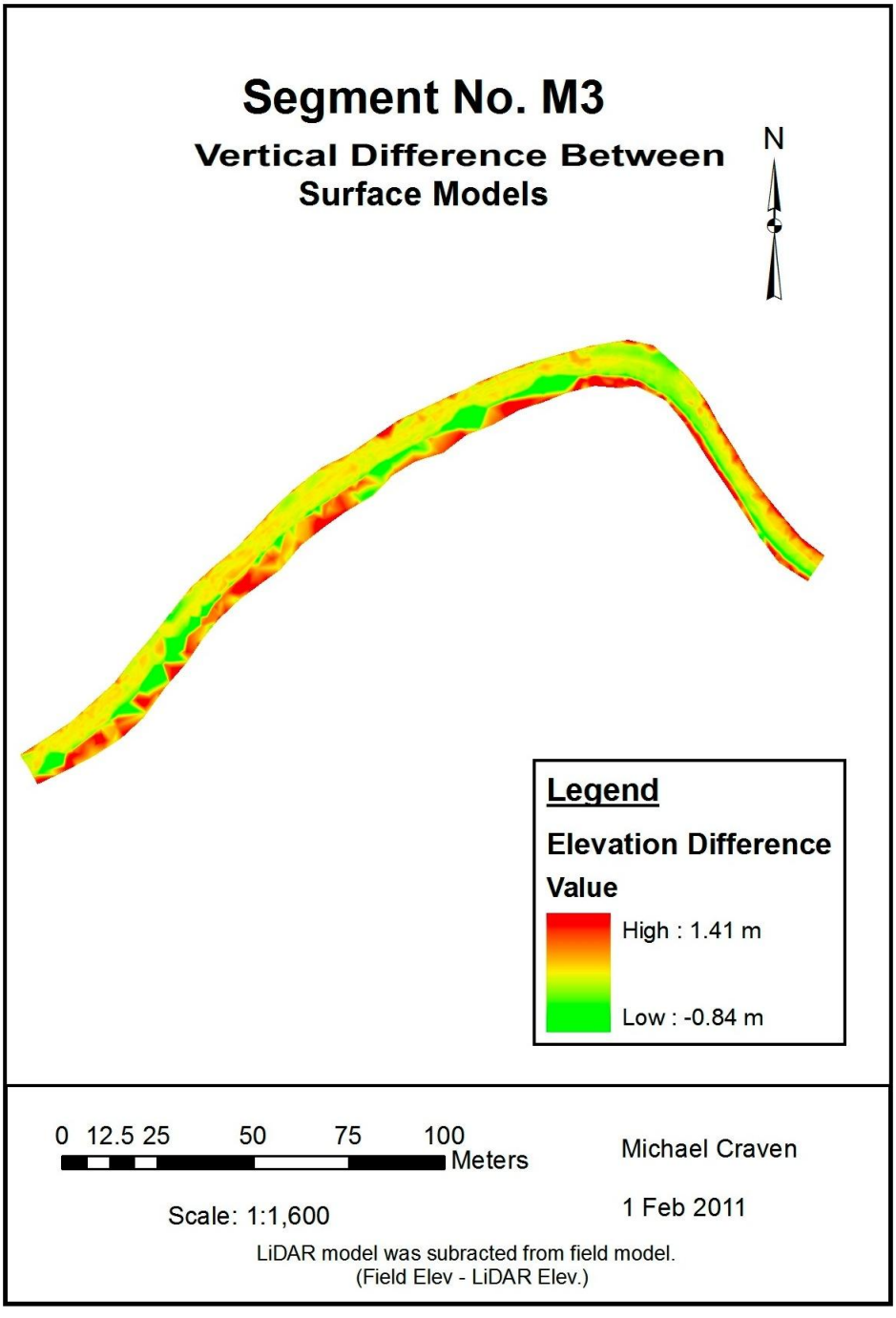

Figure A11: Elevation Difference Between TIN Models- Segment M3

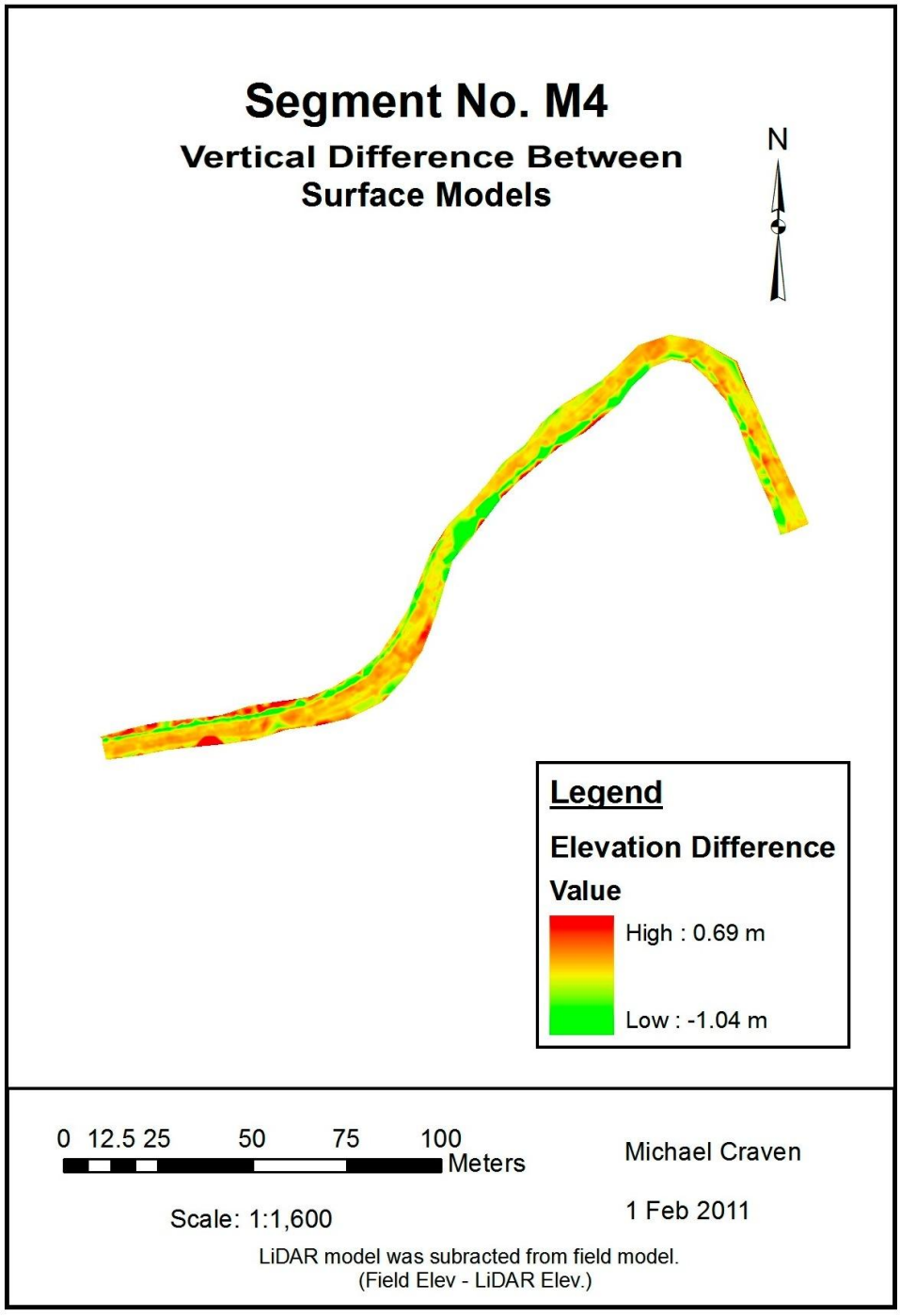

Figure A12: Elevation Difference Between TIN Models- Segment M4

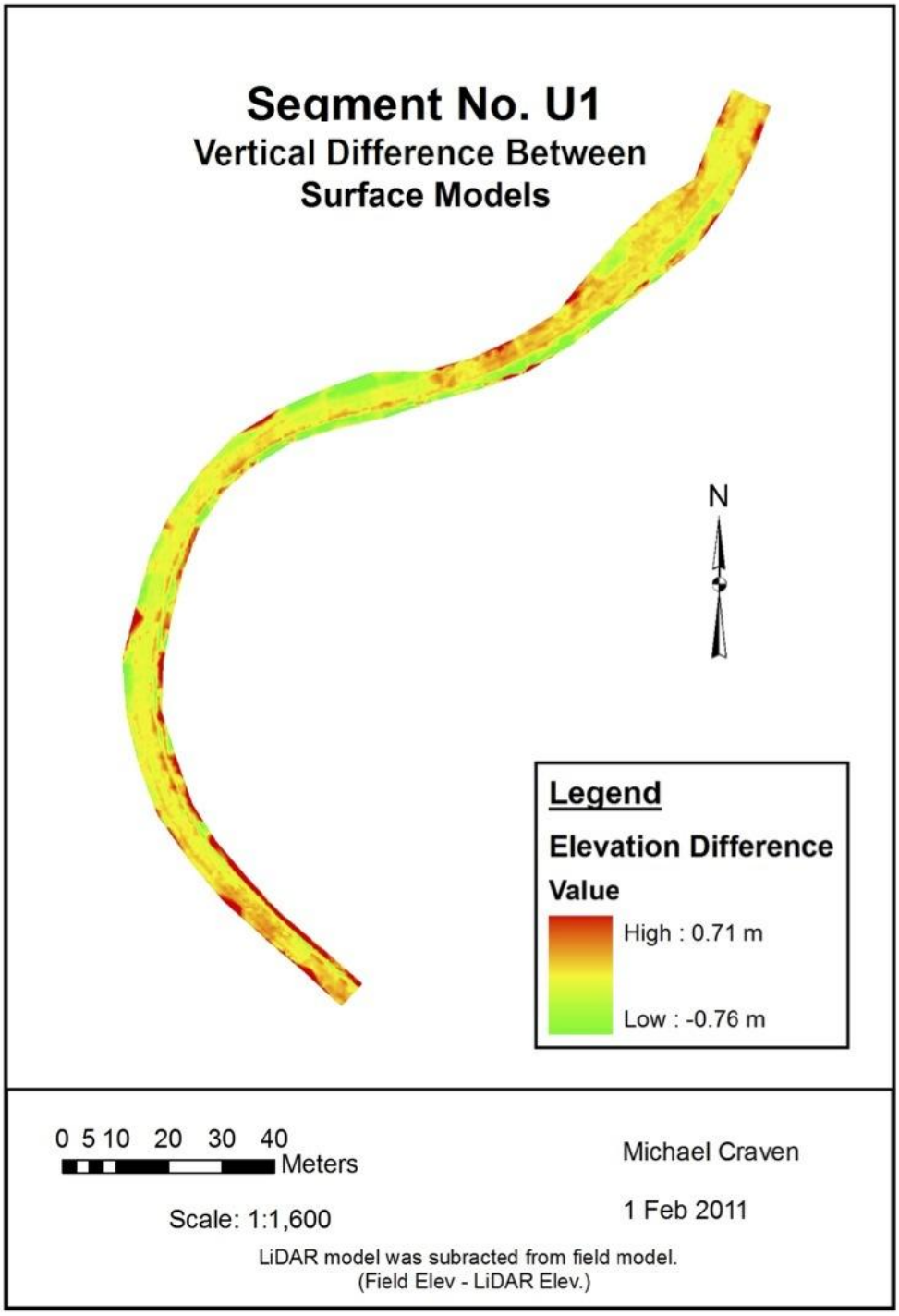

Figure A13: Elevation Difference Between TIN Models- Segment U1

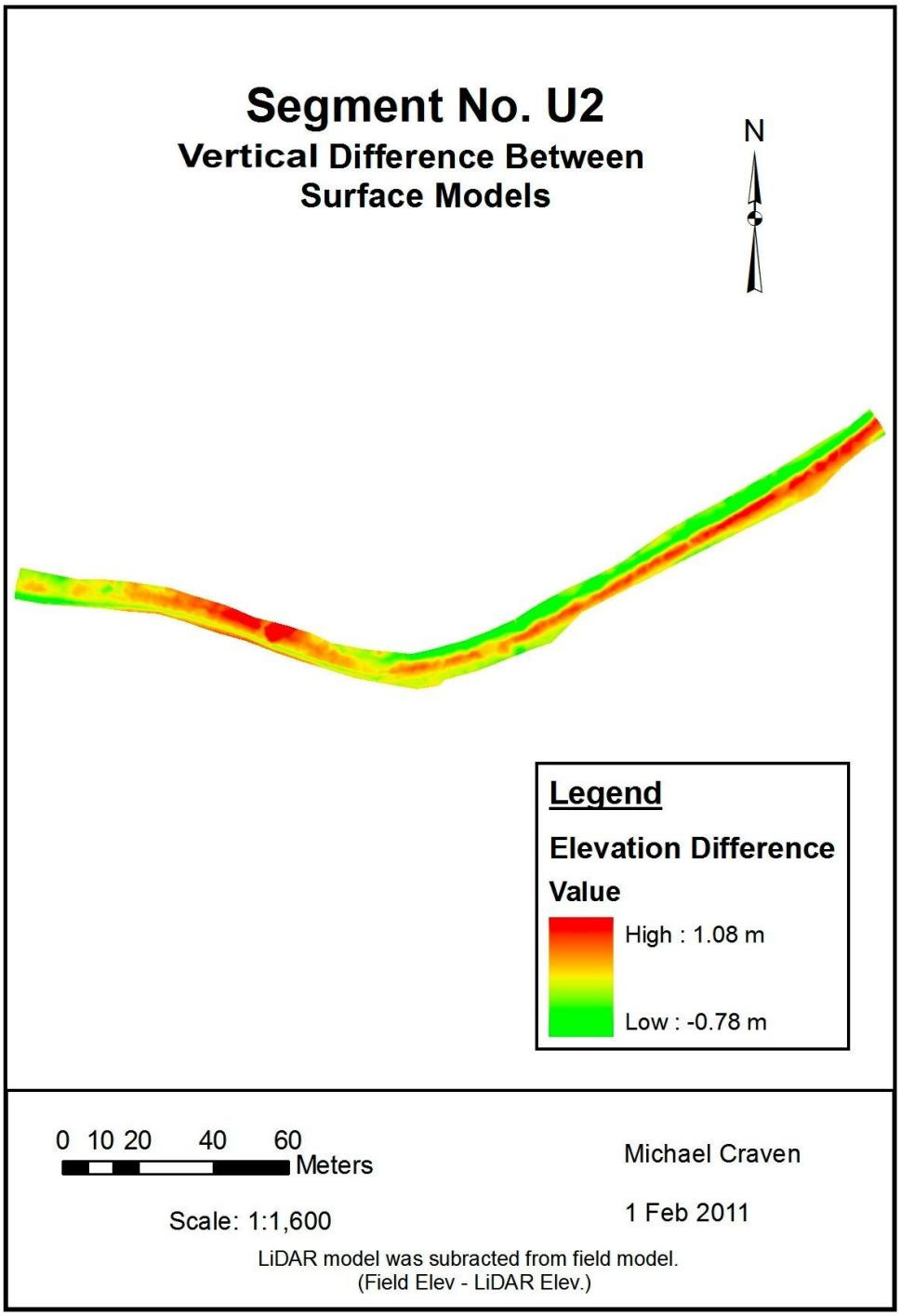

Figure A14: Elevation Difference Between TIN Models- Segment U2

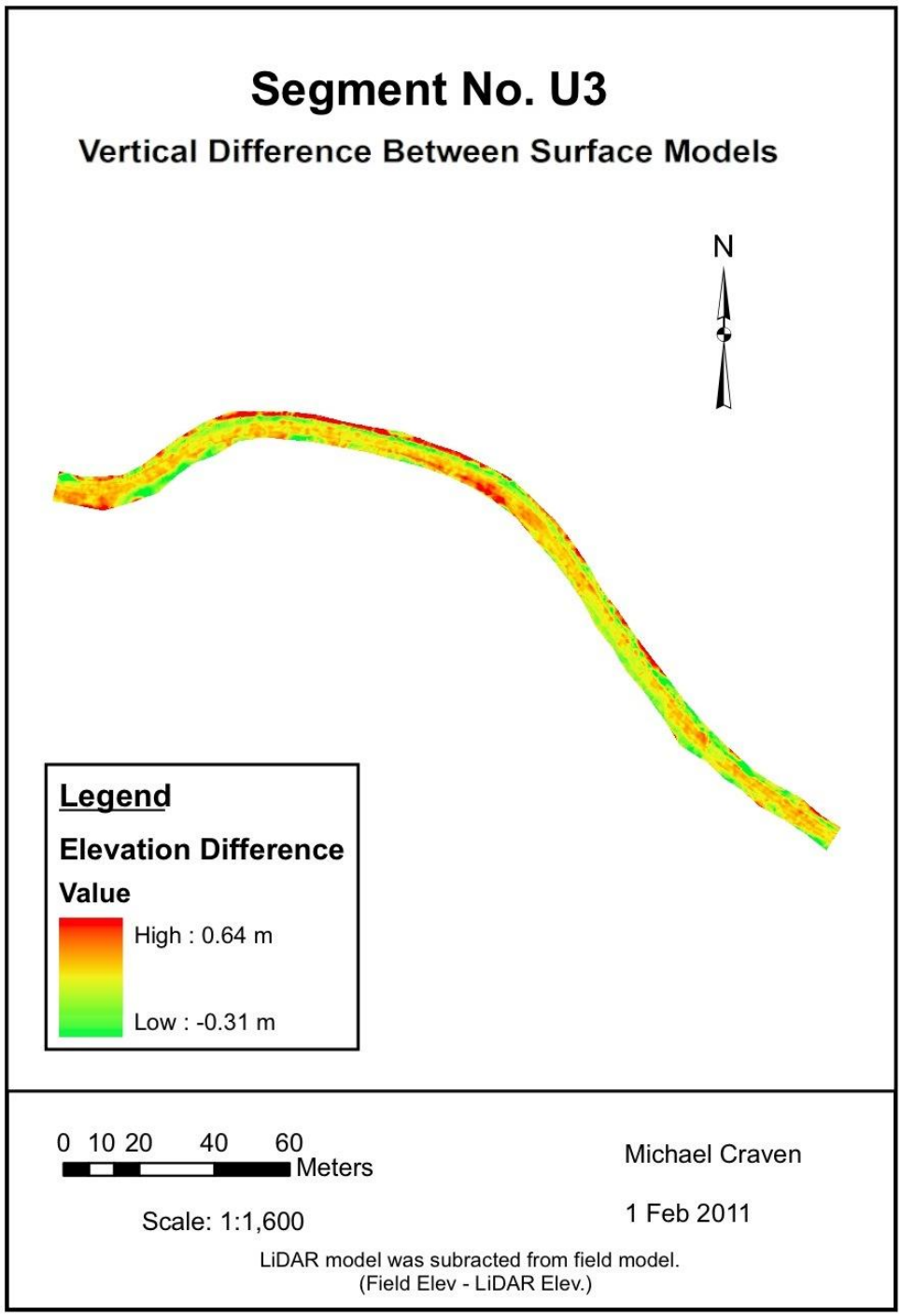

Figure A15: Elevation Difference Between TIN Models- Segment U3

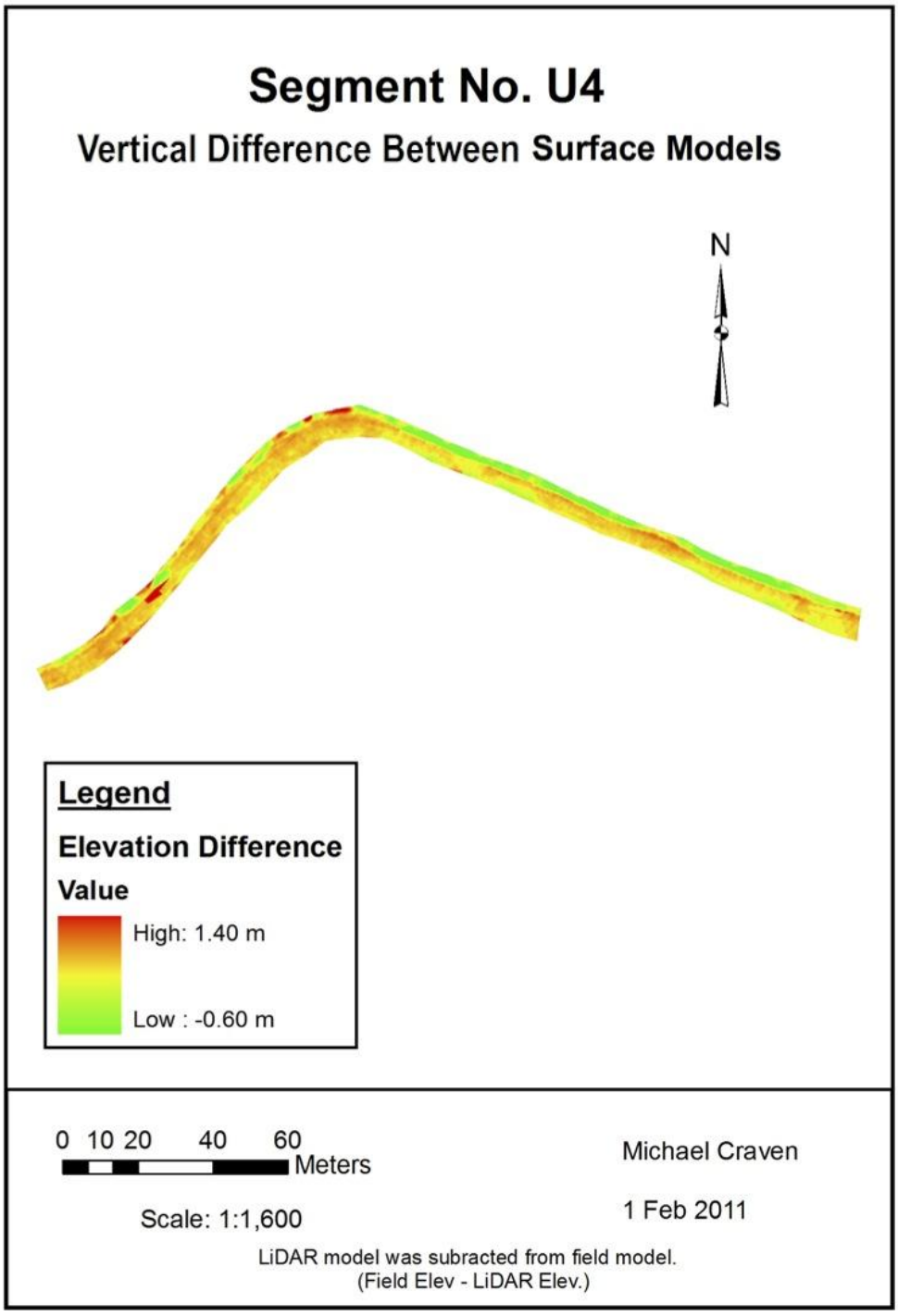

Figure A16: Elevation Difference Between TIN Models- Segment U4

Table A10: Individual Profile Results (Profile Elevation to LiDAR Elevation, in meters)

Site	Profile Point Total	Profile HD Length	Average HD Between Profile Points	Average Slope Between Profile Points (%)	Average Elevation Differnce (DEM)	Difference in SD (DEM)	Average Absolute Elevation Difference (DEM)	RMSE Absolute Difference (DEM)	Average HD Distance to Nearest LiDAR Point	Average Difference in Elevation (Nearest)	Difference in SD (Nearest)	Average Absolute Elevation Difference (Nearest)	RMSE Absolute Difference (Nearest)
Meadow	20	127.3	6.7	28	-0.01	0.17	0.14	0.37	0.30	-0.08	0.19	0.10	0.32
	14	112.5	8.7	25	-0.07	0.08	0.09	0.30	0.35	-0.13	0.19	0.15	0.39
	15	106.1	7.6	25	-0.16	0.06	0.16	0.39	0.32	-0.11	0.17	0.12	0.34
	13	108.0	9.0	29	-0.18	0.12	0.19	0.43	0.32	-0.11	0.14	0.11	0.34
Meadow Total	**62**	**453.9**	**7.8**	**27**	**-0.09**	**0.14**	**0.14**	**0.38**	**0.32**	**-0.11**	**0.18**	**0.12**	**0.35**
Clearcut	18	137.6	8.1	50	-0.21	0.24	0.25	0.50	0.41	-0.23	0.82	0.25	0.50
	20	136.9	7.2	45	-0.21	0.21	0.23	0.48	0.34	-0.30	0.38	0.30	0.54
	18	132.5	7.8	40	-0.25	0.19	0.27	0.52	0.30	-0.20	0.26	0.21	0.45
	18	128.6	7.6	38	-0.23	0.11	0.23	0.48	0.27	-0.18	0.32	0.20	0.45
Clearcut Total	**74**	**535.6**	**7.7**	**43**	**-0.22**	**0.19**	**0.25**	**0.50**	**0.33**	**-0.23**	**0.50**	**0.24**	**0.49**
Low density forest	10	77.0	8.6	51	-0.17	0.28	0.24	0.49	0.94	-0.08	0.46	0.54	0.74
	11	85.8	8.6	38	-0.09	0.20	0.19	0.43	0.80	-0.06	0.26	0.26	0.51
	6	50.1	10.0	53	-0.06	0.21	0.14	0.37	0.69	0.28	0.37	0.29	0.53
	12	59.6	5.4	56	-0.11	0.25	0.23	0.48	0.44	0.03	0.21	0.22	0.47
Low Density Total	**39**	**272.5**	**7.8**	**49**	**-0.11**	**0.23**	**0.21**	**0.46**	**0.71**	**0.01**	**0.36**	**0.32**	**0.57**
Medium density forest	26	155.0	6.2	39	-0.11	0.24	0.21	0.46	0.83	-0.28	0.27	0.38	0.62
	22	129.3	6.2	27	-0.05	0.15	0.11	0.34	0.72	-0.05	0.36	0.21	0.46
	40	230.3	5.9	43	0.03	0.21	0.17	0.41	0.74	-0.12	0.36	0.29	0.54
	17	107.0	6.7	35	0.02	0.18	0.15	0.39	0.68	-0.03	0.27	0.18	0.42
Medium Density Total	**105**	**621.6**	**6.2**	**37**	**-0.02**	**0.21**	**0.17**	**0.41**	**0.75**	**-0.13**	**0.32**	**0.28**	**0.53**
High density forest	36	280.5	8.0	35	-0.04	0.18	0.15	0.39	0.55	-0.06	0.39	0.20	0.45
	46	290.2	6.4	33	-0.05	0.24	0.18	0.43	0.82	-0.01	0.34	0.27	0.52
	40	274.2	7.0	37	0.03	0.24	0.19	0.43	0.90	0.03	0.34	0.25	0.50
	36	226.6	6.5	36	-0.10	0.24	0.20	0.45	0.70	-0.01	0.37	0.20	0.45
High Density Total	**158**	**1071.4**	**7.0**	**35**	**-0.04**	**0.23**	**0.18**	**0.43**	**0.75**	**-0.01**	**0.37**	**0.23**	**0.48**
Mixed forest	16	167.5	11.2	33	-0.10	0.17	0.16	0.40	0.81	0.17	0.10	0.32	0.57
	25	209.2	8.7	43	-0.14	0.27	0.23	0.48	0.60	-0.03	0.12	0.28	0.52
	14	108.0	8.3	52	-0.25	0.18	0.25	0.50	0.60	0.20	0.10	0.25	0.50
	12	84.7	7.7	63	-0.09	0.16	0.14	0.38	0.79	-0.01	0.09	0.29	0.54
Mixed Forest Total	**67**	**569.4**	**9.0**	**46**	**-0.14**	**0.22**	**0.20**	**0.45**	**0.68**	**0.07**	**0.10**	**0.28**	**0.53**
Grand Total	505	3524.4	7.3	38	-0.09	0.22	0.19	0.43	0.62	-0.07	0.33	0.24	0.49